INTELLIGENT TRANSPORTATION NETWORKS WITH MOBILE SHM SUPPORT AND BRIDGE PERFORMANCE ASSESSMENT

A THESIS SUBMITTED TO
THE BOARD OF GRADUATE PROGRAMS
OF
MIDDLE EAST TECHNICAL UNIVERSITY, NORTHERN CYPRUS CAMPUS

BY

ARMAN MALEKLOO

IN PARTIAL FULFILLMENT OF THE REQUIREMENTS
FOR
THE
DEGREE OF MASTER OF SCIENCE
IN
THE
SUSTAINABLE ENVIRONMENT AND ENERGY SYSTEMS

SEPTEMBER 2020

Approval of the Board of Graduate Programs

Prof. Dr.
Gürkan Karakaş
Chairperson

I certify that this thesis satisfies all the requirements as a thesis for the degree of Master of Science

Assist. Prof. Dr.
Ceren İnce Derogar
Program Coordinator

This is to certify that we have read this thesis and that in our opinion it is fully adequate, in scope and quality, as a thesis for the degree of Master of Science.

Research Assoc. Ekin Özer Co-Supervisor	Assist. Prof. Dr. Ali Atashbar Orang Supervisor

Examining Committee Members

Assoc. Prof. Dr. Mehmet Metin Kunt	Eastern Mediterranean University Civil Engineering	
Assist. Prof. Dr. Ali Atashbar Orang	METU NCC Mechanical Engineering	
Research Assoc. Ekin Özer	University of Strathclyde Civil and Environmental Engineering	
Assist. Prof. Dr. Ali Şahin Taşligedik	METU NCC Civil Engineering	
Assoc. Prof. Dr. Murat Fahrioğlu	METU NCC Electrical and Electronics Engineering	

I hereby declare that all information in this document has been obtained and presented in accordance with academic rules and ethical conduct. I also declare that, as required by these rules and conduct, I have fully cited and referenced all material and results that are not original to this work.

Name, Last name: Arman, Malekloo

Signature:

ABSTRACT

INTELLIGENT TRANSPORTATION NETWORKS WITH MOBILE SHM SUPPORT AND BRIDGE PERFORMANCE ASSESSMENT

Malekloo, Arman
MSc., Sustainable Environment and Energy Systems
Supervisor: Assist. Prof. Dr. Ali Atashbar Orang
Co-Supervisor: Research Assoc. Ekin Özer

September 2020, 137 pages

Bridge infrastructures are critical nodes in a transportation network. In earthquake-prone areas, seismic performance assessment of infrastructure is essential to identify, retrofit, reconstruct, or, if necessary, demolish the infrastructure systems based on optimal decision-making processes. As one of the crucial components of the transportation network, any bridge failure would impede the post-earthquake rescue operation. Not only the failure of such high-risk critical components during an extreme event can lead to significant direct damages, but it also affects the transportation road network. The consequences of these secondary effects can easily lead to congestion and long queues if the performance of the transportation system before or after an event was not analyzed. These indirect losses can be more prominent compared to the actual damage to bridges. Recent technological advancement in mobile sensors such as smartphones and Structural Health Monitoring (SHM) brought the opportunity to improve the accuracy of mathematical models by using experimental data and model calibration with field measurements. Engaging mobile SHM platforms with Intelligent Transportation System (ITS) and Geographical Information Systems (GIS), one can develop cost-effective and sustainable transportation infrastructure monitoring solutions targeting structural and transportation network resiliency. In line with this notion, this thesis study brings about seismic performance assessment for the Northern Cyprus transportation network from which the decision-making

platform can be modeled and implemented based on the combination of SHM and ITS. This study employs a seismic hazard analysis based on generated USGS ShakeMap scenarios for the risk assessment of the transportation network. Furthermore, identification of the resiliency and vulnerability of transportation road network is carried out by utilizing the Graph Theory concept at the network level. Moreover, link performance measures, i.e., traffic modeling of the study region is simulated in a Dynamic Traffic Assignment (DTA) simulation environment. Finally, for earthquake loss analysis of the bridges, the Hazus loss estimation tool is used. The case study of this thesis is the Western part of Northern Cyprus, comprising 20 bridges with a transportation network that is consisting of 134 links and 94 nodes with a total length of about 174 km. The results of our investigations for three different earthquake scenarios have shown that seismic retrofitting of bridges is a cost-effective measure to reduce the structural and operational losses in the region.

Keywords: Seismic risk assessment; Graph Theory; ShakeMap; SHM, ITS, DTA

ÖZ

MOBİL YAPI SAĞLIĞI TAKİP DESTEKLİ AKILLI ULAŞIM AĞLARI VE KÖPRÜ PERFORMANS DEĞERLENDİRMESİI

Malekloo, Arman
Yüksek Lisans, Sürdürülebilir Çevre ve Enerji Sistemleri Programı
Tez Yöneticisi: Dr. Öğr. Üyesi Ali Atashbar Orang
Ortak Tez Yöneticisi. Dr. Öğr. Üyesi Ekin Özer

Eylül 2020, 137 sayfa

Köprü altyapıları, ulaşım ağındaki kritik noktalardır. Depreme meyilli alanlarda, altyapının sismik performans değerlendirmesi, optimum karar verme süreçlerine dayalı olarak altyapı sistemlerini belirlemek, güçlendirmek, yeniden inşa etmek veya gerekirse yıkmak için gereklidir. Ulaşım ağının en önemli bileşenlerinden biri olan köprülerdeki herhangi bir arıza, deprem sonrası kurtarma operasyonunu engelleyecektir. Bu tür yüksek riskli kritik bileşenlerin olağandışı bir olay sırasında arızalanması doğrudan ve belirgin hasarlara yol açmakla kalmaz, aynı zamanda ulaşım yolu ağını da etkiler. Bu ikincil etkilerin sonuçları, ulaşım sisteminin performansı bir olaydan önce veya sonra analiz edilmemişse kolayca tıkanıklığa ve uzun kuyruklara yol açabilir. Dolaylı kayıplar, köprülerde oluşan gerçek hasarla karşılaştırıldığında daha mühim olabilir. Akıllı telefonlar ve Yapı Sağlığı İzleme (YSİ) gibi mobil sensörlerdeki son teknolojik gelişmeler, deneysel verileriyle ve saha ölçümleriyle model kalibrasyonunu kullanarak matematiksel modellerin doğruluğunu geliştirme fırsatı verdi. Mobil YSİ platformlarını Akıllı Ulaşım Sistemi (AUS) ve Coğrafi Bilgi Sistemleri (CBS) ile birleştirerek, yapısal ve ulaşım ağı dayanıklılığını hedefleyen uygun maliyetli ve sürdürülebilir ulaşım altyapısı izleme çözümleri geliştirilebilir. Bu fikir doğrultusunda, bu tez çalışması, Kuzey Kıbrıs ulaşım ağı için, YSİ ve AUS kombinasyonuna dayalı karar verme platformunun modellenip uygulanabileceği sismik performans değerlendirmesi yapmaktadır. Bu çalışma,

oluşturulan USGS ShakeMap senaryolarına dayalı bir sismik tehlike analizi kullanır. Ayrıca, ulaşım yolu ağının dayanıklılığı ve kırılganlığının belirlenmesi, ağ düzeyinde Grafik Teorisi kavramı kullanılarak gerçekleştirilmiştir. Ayrıca, çalışma bölgesinin trafik modellemesi gibi olan bağlantı performans ölçümleri, Dinamik Trafik Atama (DTA) simülasyon ortamında simüle edilmiştir. Son olarak, köprülerin deprem kayıp analizi için Hazus kayıp tahmin aracı kullanılmıştır. Bu tezin vaka çalışması, toplam uzunluğu yaklaşık 174 km olan 134 bağlantı ve 94 bağlantı noktasından oluşan ulaşım ağına sahip 20 köprüden oluşan Kuzey Kıbrıs'ın batı kesimini kapsamaktadır. Üç farklı deprem senaryosu için yapılan araştırmanın sonuçları, köprülerin depreme karşı güçlendirilmesinin bölgedeki yapısal ve operasyonel kayıpları azaltmak için uygun maliyetli bir önlem olduğunu göstermiştir.

Anahtar kelimeler: Sismik risk değerlendirmesi; Grafik Teorisi; ShakeMap; YSİ, AUS, DTA

ACKNOWLEDGMENTS

First and foremost, I would like to extend my sincere gratitude to Research Assoc. Ekin Özer. I feel privileged to have been working with him during these past two years. His continuous support, encouragement, and valuable and novel insights were the key contributors without which this thesis would have no foundation. A portion of this research would not have been possible without the help of my friend and research colleague, Wasim Ramadan. I would like to thank him for his support, and I cannot wait to see the fruits of the outcomes of our joint-research work in the future.

I would also like to express my appreciation to the thesis committee members Professor Mehmet Metin Kunt, Professor Ali Atashbar Orang, Professor Ali Şahin Taşligedik, and Professor Murat Fahrioğlu for taking their time to review this thesis and to provide their constructive criticism, advice, and recommendations. I am incredibly grateful to Professor Ceren İnce Derogar and Professor Bertuğ Akıntuğ for providing me with the opportunity to learn the art of teaching by allowing me to become a competent Teaching Assistant in the Civil Engineering Department at METU NCC. I am particularly grateful to Professor Fadi Al-Turjman for providing me with his valuable experiences in journal publication and reviews. I am also much appreciative of the faculties both at METU and METU NCC, whom I had the privilege to work alongside as their assistant throughout my graduate life. I also want to thank the instructors of the CVE and the SEES departments for equipping me with the necessary knowledge and skills to become a successful engineer.

The courses and research path I took, as well as the unimaginable curiosity, have all led me to this pulsating point of my life. This thesis would not have been possible without the support of my long list of friends. Special thanks to my roommate, Mohammad Abujubbeh, for all the fun times we shared, and my two delightful friends, Mahnoor Yaqoob and Sana Khan for their support and their words of encouragement that kept me going through the Master and defense process. In no particular order, Ece, Deniz, Haroon, Abdulsalam, Kamran, Ahmad, Bassel, Barış, Oğuzhan, Safa, Hamed, Narges, Negar, Shima, Ali, Erfan, Sina, and many more, thank you for your friendship.

Finally, a very special thanks goes to my family – mom, dad, and my two younger brothers – for their unconditional, unparalleled love, and support throughout my entire life. This thesis is dedicated to my family and my closest friends. Thanks for being there for me; without you the circuitous path towards the completion of this thesis would have been far-fetched.

TABLE OF CONTENTS

LIST OF TABLES

LIST OF FIGURES

LIST OF ABBREVIATIONS

AADT	Average Annual Daily Traffic
ATS	Average Travel Speed
CDF	Cumulative Distribution Function
DSHA	Deterministic Seismic Hazard Analysis
DTA	Dynamic Traffic Assignment
FEM	Finite Element Model
FFS	Free-Flow Speed
FFT	Fast Fourier Transformation
GIS	Geographical Information System
GMPE	Ground Motion Prediction Equation
Hazus	Hazard U.S.
IM	Intensity Measure
ITS	Intelligent Transportation System
KDE	Kernel Density Estimation
LOS	Level-Of-Service
ML	Machine Learning
NDT	Non-Destructive Testing
OD	Origin-Destination
PDF	Probability Density Function
PGA	Peak Ground Acceleration
PGV	Peak Ground Velocity
PHF	Peak Hour Factor
PHV	Peak Hour Volume
PHV	Peak Hour Volume
PR	Pattern Recognition
PSD	Power Spectral Density
PSHA	Probabilistic Seismic Hazard Analysis
SA	Spectral Acceleration
SHM	Structural Health Monitoring
STA	Static Traffic Assignment
STFT	Short Time Fourier Transformation
TAZ	Traffic Analysis Zone

UAV	Unmanned Aerial Vehicle
UE	User Equilibrium
WSN	Wireless Sensor Network

CHAPTER 1

INTRODUCTION

1.1 General Overview

Earthquake as a natural disaster can effectively bring parts or all the transportation network systems, especially in metropolitan areas, to an immediate halt. Underestimating the seismic risks of bridges, one of the essential components in a transportation system, would bring chaos and disorder to the disaster areas. Bridges assist in transporting goods and disaster victims to and from cities and disaster sites. They are one of the elements in search and rescue in post-earthquake operations of critical infrastructures. Therefore, without proper analysis and assessment of the risk associated with bridges, this could undoubtedly cause disruptions to the transportation network and, ultimately, collapse of the lifelines of the impacted regions. The efforts on the analysis of past events have considerably improved the proactive decision making actions taken to reduce the damage of bridges by earthquakes, but there are still cases where they fail [1]. Moreover, bridges are considered spatially dispersed and interconnected structures. Due to their interdependency, therefore, analyzing one bridge would not necessarily provide enough information to propose suggestions and alternatives for the mitigation of future losses.

Seismic risk assessment provides the necessary tools to assess damage before the main event happens. Provided that seismic hazard assessment of the region is well studied, it is possible to minimize the potential losses following a disaster. Basoz and Kiremidjian [2] presented a seismic event timeline (see Figure 1.1) that shows the actions and plans that need to take place before and after a seismic event. The first action is assessing potential risks through the use of seismic risk assessment tools such as Hazus (see 1.3.2). Next is the mitigation strategies to reduce risks such as retrofitting bridges and alternative route planning. In this regard, the highway transportation network plays a vital and integral part of such impact assessment. Consequently, the network-based risk assessment methodologies need to be

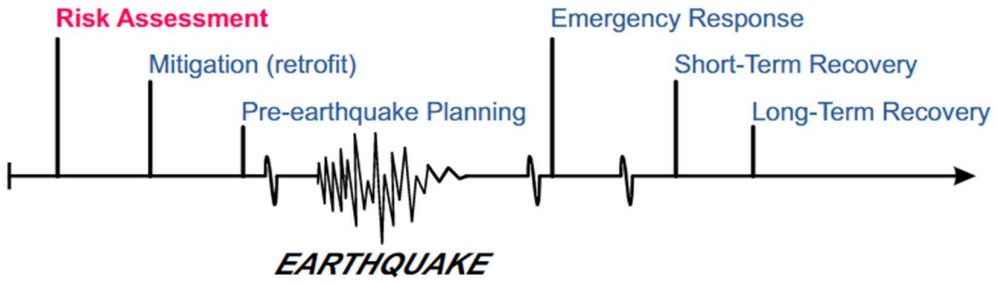

Figure 1.1. A disaster risk assessment management problem [2]

developed and enhanced further to take into consideration the ever-growing and complex transportation network.

1.2 Motivation

Seismic risk analysis with smartphone sensors augmentation as a source of data collection for fragility analysis provides a new paradigm into what is essentially has been a traditional take on damage assessment of civil infrastructures. With the proliferation of innovative technologies, it is essential to link different fields of studies into a general framework that can be used to provide better and more accurate results by working together synergistically. Disaster risks following a natural hazard can induce a lot of impacts on the vulnerable people and infrastructure of a region such as the transportation network. Hence, a decision-support system is essential for assessing the risks.

This thesis, therefore, aims to bring about a new methodology for assessing seismic risks of the Northern Cyprus transportation network. By utilizing state-of-the-art tools and methods, we try to extend the well-studied seismic hazard analysis used by researchers and scholars and expand it under the umbrella of the Intelligent Transportation Decision Support System for assessing seismic risk. The outcomes of this study hope to open the path into a fully-fledged decision-making platform with real-time network-based risk assessment providing the best mitigation strategies before and after a seismic event.

1.3 Components of the Research

There are a variety of tools and theories used for this research study. Notably, the framework behind this thesis can be further expanded and utilized for a more in-depth analysis of other hazards as well. Here we introduce the approaches we employed, albeit in varying degrees of detail, to achieve the goals of our study.

1.3.1 Structural Health Monitoring (SHM)

In the past, damage identification was based on either visually detecting damage or interval or time-based inspection techniques carried out by using Non-Destructive Testing (NDT) methods. The former method, although well-established and well-proven for small and simple systems, cannot possibly be used for more complex structures. A priori knowledge of the damaged area is necessary for such techniques, and this would be impossible for small and unreachable areas without first dismantling part of that area. Besides, such damage detection is localized, meaning they cannot represent the global behavior or the response of the system. The impracticality of visual inspection for large and complex civil infrastructures and long inspection intervals has opened the possibility of incorporating condition-based assessment techniques. As such, Structural Health Monitoring (SHM) has emerged to provide the transition from off-line local damage identification to near-real-time and online damage assessment. In layman's term, SHM is a damage-detection strategy that can observe a structure over a long period using a series of continuous measuring devices to detect any changes. A vertical hierarchy is typically considered in order to identify damage. A pioneered damage typology scheme was offered by Rytter [3]. Damage state was categorized in 4 levels, namely:

1. Existence of damage – Detection
2. Position of damage – Location
3. Severity of damage – Extent
4. Prognosis of damage – Prediction

In such a hierarchy, knowledge of the previous level is required for complete damage identification. This means that the success at each level depends on how well the lower levels perform. Damage could relate to any changes in the structural behavior of a structure that can change its current or future performance. By definition, change refers to a baseline that makes damaged and intact states comparative [4]. Many works have reviewed SHM applications in a variety of disciplines, such as [5]–[7]. The 4-stage damage identification is in the center of every SHM application. As shown in Figure 1.2, the SHM system comprises of many other elements and features.

In the SHM paradigm, we first need to answer the following questions and carry out the procedures defined below [8]:

1. Why is there a need to evaluate the damage and damage description? (Operational evaluation)
2. Which quantities need to be selected and measured, which type of sensors are required, and how often the data should be collected? (Data acquisition)

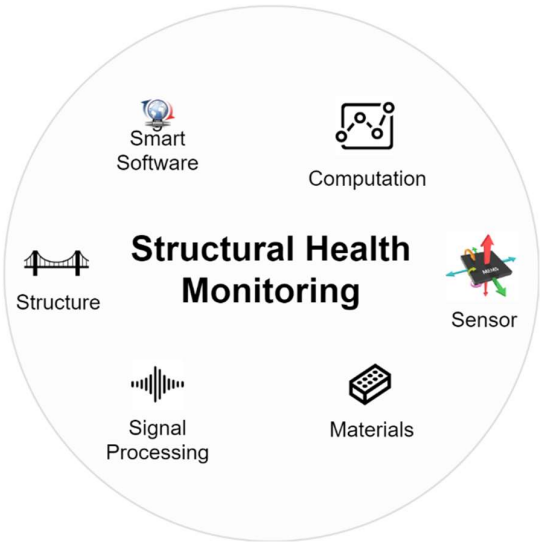

Figure 1.2. Components of SHM

3. Extracting low-dimensional feature vectors and excluding redundant information in addition to data condensation. (Feature selection)
4. Verifying the significance of the extracted feature using statistical analysis. (Feature discrimination)

In certain SHM applications, a prior model, typically the Finite Element Model (FEM) of the structure is required. Other models such as statistical, surrogate, or reduced-order models, can be used instead of FEM as well. Model updating is then performed, replacing the initially assumed assumptions with the measured values. This is then considered as the baseline or the undamaged state of the structure. Further updating of the model will, therefore, identify the damage by considering the structural changes. The comparison can also be done by assessing the changes in the modal parameters directly. This process of SHM implementation is a model-based method. This means that an accurate analytical model of the structure is required [9]. Often, coming up with an accurate model is burdensome. Model discrepancies, especially for complex structures, with little to no information about joint and bonds, are inevitable. Such an inverse problem is not well-posed [8] and requires regularization and simplification [9]. An alternative to a model-based SHM system is the data-driven model.

1.3.1.1 Machine Learning in SHM Application, A Complementary Addition

Given the amount of data gathered from many different things, it is crucial to understand the pattern that underlines it. With an increase in complexity of structures, discovering patterns using computers without automatic processes would be infeasible and impractical. Machine Learning (ML) is considered as a tool to recognize/classify information based on a learned pattern through the use of different algorithms where the model construction is dependent on

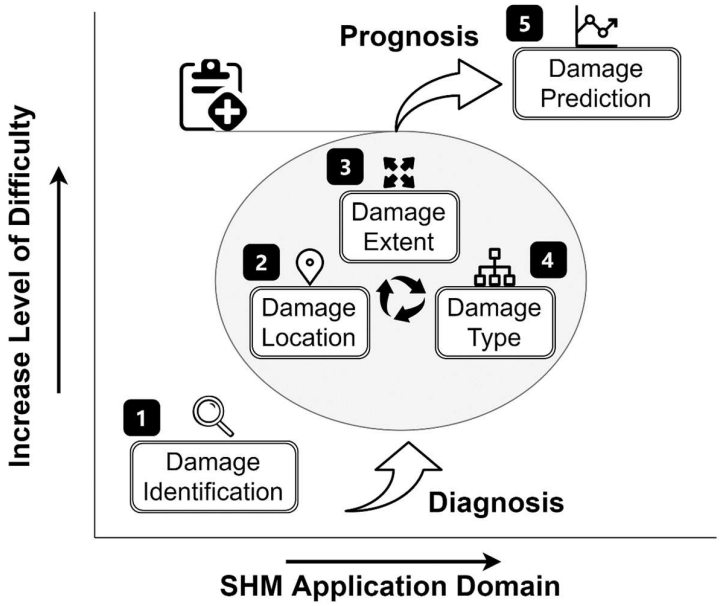

Figure 1.3. The 5-step hierarchical damage identification scheme

the statistical pattern recognition (PR) algorithms. In contrast to having a FEM and updating the model later, the data generated through the sensing devices are trained from the structure in both the damaged and undamaged states. In cases where lack of data is a problem, and the data-driven approach is still preferred over the model-based, a hybrid model of the two can be applied. The augmentation of a data-based SHM system with the FEM model can generate test data for the validation phase. With the advent of ML and statistical PR algorithms, a new level can be added to the Rytter's 4-stage damage identification. The type of damage or classification of damage is the level that is possible through the use of ML algorithms [10]. This new step lies between stages 2 and 3. Figure 1.3 depicts the 5-step hierarchical damage identification. Given that both damage and undamaged information are available, a supervised learning algorithm can effectively go through all five levels of damage detection. This, as explained before, requires extensive data to be readily available from the sensing systems, the physic-based models, or the experiments.

ML can augment SHM in many aspects where the old system is incapable. For example, environmental and operational variabilities are ongoing challenges in most SHM implementations, but it has been proven that they can significantly influence in-service structures [11]. Including these effects by leveraging the power of ML can help the SHM application achieve a better level of detection. The extension of ML into SHM is one of the future objectives of this study that we hope to achieve as the next step of our research.

1.3.2 Hazus, GIS-based Seismic Hazard Assessment Software

Geographical Information System (GIS) constitutes many components. A visually explanatory platform involving GIS manages multiple data from different sources on separate layers allowing simulation and modeling of all data and their influence on one another. GIS and its useful applications in many disciplines, especially in disaster management cases, come with shortcomings, however. The time, effort, and possibly money that is essential for advanced GIS applications may deter usage of the tools altogether. Applicability constraints clearly can be seen when analyzing earthquake disasters and its implication on the network, which could produce tens of thousands of spatially – possibility not uniformly distributed data that can make the processing and analyzing a complicated and time-consuming process [12]. GIS maps with different layers are available online[1] , but the currency of the information provided may be of concern. Therefore, in some cases where there is a lack of information on GIS maps (e.g., unknown bridge locations or highway network information), one needs to spend hours to acquire these data and import them into the correct location on the maps. GIS is considered as a database management system capable of storing, analyzing, and displaying data in a standard graphical interface. In the area of bridge performance assessment, standalone applications of GIS are mostly associated with risk assessment and life-cycle risk analysis. Spatially distributed information along with multiple independent parameters of bridges and networks, call for a management system that could operate and analyze different scenarios. Integrating bridge inventory information with earthquake parameters required to produce fragility curves to determine bridge damage state as one of the input parameters for initializing spatial analysis is widely used in many studies [13]–[15].

Hazard U.S. (Hazus) is a general-purpose multi-hazard GIS-based loss estimation software. Earthquake loss estimation methods of Hazus is heavily used by the locals, states, and regional officials in the U.S. as a state-of-the-art decision support software. Development of earthquake hazard mitigation strategies, development of contingency planning measures, and finally, the anticipation of the nature and scope of response and recovery efforts are some of the pre-earthquake applications of Hazus. It can also be used for post-earthquakes analysis for the projection of immediate economic impact assessment and long-term reconstruction plans. One of the new additions to Hazus was the ability to import ShakeMap data for rapid post-earthquake loss estimation in the affected region. ShakeMap can provide deterministic seismic hazard maps that are used to predict the shaking intensities of earthquakes. The risk assessment results that Hazus provides are vast in terms of both direct and indirect losses. For this study, we will only be utilizing the damage assessment of bridges in our study region. The assessment

[1] Natural Earth Data, Esri Open Data, USGS Earth Explorer, OpenStreetMap

in Hazus is based on fragility curves developed for 28 classes of bridges in the U.S. A Fragility curve represents the probability of exceeding a given damage state as a function of an engineering demand parameter.

1.3.3 Travel Time Loss Estimation with Dynamic Traffic Modeling

One of the outcomes of this research is to show how damaged bridges in the transportation network can significantly influence the travel time and traffic planning. Travel forecasting models are widely used in transportation planning. They qualitatively and quantitatively evaluate the impacts of future changes in the transportation network [16]. The mesoscopic simulation of the network can share a great deal of information on how individual users choose their paths and what determines their decision on changing routes. Dynamic Traffic Assignment (DTA) modeling can perform such analysis with varying degrees of accuracy, provided that enough information is used to support the simulation. By leveraging the potential of DTA, we can have a better insight into what would happen when some bridges are completely failed or have reduced capacity due to a decrease in serviceability.

1.4 Research Objectives

We are primarily interested in modeling the transportation network of Northern Cyprus, and in particular, the performance of such a network under earthquakes hazards. The goal of our study is to determine the most critical components in the network and provide alternative solutions or measures that need to be taken to reduce the impacts of risk associated with earthquake hazards. We will apply what we described in the brief introduction of our study in the western part of Northern Cyprus, which includes 20 historical as well as newly built bridges. Therefore, the objectives of this thesis are:

1. To develop the seismic hazard maps for scenario-based earthquake analysis.
2. Providing a novel framework for implementing mobile SHM and analytical fragility analysis of the bridges
3. To build the bridge inventory of the study region and the linked transportation network and to analyze the structural integrity of the network by employing Graph Theory.
4. To simulate the dynamic traffic assignment for travel forecasting purposes, such as determining the travel time in the network based on a mesoscopic model.
5. To show the international adaptation of Hazus as a tool for seismic risk assessment for Northern Cyprus.

Ultimately, the end goal of this thesis is to show a different approach for assessing risks related to earthquakes by considering state-of-the-art technologies and by introducing a flexible decision platform system for governments for pre- and post-earthquake disaster scenarios.

1.5 Contribution and Thesis Organization

The first significant contribution of this thesis is the fact that there have been no case studies on a national scale on the Northern Cyprus transportation network. Most prior works dealt with ground motions probabilistic assessment of the region. We extend their work and find the risk associated with the results of their studies. Therefore, this thesis can provide a comprehensive multi-purpose tool for the responsible agencies in the urban planning sector. The methods used to derive the assessment of the transportation network can also be used in other hazards analyses such as flood hazard. In reality, floods have been more damaging to Northern Cyprus in the past 50 years than the earthquakes. The extension of our analysis to multi-hazard assessment is one of the other valuable outcomes of our study. The second major contribution is the implementation of mobile SHM and analytical fragility analysis of the bridges. The incorporation of SHM and Intelligent Transportation System (ITS) in seismic risk assessment can bring a new domain of intelligent sensing and real-time loss estimation. The initial strides towards developing the fragility curves have already been taken, and we aim to finalize this portion of the study in the near future.

Furthermore, we incorporate dynamic traffic analysis (DTA) as part of our study for travel time estimation. There have been few works that leveraged DTA in their analyses for risk assessment of the transportation network. We also demonstrate the tractability of adapting Hazus for our case study. It goes to show the effectiveness of applying a well-known risk assessment software for a region that it was not initially intended for. Finally, under the framework laid out in this thesis, we believe that the roadmap of utilizing new technologies such as 1) ML application for diagnosis and prognosis of bridge structures, 2) cloud-based decision-based system, and 3) the integration of ITS with SHM-based bridge monitoring system is defined in such a way as to guide the future implementation of this paradigm.

In light of these outcomes, this thesis explores the above contributions in its seven main chapters and appendices:

Chapter 2 presents a detailed literature review of SHM, ITS, their integration, and finally, seismic risk assessment implementation in different parts of the world. This chapter also aims to outline the research gaps in the current body of literature.

Chapter 3 describes the seismic hazard risk analysis of Northern Cyprus. We introduce the Probabilistic Seismic Hazard Analysis (PSHA) in detail and give a case study example of how it works. In addition, we outline the necessary assumptions and criteria for generating ShakeMap data for Hazus analysis. The results of this chapter are integral parts of our study, which describe the basis of our case study earthquake scenario-based analysis. Finally, we establish the SHM part of our research and discuss the future steps that will be taken to develop the fragility curves of the bridges.

Chapter 4 provides an essential understanding of the transportation network system of Northern Cyprus. We introduce the idea of network reliability and vulnerability. We further extend these concepts into assessing the structural integrity of the network based on topological vulnerability metrics using Graph Theory concepts. The findings of this part of the chapter indicate the structural measures at network, node, and link-level, which then can be used as a baseline comparison of post-earthquake analysis. In the second part of this chapter, we propose the DTA of our study region transportation network. We introduce the concept of link performance measure as part of 4-step travel demand modeling for evaluating the overall travel time of the network based on a dynamic traffic assignment assumption under the mesoscopic travel model.

Chapter 5 shows the adaptation of Hazus earthquake methodology for seismic risk assessment of Northern Cyprus. In this chapter, we outline the exact procedures taken to convert the Hazus default U.S. inventory to the inventory of our study region, including the administrative boundary, roads, and bridges.

Chapter 6 introduces our case-study region, where we apply the methodologies and approaches described in earlier chapters to perform the seismic risk assessment of the transportation network. The outcomes of this chapter include the mitigation strategies to reduce indirect losses to the network, as well as to identify vulnerable bridges and provide bridge prioritization seismic retrofit strategies.

Chapter 7 summarizes the main contributions and explores future works to enhance the current capabilities of this research. For example, we introduce our aim to synergistically combine SHM and GIS for a cloud-based bridge monitoring system with a further extension in ITS in the smart city paradigm.

Finally, in addition to the chapters, supplements files are provided for some sections of the main chapters. **Appendix A** outlines the data sources used for the case-study. **Appendix B** provides the ShakeMap PGA intensity maps for the four earthquake scenarios simulated in this thesis. **Appendix C** provides the damage state probabilities in the form of tables from Hazus based on the ShakeMap data for the four scenarios. Finally, **Appendix D** presents a

very simple case-study for developing an optimal retrofit strategy under a budget constraint as a mixed-integer linear program optimization model that we hope to incorporate more comprehensively in the later research. Collectively, these four appendices deliver the necessary supporting materials and details to extend the impact of this thesis. A flowchart of the thesis structure is depicted in Figure 1.4.

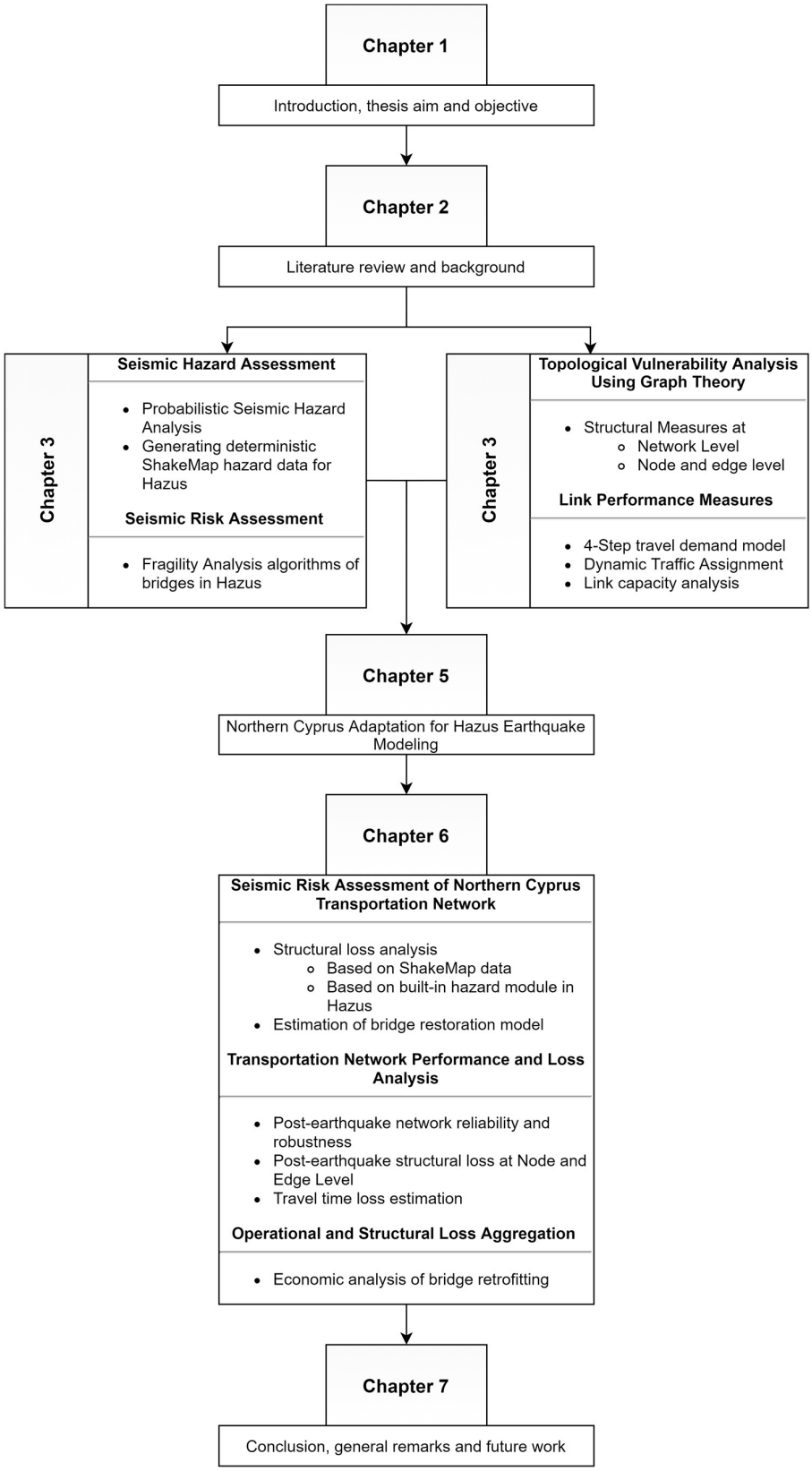

Figure 1.4. Flowchart of thesis structure

CHAPTER 2

LITERATURE REVIEW

2.1 Introduction

In this chapter, a thorough review of the past research studies in ITS and SHM, as well as many proposed seismic risk assessment approaches in evaluating the performance of transportation networks under seismic hazards will be analyzed and compared. It should be noted that making comparisons in this area of research especially in seismic risk assessment studies, is not a straightforward task. Considering the regional differences, both geologically and socioeconomically, each study, therefore, delivers its own set of outputs. Although, by tackling different studies, we can observe the changes that some fundamental parameters undergo leading to the emergence of new ways that can enable us to analyze the effectiveness of utilizing state-of-the-art methods and technologies in seismic risk assessment. In the up-to-date literature, the interaction between ITS and SHM in bridge performance under seismic activities has yet to be explored. However, the components of this process can still be investigated individually. Consequently, each section of this chapter investigates, from a broader perspective, the work that goes to bring about innovative bridge monitoring technologies for the performance assessment of these components in the transportation network.

2.2 Structural Health Monitoring of Bridges

SHM, or also referred to as rapid condition monitoring, is a form of condition-based damage identification in infrastructures. SHM studies are broad and cover many engineering disciplines. In civil infrastructures, however, we are mostly interested in vibration-based induced damages. An extensive review of pre-1996 SHM applications for structural and mechanical systems that experience changes in their vibrational characteristics was conducted in [17]. In their report, the authors emphasized the use of the continuous mechanism of bridge

damage detection techniques that could replace the unreliable visual-based inspection methods. However, introducing an automated approach requires a comprehensive understanding of several critical elements such as attention to the non-linearity behavior of bridges, location of sensors, and accurate detection. Reducing dependency on non-destructive vibration-induced loads is the next goal in long term infrastructural health monitoring, as noted by the authors. Another study in utilizing SHM was described in [18]. The authors in their paper provided several case studies of SHM applications explaining the recent history of the SHM system. Bridges, as one of the critical lifeline structures, must be controlled and maintained regularly. As the authors pointed out, SHM needs to be integrated into the bridge management program in the design stage. There are some bottlenecks in achieving complete SHM integration in today's civil infrastructure ecosystem. The reasons are primarily due to low SHM system reliability considering the existing issues such as big data, communication overhead especially in rural areas, and lack of accurate data mining algorithms to convert data to useful information. In order to solve some of the issues mentioned above, authors in [19] and [20] reviewed many solutions in the literature to improve the reliability of SHM using Wireless Sensors Network (WSN) as the backbone of SHM systems. One of the open research issues mentioned in [20] was about the smartphone sensing paradigm for information collection using the embedded sensors in our smartphones. This specific open research topic is investigated in this thesis under the framework of the smartphone platform.

In line with the suggestion of the previous studies in utilizing smartphones for sensing and measuring critical information, authors in [21] overviewed the development of smartphone-based systems. It is clear that classical SHM systems are expensive and require constant maintenance. Shifting toward mobile sensing for SHM can improve the overall quality and practicality of the system. Embedded sensors in smartphones with a variety of communication technologies can enable an effective solution to many issues in present classical SHM systems. However, further research must be carried out in order to enhance the capabilities of smartphones and to compete with the quality of the stationary sensors-based SHM systems. Other challenges, such as energy consumption and privacy issues with crowdsourcing applications must also be taken into consideration.

The authors in [22] presented a review of the recent smartphone-driven civil infrastructure monitoring projects. Compared to the previous review above, the authors focused on the influence of the citizen-centered monitoring aspect of civil engineering projects. This method of sensing can allow rapid assessment of damages during or after a disaster. The application domain of crowdsourced smartphone-based sensing needs to further integrate into other areas of civil engineering, as authors suggested. Furthermore, to improve the capabilities of these systems, external sensors may be required to work in conjunction with the built-in sensors.

Moreover, robust calibration is necessary to address the influence induced by citizens or other external factors.

The work in [5] presented a very recent review of SHM techniques and introduced a framework based on the Internet of Things (IoT), addressing SHM deployments, challenges, and solutions. This paper emphasized one of the critical issues in SHM deployments, i.e., communication. In today's heterogeneous, highly scalable world, communication network technology has always been the front line in the IoT paradigm. To overcome the challenges, further advancement in many topics such as security and privacy, as well as interoperability are needed. The authors' proposed framework in their paper aimed to enhance the SHM paradigm in these matters.

The authors in [23] overviewed the next generation of smart sensing technologies in SHM. They classified four smart-sensing technologies in their paper, namely: 1) camera-based, 2) UAV-based, 3) smartphone-based, and lastly, 4) mobile sensor-based. They reviewed these four forms of sensing technologies in the literature and compiled a comprehensive list comparing each technology used by various researchers in their case-studies. Moreover, key findings from each technology were noted, and challenges were also identified.

Quantifying the usefulness and practicality of utilizing SHM in measuring seismic damages is not dissimilar to seismic risk assessment, where we try to evaluate the performance of a given structure. In fact, by doing so, we try to have a general idea of the economic benefits of different mitigation strategies and measures — an example of cost-benefit analysis of SHM was shown in [24]. The authors employed a Bayesian pre-posterior decision analysis intending to minimize the total cost or risk from damage on a bridge caused by the mainshock further progressed in an aftershock.

2.3 Intelligent Transportation System

ITS by itself is not capable of providing useful information about bridge performance per se. However, fusing ITS and SHM in a seamless and integrated manner can offer numerous unprecedented perks of the combined use of the two systems. ITS is an emerging smart system with advanced sensory technologies capable of integrating information, communication, and control technologies to provide innovative services to different modes of transport. Advanced traffic management, advanced transit system, and travel time prediction are a handful of services offered by the combined usage. Depending on how they are integrated and how they exchange information, they can deliver an overall better system.

There are two possible ways to merge these two systems into one. The data collected through the ITS can be fed to the SHM system and, in turn, improve the reliability of the SHM

system; this is commonly known as the ITS-Informed-SHM system. An example of this approach was discussed in [25], which showed the impact of traffic load for fatigue damage evaluation on bridges. On the other hand, when providing the data collected from the SHM system to the ITS, we can make use of the information for real-time traffic management, especially under critical events such as an earthquake. This form of integration is referred to as SHM-Informed-ITS. In the latter case, in case of a disaster, the most beneficial use-case of the system is to inform citizens about bridge closure and the suggestion of alternative routes. Alternatively, in case of retrofitting or repairing, the system can also be used as an early information system for the possible full or partial closure of damaged bridges. This is further enhanced when the system is integrated as part of smart cities [26] where the information could be used for other services provided in this context, enabling interoperability, which in turn leads to an enhancement in the Quality of Service (QoS).

2.4 ITS and SHM integration

The review presented by [27] assessed the works related to both of the forms of ITS and SHM integration described earlier. In their paper, the authors discussed the limitation of standalone SHM and ITS in monitoring applications such as bridges, especially bridge vibration characteristic, which is influenced by the mass and speed of the moving vehicles. This review mostly tackled the studies related to traffic influence on bridge monitoring and bridge management in both applications. However, during or after disaster scenarios, this integration is significant and is beneficial to both the citizens and the bridge owners. Therefore, it is vital to expand on this and research further to incorporate these systems in critical lifeline infrastructures. As noted by the authors, there are still significant challenges such as big data [28], communication overhead, seamless integrations, and transition from local to national level that need be adequately addressed for large scale implementation of such an integrated system.

The authors in [29] presented an application for assessing existing roads and bridges utilizing Weigh-in-Motion (WIM) sensors. Generally, WIM sensors are used in ITS for traffic counting and vehicle load measurements. The authors used these key data to improve numerical models for bridge vibration characteristics. The integration of ITS with SHM in this scenario enhanced the capability of SHM and provided even more useful information that could be used further to calibrate certain variables while assessing the performance of bridges.

As described in [30], many long-span bridges are in the process of integrating ITS with SHM. This proves compelling benefits for the optimal management of bridges. The authors, therefore, reviewed the state of this integration for long-span bridges in the U.S. It was

suggested that there should be further efforts in adapting ITS in the existing bridges, a paradigm in which this seamless integration can be realized.

Disaster mitigation with the help of the integrated operation of ITS and SHM is crucial for emergency management. This idea was envisioned by [31]. The authors established this relation and explained how ITS takes advantage of an integrated information system allowing different users to access, review, and analyze real-time information. The authors went further to expand this link with earthquake disaster mitigation applications and how this interaction can bring people from many disciplines of engineering together for close coordinated research projects. This paper also showed examples and initiatives of this vision on the Commodore Barry Bridge in Philadelphia, U.S.

2.5 Seismic Risk Assessment

Evaluation of any risk in civil infrastructural systems, especially those that are critical to the function of a city, is an important task. One area where this assessment is crucial is in the transportation network system, which includes bridges and roadways. Seismic risk assessment is therefore needed to be carried out in locations where the risk of earthquakes is high. This assessment requires evaluating every individual component of the network system and then the system as a whole [32]. Understandably, under the umbrella of sustainability and the risk associated with seismic damages, one needs to understand the overall predisposition to social, environmental, political, and economic losses [33]–[35]. The objective of seismic risk assessment is to provide a decision-making platform that can be used as a guide in mitigation scenarios to alleviate the losses during a disaster. Combined with SHM and ITS, this allows for quick and critical decisions to be taken prior to the event, such as early retrofitting, and early warning systems. Overall system resiliency (ability to withstand, adapt and recover) is a challenge that needs to be addressed in every assessment scenario. The issue with achieving this in today's transportation network system is the interdependency and interconnectivity of the transportation system [36], [37]. One failed component in the network can significantly influence the functionality of the whole system.

To address some of the issues discussed above, the authors in [37] developed a risk assessment software that takes into account the resiliency of the transportation network. This tool was created to overcome the existing issues with other assessment strategies such as lack of including indirect cost, assumption of deterministic scenarios, and those where no quantification of the resiliency was made. Many indicators and different sources of uncertainty were coupled into a GIS-based package where both direct and indirect losses were assessed, giving the stakeholders the ability to decide on the best mitigation strategy.

In a comprehensive review of seismic fragility assessments, the authors in [38] systematically analyzed the existing literature, revealing state-of-the-art fragility assessment methods in addition to the development phase of each of them in detail. The authors believe that there exist many advanced fragility methodologies in the assessment of highway bridges under seismic activities. However, there needs to be more research on the hybrid approach of developing fragility curves. They proposed a combination of the empirical, experimental, and analytical methods of developing such curves. However, they did not test the adequacy of their method and suggested it to be further enhanced by researchers.

The work in [39] presented an extensive review of the multi-hazard assessment of highway bridges in the U.S. In the analysis for hazards related to earthquakes, the authors found out that the bridge classes defined for assessing the risk are limited and suggested to expand on a border range of bridge typologies. Moreover, it was stated that almost all of the research efforts are dedicated to mainshock damages, and very few consider mainshock as well as aftershock effect. Finally, the authors emphasized that future efforts should be put on areas where currently, there is a complete lack of fragility models related to other types of hazards such as wind, tornado, and fire.

There may be cases where a rapid post-assessment of a bridge is required to give an insight into the condition of the said bridge. A methodology was therefore developed by [40] that enables a quick assessment of bridges based on bridge prioritization given the effect of failure on the network. The authors evaluated their method in the transportation network of Wellington, New Zealand, and quantified the damages with SHM sensors.

Fixed or variable traffic demand may reduce and impair the highway traffic carrying capacity and influence the network functionality. Variable traffic demand, compared to fixed demand, more or less, reflects the real-life scenario. However, incorporating this demand not only makes the overall assessment more complicated but also introduces other intricate indicators. The authors in [41] introduced a framework to include post-disaster traffic demand in emergency conditions. Network topology, bridge link vulnerability, and traffic flow analysis were part of their proposed methodology. In their findings, a strong correlation between the damage level of the bridge link and traffic flow was observed. Moreover, it was shown that network topological features reflect a different aspect of the traffic flow of the bridge network.

The authors in [42] carried out a thorough analysis of the post-earthquake travel characteristics. Their method was proven to be more effective than the conventional approaches in transportation modeling. Their method, however, only considered bridges as the only component of the system to be susceptible to damage. However, they mentioned that with

little effort, this framework could be extended to other network components such as roadway segments.

In their work [43], the authors proposed a seismic risk assessment model for bridges in Charleston, South Carolina. They assessed the risk only in terms of direct losses. However, as they pointed out, there are uncertainties in every study that reflects the reliability of the tools and the models used. Applying sensitivity analysis can ensure that the assessment indicates the most appropriate result of the study. By doing so, we can both identify the sensitive components in the model and try to calibrate then, if possible. Authors in their study, therefore, analyzed two input models, namely, the fragility models and repair cost model. The findings revealed that repair cost associated with damage ratio models is more sensitive in determining the total direct economic loss.

The study [34] evaluated the socio-economic cost of bridges for two sets of scenarios, before or after the seismic retrofit. They evaluated the social cost in terms of travel delay with the assumption of a reduction in traffic flow after an earthquake and an opportunity cost. The latter reflects the loss of value in the inability to perform an activity by the drivers. It was found that retrofitting is more cost-effective for lower discount rates and bridges with higher average service life.

As it was discussed in the previous study above and also noted by the authors, different models and different assumptions can produce different results. Therefore, there are no unique models that best describe and assess the risk of seismic hazards. A similar study in [44] was presented, albeit with the focus only on travel time delay for deciding whether or not to retrofit bridges. The authors indicated the significance of bridge retrofitting on reducing travel time after an earthquake event.

A complete risk assessment methodology was presented in [45]. In most of the research papers, bridge performance assessment under seismic activities is only evaluated based on one hazard, generally ground shaking. However, the authors in their paper expanded their approach and included liquefication and landslide hazards as well. Annual risk curves for the San Francisco Bay area network, indicating both direct and indirect loss for different possible occurrence rate events, were generated. In this model, the loss due to traffic delay was found to be higher than the cost of repairing damaged bridges.

A similar paper [32] showed that for a single deterministic earthquake scenario of a magnitude M7.0, liquefaction accounts for the most substantial damage to the transportation network. In their study, the authors found that for their variable traffic demand case, they observe lower travel time delay. This is opposite to other works discussed previously in which most observed more travel time with variable traffic demand.

The works in [46] and [47] discussed the estimation of the direct and indirect losses to bridges in the St. Louis Metropolitan Area, respectively. Three deterministic earthquake magnitudes in different locations, including areas with liquefaction vulnerability, were considered in the former case. However, in the indirect loss estimation scenario, only one magnitude earthquake was considered. For the worst-case scenario in the direct loss estimation case, the associated indirect cost was found to be more than half of the cost of the direst losses, clearly indicating the importance of evaluating this form of loss.

Finally, the authors in [48] illustrated a seismic risk assessment of both industrial plants and tunnels and bridges of the Friuli–Venezia Giulia highway network in Italy. In their study, unlike other papers where they evaluate the losses in dollar figures, the authors relied on a simple probability estimate percentage for a 50-year return period ground motion. The methodologies used in estimating the losses were derived from the fragility curves developed for U.S bridges.

2.6 Hazus International Adaptations, Seismic Risk Assessment Tools

Hazus software was initially intended only for risk assessment of different hazards in the U.S regions. However, with further developments, transitioning to a more versatile data management scheme, and the introduction of Hazus specific open-source tools, it is now easier to implement Hazus in different regions around the world [49]. At the current stage, the adaptation of the international regions to Hazus requires extensive data collection, in addition to conforming to the original data format. This can prove to be difficult for those regions that do not follow exact Hazus definitions of administrative boundaries, hazard-specific fragility classifications, and much more. Therefore, for the complete adaptation, lots of effort and time are needed to achieve the level of precision that exists in the current inventory of Hazus for the regions in the U.S.

An example of one use-case of Hazus software in regions other than the U.S. was discussed in [50]. The authors investigated the sensitivity of the Canadian version of Hazus for flood risk assessment. They applied three different models for the City of Fredericton in the New Brunswick Province. They concluded that many uncertainties in their models could be reduced by acquiring additional data in addition to selecting and modifying the input parameters specific to the study area.

Another example was presented in [51]. The authors in their paper studied the risk assessment of hospitals in the city of Yazd in Iran. They evaluated the potential seismic risk and losses of hospital buildings. They prepared fragility curves for each hospital to enrich the

Hazus inventory and perform their analysis for both hospital and its main components such as the water and fuel tank, power, and gas station.

Other than Hazus, different risk assessment tools are continually being developed all around the world. It should be noted that almost all the newly developed tools inherent some of the methodologies described by Hazus. AFAD-RED is Turkey's first national operational tool for the prevention, preparedness, and response of seismic hazards. The open-source OpenQuake project as part of the Global Earthquake Model (GEM)[2] initiated a worldwide collaborative effort to bring the state-of-the-art science behind seismic risk assessment tools developed by different organizations and individual researchers to a common, uniform, and open standard way of communicating earthquake risks [52]. The OpenQuake engine is now the primary tool used by the new risk analysis platforms and large-scale real case implementations such as the Euro-Mediterranean Seismic Hazard Model (ESHM13) European Union project [54]. CAPRA is a probabilistic risk assessment system. The modules available in the CARPA platform are capable of both hazard and climate change risk analysis. Initially developed for Colombia, the tool is now widely used in South America and a handful of European countries. SELENA is a tool developed by the Norwegian seismic array (NORSAR) in Kjeller for Norway. Ergo is another open-source seismic risk assessment platform and application developed by the National Center for Supercomputing Applications at the University of Illinois at Urbana-Champaign. This tool is based on the core functionalities of the old MAEViz platform.

A complete list of new and old tools used for seismic hazard and risk assessment is provided in [53]. In the end, no matter what seismic risk tool is used, for achieving a reasonable estimate of the losses incurred due to natural hazards, region-specific parameters, and updated inventory of regions are required. Therefore, the effort should be put on creating real-time platforms capable of instantaneous monitoring and updating of the necessary inventories and parameters needed for risk assessment.

2.7 Chapter Summary

In this chapter, we collectively overviewed the components that constitute this thesis. We discussed the concept behind SHM and ITS and their joint integration for seismic risk assessment. Finally, we presented some of the seismic risk assessment tools used globally—most of the methodologies behind the current tools inherent the core functionalities of Hazus and Hazus earthquake risk assessment methodology. The concepts defined in this chapter

[2] http://www.globalquakemodel.org/

paves the way for future implementation of our goal, i.e., to incorporate SHM in assessing bridges using mobile sensing platforms. Following the framework and the integration of the transportation network by employing ITS, we expect to develop a general-purpose decision-making support system.

CHAPTER 3

SEISMIC HAZARD ANALYSIS OF NORTHERN CYPRUS

3.1 Introduction

One of the most significant forms of earthquake impacts is the disconnection of a transportation network due to bridge failure. Any failures would impede post-earthquake rescue operations or could create bottlenecks in the network, creating long queues and a decrease in the performance. Therefore, analyzing the risk associated with bridges is of utmost importance. Thus, seismic hazard analysis can be performed to quantify hazards in terms of useful information that can be used to assess the risk associated with bridges and to make a better risk-informed decision. Many earthquakes with a variety of magnitudes and depths can occur in a given location, though it is impractical to assess each earthquake individually. It is also possible that with the current tectonic movements, some regions would never experience large and devastating earthquakes, such as the case of Northern Cyprus. However, the uncertainties in tectonic models, as well as faults' characteristics, can lead to significant events; therefore, it is essential to consider rare scenarios as well. In line with this notion, this chapter discusses and demonstrates the seismicity of Northern Cyprus, in addition to creating deterministic hazard maps via ShakeMap scenarios with different event magnitudes. These maps are then imported to Hazus ground motion hazard analysis as one measure of seismic risk assessment of the bridge transportation network.

3.2 Seismicity of Cyprus

Just like any other part of the Mediterranean region, there have been historical records of devasting earthquakes in Cyprus dating back as far as 1500 B.C. [54]. It was until recently, in 1997, where Southern Cyprus started modern instrumentation of seismometers around the

Figure 3.1. The distribution of 13 seismometers in Cyprus

region (Cyprus Broadband Seismological Network) [55]. Following the work, the Northern Cyprus seismography operation started in 2007 [56]. In total, there are 13 seismometers (5 in the northern part) with different sampling rates ranging from 50 Hz to 100 Hz at different orientations operating 24 hrs. Figure 3.1 shows the distribution of these seismometers in Cyprus.

There have been several attempts in identifying the fault lines as well as the seismic sources of Cyprus with varying degrees of details. The two recent studies, namely the work by Cagnan and Tanircan [54] in 2010 and the 2013 Euro-Mediterranean Seismic Hazard Model (ESHM13) European Union project [57] attempted to model the seismic hazard of Cyprus. The basis of the two projects was based on the tectonic map of the region, which was developed by the United States Geological Survey (USGS) [58] in 2000 after the work by Barka and Reilinger [59], as shown in Figure 3.2. Looking closely at the Cyprus region, the inferred shore faults of possible Quaternary age indicate potential hazards of the cities around the coastlines.

It should be noted that, however, not every fault can generate large earthquake magnitudes. Given that many earthquake epicenters are shallow, i.e., originating within 60 km of the Earth's other surface, this warns for taking necessary measures to ensure the safety of the region in terms of the possible earthquake hazards. The ESHM13 study resulted in identifying the faults capable of generating earthquakes with magnitude M5.5 or larger. For the case of Cyprus, it has been shown that the regional faults can generate magnitudes larger than M6.0. Figure 3.4 illustrates the faults with the maximum possible magnitude and the distribution of earthquakes from 1956 to 2020 collected from the USGS earthquake catalog. Take into account that these faults have been identified based on the homogeneous earthquakes aggregated from two sub-catalogs, 1000-1899 [60] and 1900-2006 [61].

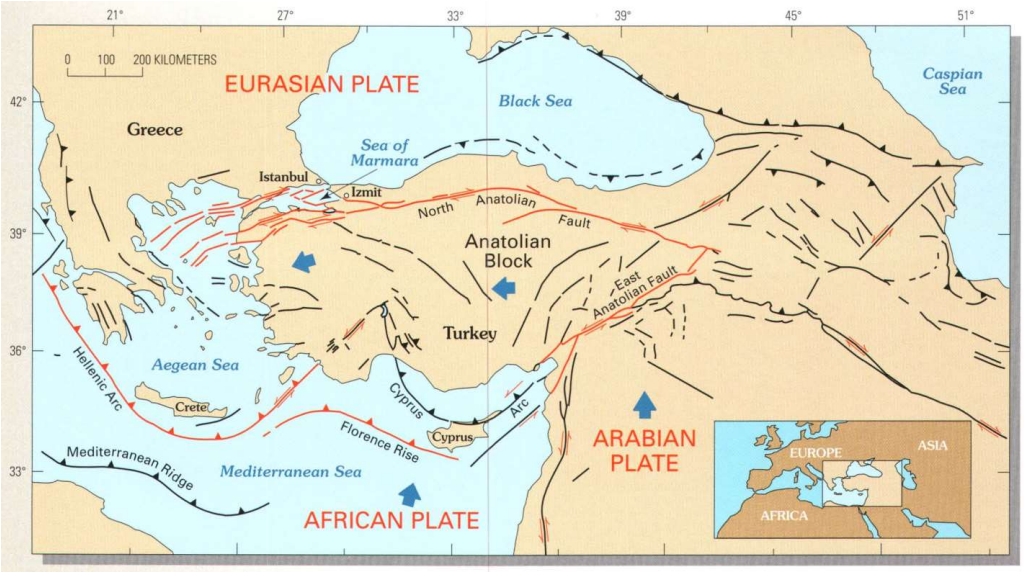

Figure 3.2. Tectonic Map of East-Mediterranean region developed by USGS in 2000 [58]

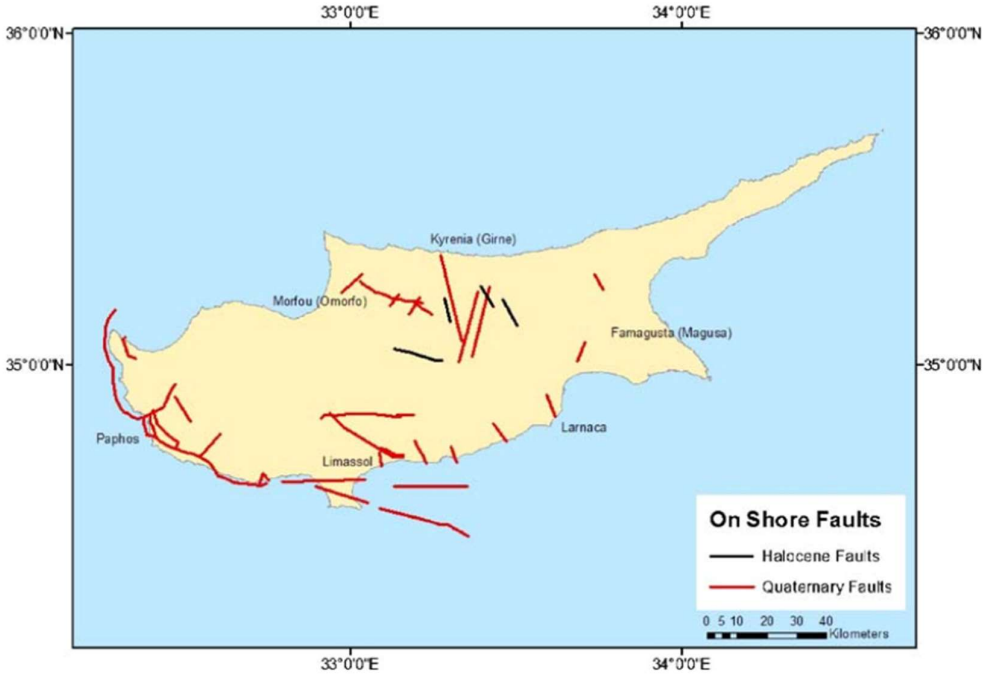

Figure 3.3. Inferred shore faults on Northern Cyprus of possible Quaternary age [54]

3.3 Probabilistic Seismic Hazard Analysis

The concept behind Probabilistic Seismic Hazard Analysis (PSHA) was first introduced by Cornell [62]. Assuming all scenarios of earthquake magnitudes, distances, and effects, PSHA is found to be superior to Deterministic Seismic Hazard Analysis (DSHA), where single and fixed magnitudes and distances are assumed. PSHA can be achieved in 5 steps as [63]:

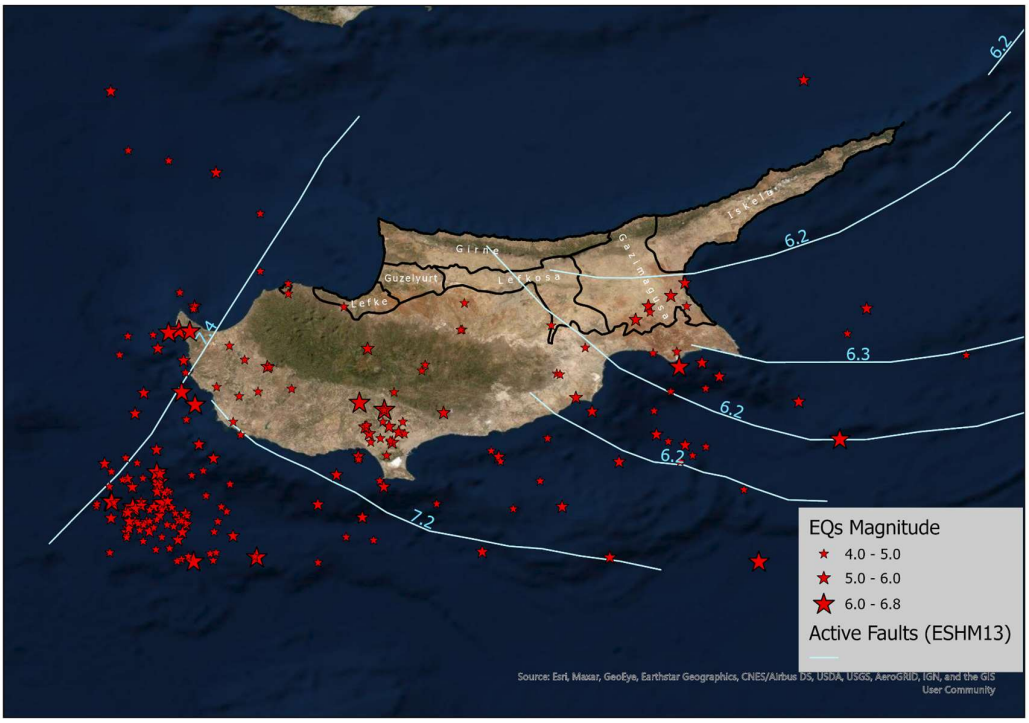

Figure 3.4. Active faults from ESHM13 with maximum possible magnitudes and earthquake distribution in Northern Cyprus since 1956

1. Identify earthquake sources
2. Characterize the distribution of earthquake magnitudes from each source
3. Characterize the distribution of source-to-site distances from each source
4. Predict the outcome of the ground motion intensity distribution, and
5. Combine the four steps above to compute the annual rate of exceeding a given ground motion intensity

In the following sections, we will present an example performing PSHA, which will be an introduction in creating shaking and intensity maps using ShakeMap DSHA software developed by USGS [64]. Since PSHA are out of the scope of this study, instead, we try to simulate the past PSHA studies for Cyprus using ShakeMap DSHA. Some essential aspects of the developing ShakeMap data are also provided in these sections. The PSHA steps below are adapted mainly from [63] with slight modifications related to the scope of our thesis.

3.3.1 Identifying Earthquake Sources

As described previously, in performing PSHA, we would need to acquire all earthquake magnitudes that are capable of causing significant damaging ground motions for a given location. Earthquakes occur from the movement of the boundaries of the tectonic plates. Each type of boundary is associated with a fault mechanism, namely, 1) normal faulting (divergent

boundary), 2) reverse faulting (convergent boundary), and 3) strike-slip faulting (transform boundary). Identifying these planar surfaces is usually done by observing past earthquakes or geological evidence. Earthquake catalogs in determining earthquake sources are a vital part of PSHA. They can include events ranging anywhere from the last 100 decades or as far as 2150 BC. Depending on the decision and the form of analysis, different earthquake catalogs from various sources can be used. As discussed previously, ESHM13 included all events (excluding the foreshocks and aftershocks) between 1000 and 2006. In a recent study [65], a new catalog of Eastern Mediterranean earthquakes as part of the project titled "Seismic Hazard Assessment for Cyprus and Neighboring Regions" was developed. The authors identified a total of 2581 events, including only the mainshocks. Once an inventory of possible earthquakes is created, then the distribution of magnitudes and source-to-site distances of these earthquake sources can be identified.

3.3.2 Identifying Earthquake Magnitudes

Various magnitudes of earthquakes can occur along a given fault. In order to determine the seismicity rate, i.e., the possible number of earthquakes that could occur that are greater than a given magnitude; the distribution usually follows the model developed by Gutenberg & Richter [66] as:

$$\log_{10} \lambda_m = a - bm \tag{3.1}$$

where λ_m is the rate of earthquakes for a specific location per year with magnitudes that are greater than m, and a and b are regression coefficients. These constant parameters are estimated from the statistical analysis of past observations. Here a indicates the overall rate of earthquakes in a region, whereas b indicates the relative ratio of the small and large magnitudes, generally taken as 1 for seismically active regions.

To compute the cumulative distribution function (CDF) as well as the probability density function (PDF) for earthquake magnitudes larger than a given minimum magnitude m_{min} and less than a theoretical maximum magnitude of a given fault m_{max} the following equations can be used [63]:

$$F_M(m) = \frac{1 - 10^{-b(m-m_{min})}}{1 - 10^{-b(m_{max}-m_{min})}} \tag{3.2}$$

$$f_M(m) = \frac{d}{dm} F_M(m) = \frac{b \ln (10)(10^{-b(m-m_{\min})}}{1 - 10^{-b(m_{max}-m_{min})}} \tag{3.3}$$

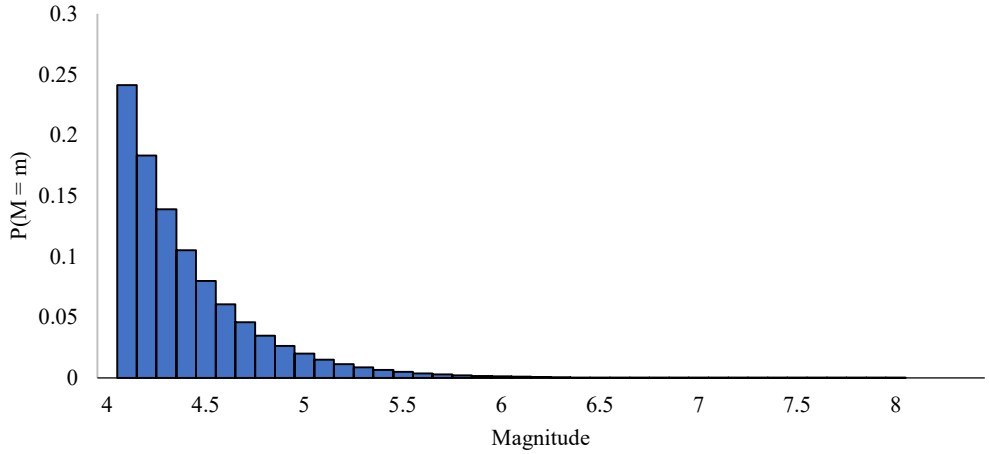

Figure 3.5. The discrete probability distribution for a minimum magnitude of M4.0 and a maximum magnitude of M7.4

where $F_M(m)$ and $f_M(m)$ denote the CDF and PDF of M, respectively. For later equations, the above CDF equation is discretized so that the probability of an ordered set of magnitude m_j is given as:

$$P(M = m_j) = F_M(m_{j+1}) - F_M(m_j) \tag{3.4}$$

Figure 3.5 illustrates discrete probability distribution for a minimum magnitude of 4 and a maximum magnitude of 7.4 (see Figure 3.4 for maximum fault magnitude) with parameter b set equal to 1.2, suggested by [54] for the selected fault zone.

3.3.3 Identifying Earthquake Distances

Given an earthquake source, it is generally accepted that future earthquakes would have an equal probability of occurrence along the fault. It is, therefore, essential to identify the distribution of source-to-site distances. It is also possible to assume a non-uniform distribution of distances, as some of the ground motion prediction equations rely on such an assumption for greater accuracy, as will be discussed in the next section. However, for the sake of simplicity of the current example, we demonstrate two possible models of source-to-site distance distributions.

3.3.3.1 Area Source

In specific locations, when faults are not responsible for the generation of earthquakes – they are instead caused by tectonic subsidence with loading mechanism, area sources are often used to determine the probability of future earthquakes distances. Assume a circular source area with a maximum radius of R, given equal likelihood probability, we can say that:

$$F_R(r) = P(R \leq r) = \frac{\text{circle with Area } r}{\text{circle with Area } R} \tag{3.5}$$

$$F_R(r) = \begin{cases} 0 & \text{if } r < 0 \\ \left(\frac{r}{R}\right)^2 & \text{if } 0 \leq r < R \\ 1 & \text{if } r \geq R \end{cases} \tag{3.6}$$

where $F_R(r)$ is the CDF for R, i.e., the distance from a site to the source (epicenter).

3.3.3.2 Line Source

When faults can be identified on the boundary of two tectonic plates, the line source model can be employed. Assume, a fault with a total length of D and a site location that is S distance from the fault's center $\frac{D}{2}$, again given equal likelihood probability, we can say that:

$$F_R(r) = P(R \leq r) = \frac{\text{length of fault within distance } r}{\text{total length of fault}} \tag{3.7}$$

For a distance r from the site to the epicenter and using the Pythagorean theorem, the CDF of R is given as:

$$F_R(r) = \begin{cases} 0 & \text{if } r < S \\ \frac{2\sqrt{r^2 - S^2}}{D} & \text{if } S \leq r < D/2 \\ 1 & \text{if } r \geq D/2 \end{cases} \tag{3.8}$$

Assuming R, D as 100 km, and S as 10 km, the CDF of the two models are plotted in Figure 3.6. The PDF of R for both models can be found by taking the derivative of the CDF.

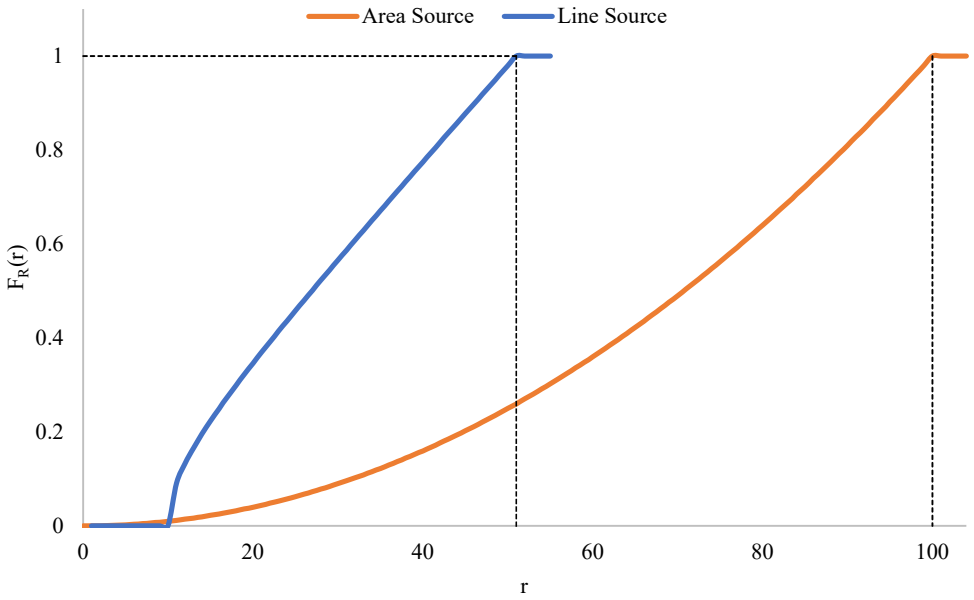

Figure 3.6. An Illustration of two different source-to-site distance modeling

As described before, the choice of a ground motion prediction model can influence the PSHA greatly. Nowadays, most models are adopting a form of Joyner-Boore Distance R_{JB} [67], [68], which is defined as the shortest distance from a seismic station or any other site to the surface projection of the rupture surface of the seismic event given as:

$$R = \sqrt{R_{JB}^2 + h^2} \tag{3.9}$$

where h is a coefficient that depends on the choice of the ground motion prediction model.

3.3.4 Ground Motion Prediction Model

For seismic analysis, we are interested in ground motion intensity measures (IM) such as Peak Ground Acceleration (PGA) or Spectral Acceleration (SA) at different periods. We can use Ground Motion Prediction Equations (GMPEs) developed globally or individually for a region to predict the level of ground shaking. As more information about a region is gathered, more and more complex GMPEs are developed that take other parameters and coefficients such as [63]: near-surface site conditions, fault mechanism, and may more in addition to the magnitude and distance. Such GMPEs are developed using statistical regression from the recorded ground motions intensities in the past. The general form of a GMPE is given as [63]:

$$\ln IM = \overline{\ln IM}\,(M, R, \theta) + \sigma(M, R, \theta) \cdot \epsilon \tag{3.10}$$

where $\overline{\ln IM}\,(M, R, \theta)$ and $\sigma(M, R, \theta)$ represent the mean and the standard deviation of the output of the ground motion prediction model, respectively, based on the given magnitude (M), distance (R), and other parameters (θ). And ϵ refer to the standard normal random variable of the variabilities in $\ln IM$. Over the past 60 years, there have been several GMPEs developed for different regions around the world. A complete and very recent summary of the GMPEs from 1964 until 2019 is provided in [69]. For the sake of demonstration, we will show one of the oldest predictive models of ground motions developed by Cornell et al. [70] and use this to show how GMPE works. The model predicts the natural log of mean PGA $\overline{\ln PGA}$ in units of g with a standard deviation of 0.57 as:

$$\overline{\ln PGA} = -0.152 + 0.859M - 1.803\ln\,(R + 25) \tag{3.11}$$

An example of the predictive model above is illustrated in Figure 3.7. It should be noted that, for this study, however, we decided to use three different GMPEs (MultiGMPE) developed by Boore and Atkinson in 2008 [71], Campbell and Bozorgnia in 2014 [72], and finally, Akkar and Bommer in 2010 [73] when creating ShakeMap data. To account for the use of multiple GMPEs, we incorporated weights for each GMPE such that Boore and Atkinson [71], Campbell and Bozorgnia [72], and Akkar and Bommer [73] were each assigned

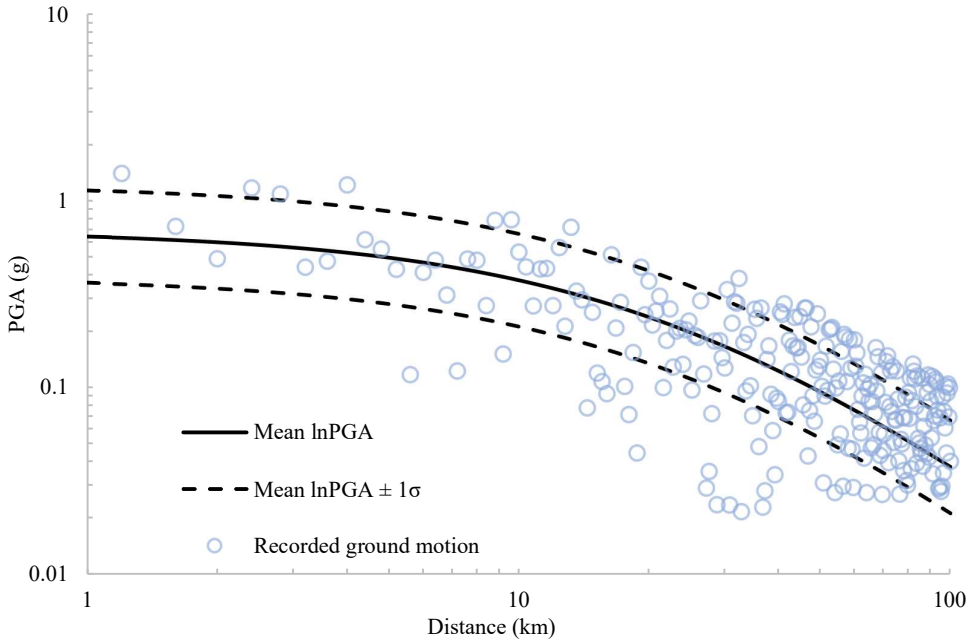

Figure 3.7. An example of GMPE developed by Cornell et al. [63]

with the weights of 0.4, 0.4 and 0.2, respectively. The two reasons for the selection of the above weights and GMPES are that first, these models are developed for shallow earthquakes, as in the case of our region and second, weights are distributed based on more recent and up-to-date regional data, as suggested by [36].

Following the Cornell et al. [70] model, for a normally distributed set of PGA, probability of exceedance can be computed as:

$$P(PGA > x|m,r) = 1 - \Phi\left(\frac{\ln x - \overline{\ln PGA}}{\sigma_{\ln PGA}}\right) \tag{3.12}$$

Where Φ is the standard normal cumulative distribution function. Using the same discretization approach used in identifying continues earthquake magnitudes; we can find the probability of each PGA value as:

$$P(PGA = x_j) = P(PGA > x_j) - P(PGA > x_{j+1}) \tag{3.13}$$

3.3.5 Combining All Information and a Case Study Example

Now that we know the necessary information for deriving PSHA equations, we can use the total probability theorem to combine the previously defined probabilities, i.e., PDFs or CDFs. For a set of magnitudes and distances of earthquakes, we therefore have:

$$P(IM > x) = \int_{m_{min}}^{m_{max}} \int_{0}^{r_{max}} P(IM > x|m,r) f_M(m) f_R(r)\ dr\ dm \tag{3.14}$$

where $P(IM > x|m,r)$ is the output of the ground motion prediction model for a given IM, $f_M(m)$ and $f_R(r)$ are the PDFs of the magnitude and distance for each earthquake, respectively. Aside from the probability of exceedance defined above, we are also interested in the temporal distribution of earthquake recurrence for a certain IM. Such a distribution is typically defined according to the Poisson Model as:

$$P(N = n) = \frac{(\lambda \cdot t)^n\ e^{-\lambda \cdot t}}{n!} \tag{3.15}$$

where λ is the annual rate of occurrence of earthquakes that is reciprocal of a given a Return Period $T_R = 1/\lambda$ and t is the time interval of interest. The probability of exceedance of at least one earthquake in a period of t can be calculated as:

$$P(N \geq 1) = 1 - P(N = 0) = 1 - e^{\lambda \cdot t} \tag{3.16}$$

where λ here can be further defined as the occurrence rate for any IM such as magnitude, distance, PGA, etc.

Generally, when creating hazard maps, we refer to the estimate of the probability of exceeding a certain amount of ground shaking in a given time, say 50 years. Therefore, for specific exceedance probabilities, we can modify the equation above to:

$$\lambda = -\frac{\ln\ (1 - P)}{t} \tag{3.17}$$

where P denotes an event with an $P\%$ exceedance probability. For example, a 10% probability of exceedance in 50 years would result in $\lambda = -\ln(1 - 0.1)\ /50 = 0.00021/\text{year}$ with a corresponding return period of $T_R = 1/\lambda = 475\ \text{years}$. We can incorporate this uncertainty in equation (3.14) such that:

$$\lambda(IM > x) = \lambda_{m_{min}} \int_{m_{min}}^{m_{max}} \int_{0}^{r_{max}} P(IM > x|m,r) f_M(m) f_R(r)\ dr\ dm \tag{3.18}$$

where $\lambda_{m_{min}}$ is the rate of occurrence of earthquakes greater than m_{min} or simply written as $\lambda(M > m_{min})$. To simplify the above equation for multiple sources, we can discretize the distribution into discrete summations as:

$$\lambda(IM > x) = \sum_{i=1}^{n_{sources}} \lambda(M_i > m_{min}) \sum_{j=1}^{n_M} \sum_{k=1}^{n_R} P(IM > x|m,r) P(M_i = m_j) P(R_i = r_k) \tag{3.19}$$

Table 3.1. Five exceedance probabilities in a 50-year period

Exceedance Probability, P	Annual Rate (year $^{-1}$)	Return Period (year)
0.02	0.000404	2475
0.05	0.001026	975
0.1	0.002107	475
0.3	0.007133	140
0.5	0.013863	72

To illustrate a PSHA example, assume a minimum magnitude of M4.0 and a maximum magnitude of M7.4 with b value of 1.2 (the same example we did when creating Figure 3.5). We use Equation (3.4) to find the distribution of magnitudes. Also, we assume a fixed 10 km distance between the source with varying M and R values. We demonstrate PHSA in terms of five exceedance probabilities P in a $t = 50$-year period. These values are shown in Table 3.1. A 50-year period is typically used as it usually represents the service life of buildings. The results are depicted in Figure 3.8.

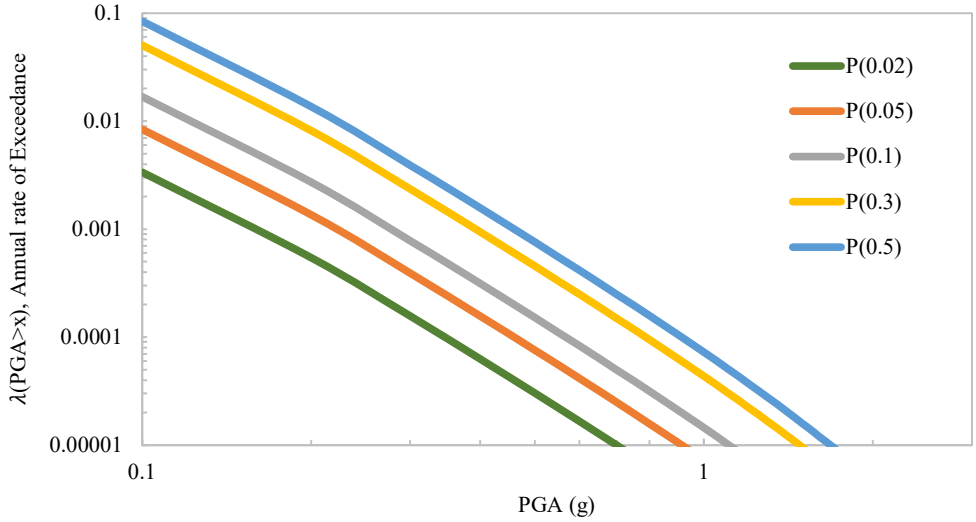

Figure 3.8. A demonstration of PGA distribution of PHSA for five different exceedance probability

In this section, we showed a very simple use-case of PSHA. Incorporating other parameters into the analysis can be time-consuming and require extensive research and understating of the local conditions of the region. As pointed out before, two research studies have already analyzed the seismic hazard associated with Cyprus. Both studies have concluded that Northern Cyprus would experience PGA values between 0.2 g and 0.3 g. The result of the study for 10% PGA probability of exceedance in 50 years by Cagnan and Tanircan [54] and ESHM13 [57] are shown in Figure 3.9 and Figure 3.10, respectively. Although the PGA values of Northern Cyprus are relatively low, however, we can still create different scenarios based

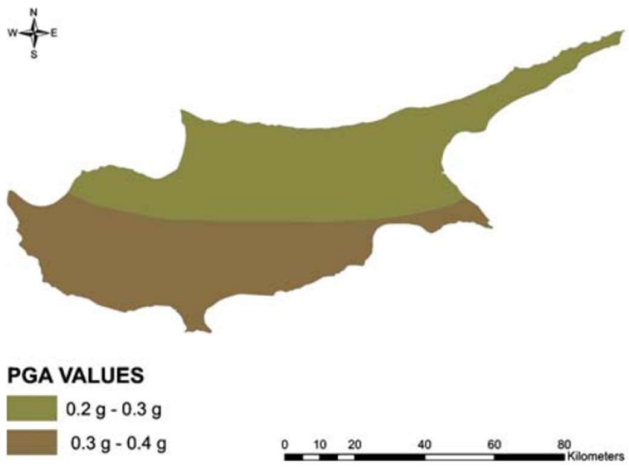

Figure 3.9. Cyprus PGA distribution with 10% probability of exceedance in 50 years for rock conditions [54]

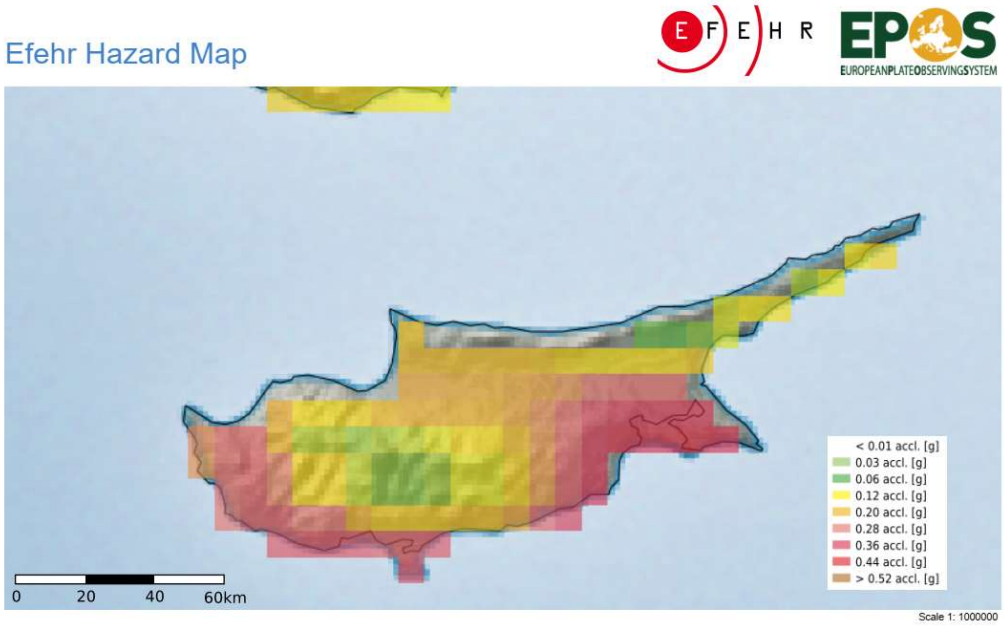

Figure 3.10. Cyprus PGA distribution according to ESHM13 probabilistic seismic hazard assessment for 10% probability of exceedance in 50 years [57]

on different earthquake magnitudes and distances. As PSHA contains many assumptions with degrees of uncertainty, we can leverage this fact and determine the worst-case scenario (higher return periods) when performing seismic hazard assessment of the bridge transportation network.

3.4 Generating ShakeMap Data for Hazus

As part of our analysis in Hazus, we can create different scenarios based on different magnitudes, depths, and different GMPEs. To achieve this, we create ShakeMap scenario data

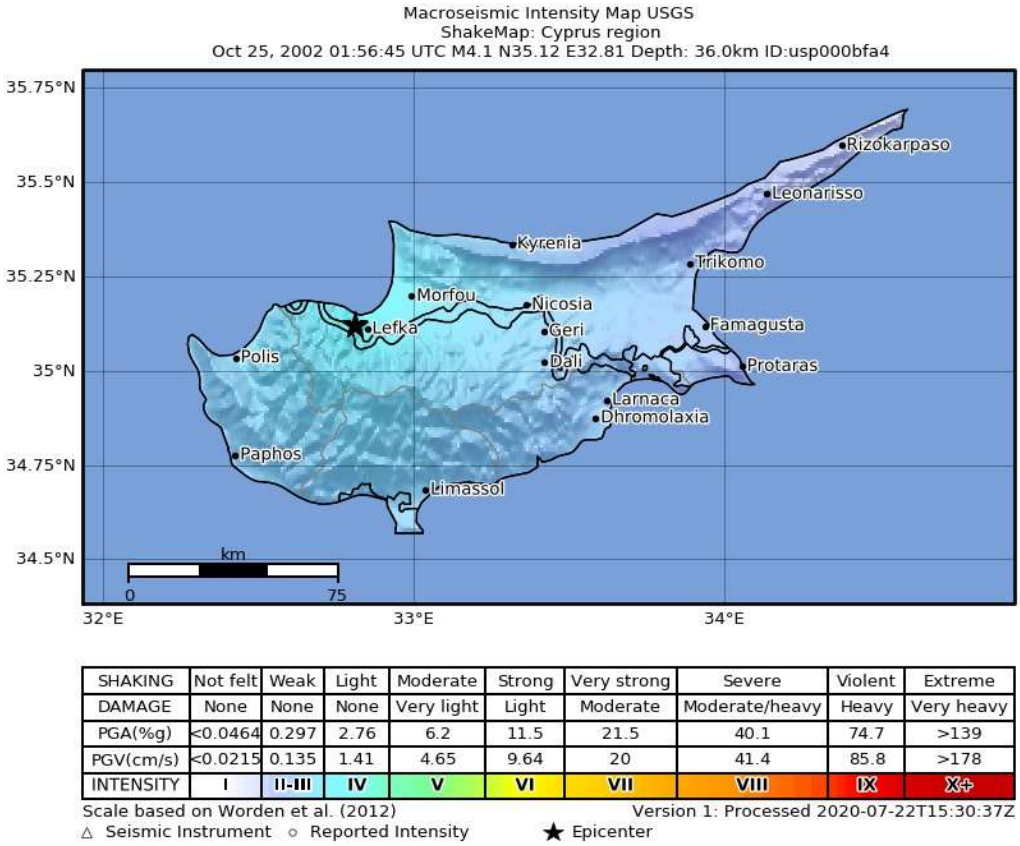

Figure 3.11. ShakeMap representation of an M4.1 Earthquake event

for our region. ShakeMap software is developed by USGS written in Python programming language. With the geological information, ShakeMap can automatically generate shaking and intensity maps in real-time when an earthquake occurs. It is one of the emergency tools used by many agencies in the U.S. for rapid loss estimation. ShakeMap is capable of producing PGA, Peak Ground Velocity (PGV), and SA at 0.3, 1.0 and, 3.0 s. These are precisely the default IM requirements of the Hazus loss estimation methodology. This enormously eases the task of analyzing different earthquake scenarios in Hazus. We use the command line interface described in the ShakeMap Manual [74] for the creation of the maps. To demonstrate ShakeMap, we will generate the ground motion prediction model of an earthquake that occurred on October 25, 2002, near the European University of Lefke, which occurred at 35.121°N, 32.809°E with a moment magnitude M4.1 at 36.0 km depth as shown in Figure 3.11.

Assuming the MultiGMPE criteria and with the given weights as already discussed in 3.3.4, we can generate the PGA of the earthquake. The result is shown in Figure 3.12. According to the contour maps, we can observe a maximum of 2%g PGA in the vicinity of the epicenter. Such small magnitude (light) earthquakes can cause no or minor damages to the infrastructure

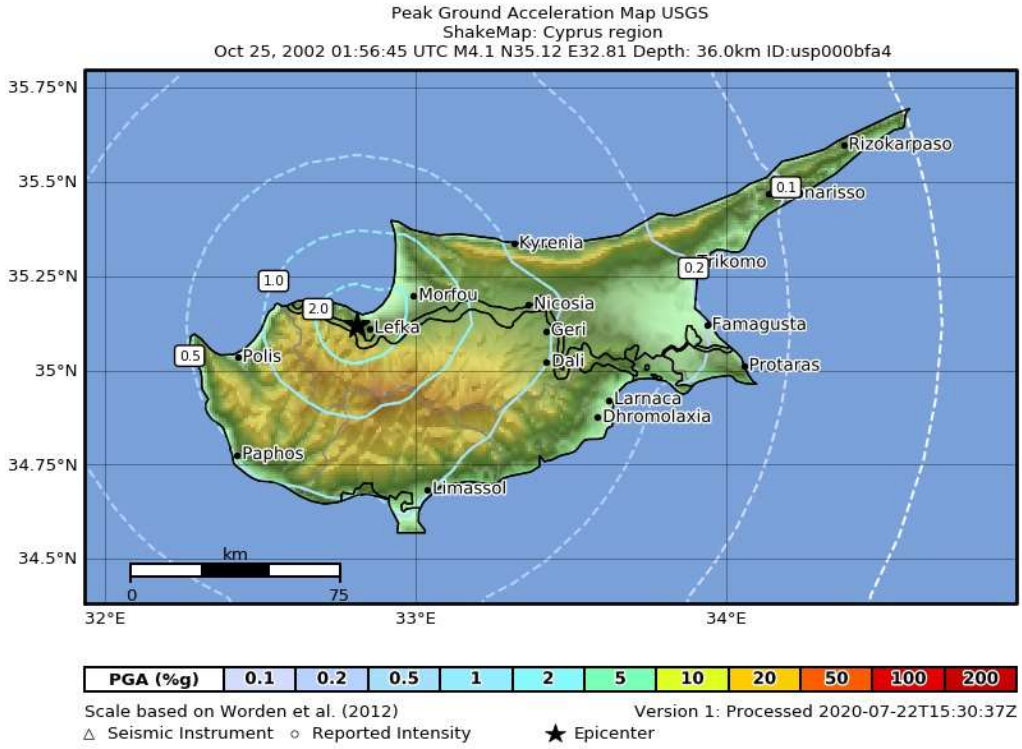

Figure 3.12. PGA map generated from ShakeMap for an M4.1 Earthquake event

system. The site condition of the majority of Northern Cyprus shows high shear wave velocity (see Table 5.5), and the higher the velocity, the less the ground shaking amplification. Hence for observing damage, earthquake magnitudes of M5.0 or above are required. For the current active fault lines of Cyprus, we can expect magnitudes of up to 7.4 for the Western part of Northern Cyprus at depths less than or equal to 70 km. Therefore, as one of the scenarios, we can simulate the damage of the same earthquake except with a higher magnitude.

It should be noted that the direction taken in generation shaking distribution under scenario modeling is not as complex and it is more uniform compared with the real events shaking maps. In real shaking intensity distribution, 2D and 3D wave propagation, basin-edge effects, and other complex site effects are usually accounted for. Nevertheless, using this tool we can analyze different hazard levels for better preparedness and emergency response.

3.5 Seismic Risk Assessment Through Fragility Analysis of Bridges

In contrast to the seismic hazard analysis discussed previously, seismic risk assessment describes the potential for damages or losses that a region is prone to experience after a seismic event. They can also be defined as the integrated product of the seismic hazard, that determines

the value and fragility of assets [75]. This link between ground motion intensity and the structural damage is related by fragility function. They are also known as damage functions that are usually represented by conditional cumulative log-normal distribution functions, that are depicted as curves for a given level of damage. These curves are the key input for seismic risk assessment for evaluating the bridges and the corresponding loss of serviceability for a defined damage level. Depending on the form of fragility analysis, the conditional probability that a given structure exceeds the prescribed damage limit state (ds) is usually defined as:

$$P[ds_i|x = IM] = \Phi\left[\frac{1}{\beta_{ds}} ln\left(\frac{IM}{S_{median}}\right)\right] \tag{3.20}$$

where, IM represent the intensity measure, e.g., PGA, SA(T=1s); Φ is the standard log-normal cumulative distribution function; β_{ds} indicates the lognormal standard deviation of IM; and S_{median} denotes the median (or expected value) of the IM. Here the damage state ds can be varied depending on how Equation (3.20) is defined for a structure. As an example, according to Hazus methodology [76], bridge damage states can be summarized in Table 3.2.

Table 3.2. Definition of 5 bridge damages states according to Hazus [76]

Hazus Damage State	Definition
ds_1: None	
ds_2: Slight/Minor Damage	Minor cracking and spalling to the abutment, cracks in shear keys at abutments, minor spalling and cracks at hinges, minor spalling at the column (damage requires no more than cosmetic repair) or minor cracking to the deck
ds_3: Moderate Damage	Any column experiencing moderate (shear cracks) cracking and spalling (column structurally still sound), moderate movement of the abutment (<2"), extensive cracking and spalling of shear keys, any connection having cracked shear keys or bent bolts, keeper bar failure without unseating, rocker bearing failure or moderate settlement of the approach
ds_4: Extensive Damage	Any column degrading without collapse – shear failure - (column structurally unsafe), significant residual movement at connections, or major settlement approach, vertical offset of the abutment, differential settlement at connections, shear key failure at abutments.
ds_5: Complete Damage	Any column collapsing and connection losing all bearing support, which may lead to imminent deck collapse, tilting of substructure due to foundation failure

There are three different methods for developing fragility curves: heuristic, empirical, and analytical [77]. Heuristic methods rely on the engineering judgments on the structural response; empirical curves are based on past earthquake data, and the analytical approach takes into consideration the complete non-linear simulation of the structural response based on mathematical frameworks. Additionally, with a combination of one or two of the above methods, one can achieve hybrid fragility analysis as well.

By the definition of cumulative distribution, the following formula allows for identifying the damage state probability for each defined damage sate as:

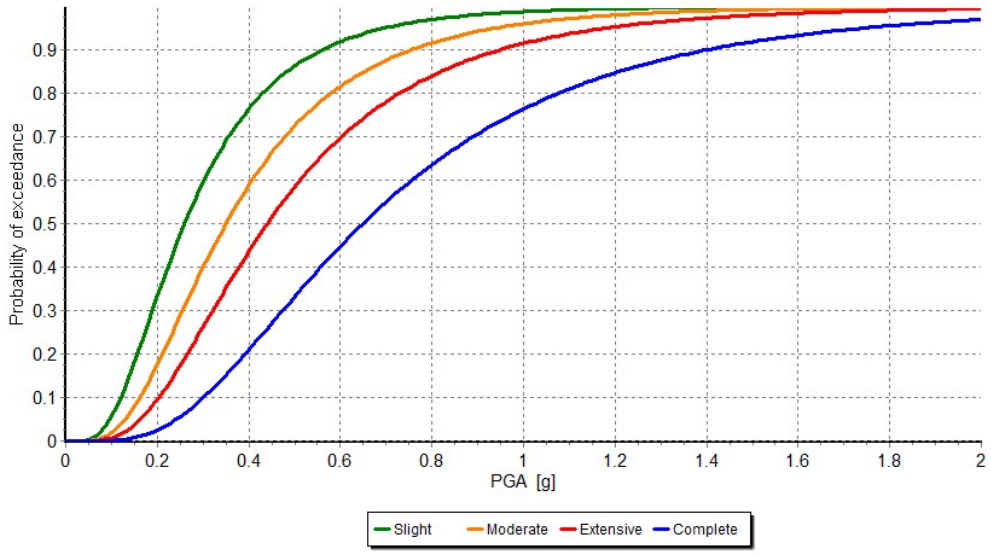

Figure 3.13. An example of a single span reinforced concrete bridge fragility curves, adapted from [78]

$$
\begin{aligned}
P[ds_1] &= 1 - P[ds_2] \\
P[ds_2] &= P[ds_2] - P[ds_3] \\
P[ds_3] &= P[ds_3] - P[ds_4] \\
P[ds_4] &= P[ds_4] - P[ds_5] \\
P[ds_5] &= P[ds_5]
\end{aligned} \tag{3.21}
$$

To illustrate the fragility curves concept, Figure 3.13 shows the analytically predicted fragility curves developed for single-span reinforced concrete bridges validated empirically from the earthquake damages to the bridges in the 1994 Northridge and 1989 Loma Prieta earthquakes [78]. For an intensity measure such as PGA, as shown in the figure, one can find the probability that provides the likelihood for a bridge that will meet or exceed a specified level of damage.

In Hazus, 28 primary bridge classifications are defined for the entire U.S. As a result, for four damage limits defined previously, 112 fragility curves are developed according to the study in [79]. These 'standard' curves have to be modified to reflect the characteristics of the bridge such as 2-dimensional piers' capacity to 3-dimensional arch action in the deck K_{3D}, shape factor K_{shape}, and finally skewness of the bridge K_{skew} through an scaling procedure defined in the Hazus manual. To demonstrate the how fragility curve analysis in Hazus is performed, we will show an example of one of the bridges of our study region.

Consider bridge KK000016 (see Table 5.7 on page 89 for description) shown in Figure 3.14. According to the Hazus classification, such a bridge would be considered as HWB5 (see Table 5.4 on page 84). We will use Earthquake Loss Estimation Routine (ELER)

Figure 3.14. Bridge KK000016 located at 35.217°N, 33.005°E

software developed under the Network of Research Infrastructures for European Seismology (NERIES) [80] to estimate ground motion parameters by assuming the following parameters:

- Point source (M6.5 at depth 36.0 km located at 35.121°N, 32.809°E)
- Site correction, according to Borcherdt [81], requires shear wave velocity to 30 meters depth, V_{30}
    - V_{30} –grid from USGS ($V_{30} \cong 350\ m/s$)
- Boore and Atkinson GMPE [71]
- Instrumental Intensity Measure (IIM) from Wald et al. [82]
    - Default ShakeMap IIM

The damage assessment in Hazus for bridges are determined from SA at 0.3 and 1.0 sec period; therefore, we will create the SA contour maps for the specified earthquake event with the parameter above using ELER software. The results are shown in Figure 3.15 and Figure 3.16. We can deduce from the figures that for the specified bridge, we can observe SA of approximately 35.0% g and 21.0% g at 0.3 and 1.0 sec period, respectively.

Using the scaling procedure in Hazus, we can use the following set of equations to modify the median value $S_{SA(1.0\ \mathrm{sec})}$. Before the scaling procedure is applied, the ground motion data have to be amplified according to the factors in Table 4.9 of the Hazus manual. However, since ELER already takes into account the site condition, the amplification step is therefore skipped. Using the equation below, the skewness factor can be calculated as:

$$K_{skew} = \sqrt{sin(90 - \alpha_{skew})} = 1 \tag{3.22}$$

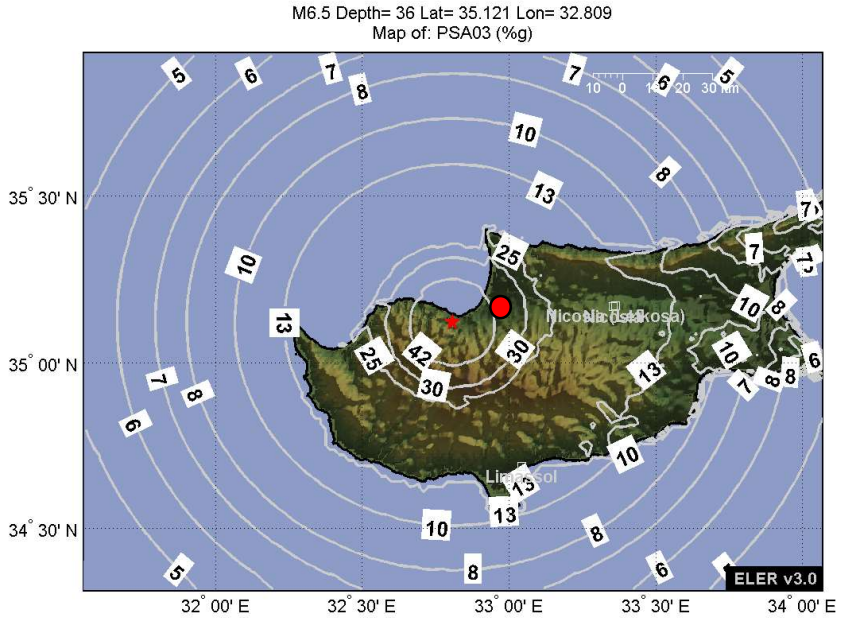

Figure 3.15. SA(0.3 sec) for M6.5 at 36.0 km generated from ELER software

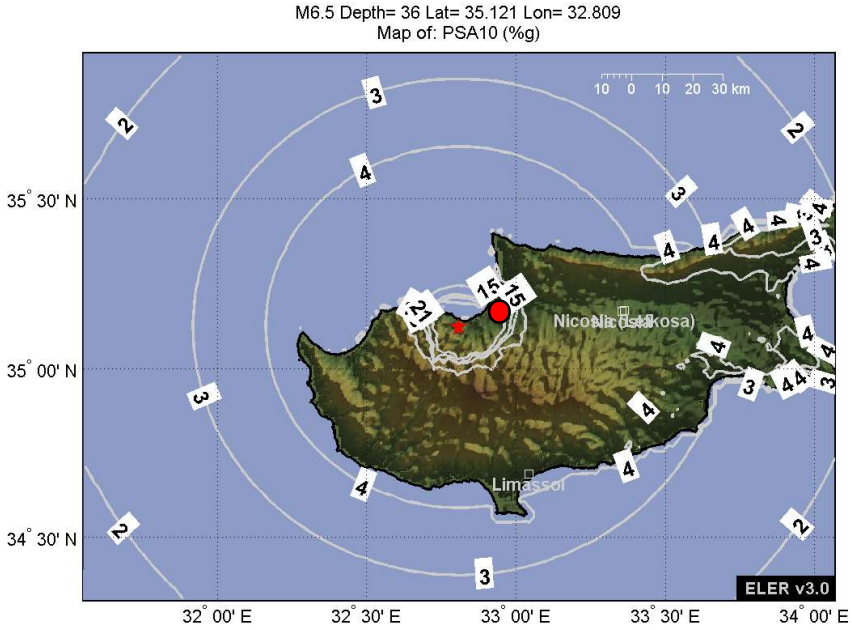

Figure 3.16. SA(1.0 sec) for M6.5 at 36.0 km generated from ELER software

where α_{skew} is the skew angle, i.e. the angle between a line normal to the centerline of the bridge and the centerline of the support. The bridge in question is not skewed; therefore, the skewness factor is 1. For the shape factor, we have:

$$K_{shape} = \frac{SA(1.0)}{SA(0.3)} \times 2.5 = \frac{0.21}{0.35} \times 2.5 = 1.5 \tag{3.23}$$

Furthermore, the 3D scaling factor depending on the bridge classification (see tables 7.2 and 7.3 of Hazus manual) can be calculated from:

$$K_{3D} = 1 + \frac{0.25}{n-1} = 1.25 \tag{3.24}$$

where n is the number of spans that is set equal to 2. The modification of the medians of the fragility curves can be determined as follows:

$$\text{New}[ds_2] = \text{Old}[ds_2] \times Factor_{Slight} \tag{3.25}$$

where $Factor_{Sligh}$ is 1 if I_{shape} (read from Table 7.2 of Hazus manual) is 0, otherwise $\min\,(1, K_{shape})$ if $I_{shape} = 1$. The HWB5 bridge class has an I_{shape} factor of 0.

$$\text{New}[ds_{3,4,5}] = \text{Old}[ds_{3,4,5}] \times K_{skew} \times K_{3D} \tag{3.26}$$

Using the standard fragility curves defined for HWB 5, we can apply modification factors to the median values, as shown in Table 3.3. The resulting fragility curves derived from Equation (3.20) with β_{ds} set to 0.6 as per the recommendation in [79] can be seen from Figure 3.17 resulting in exceedance probabilities for a $SA(1.0\ \text{sec})$ of about 21%g.

Table 3.3 Modification to the standard median fragility curves for bridge KK000016 (Hazus HWB5 class)

Hazus Damage State	Standard Values for $S_{SA(1.0\ sec\ in\ g)}$	Modified Values for $S_{SA(1.0\ sec\ in\ g)}$	Exceedance Probability for $S_{SA(1.0\ sec\ in\ g)}$	Discrete Damage State Probabilities from Equation (3.21)
ds_1	-	-	-	0.61
ds_2	0.25	0.25	0.39	0.28
ds_3	0.35	0.44	0.11	0.06
ds_4	0.45	0.56	0.05	0.04
ds_5	0.70	0.88	0.01	0.01

These discrete damage state probabilities are subjective and can vary depending on the methodology used. Since Hazus is used in this study, the definition of the damage in terms of the structural losses (cost) for an event m can be defined such that:

$$Direct\ Loss_m = \sum_{n=1}^{\#bridges} \overbrace{\sum_{k=1}^{\#DS} DR_k \underbrace{P[ds_{nm}]}_{\substack{proabilty\ of\ being\ in\ a\ specific\ damage\ state}}}^{compounded\ damage\ ratio\ (DR_C)} \times Repair\ Cost_{\,n} \tag{3.27}$$

where DR_k denotes the damage ratio in terms of the replacement cost. Hazus defines bounds for each damage state according to the severity of the damage, as shown in Table 3.4.

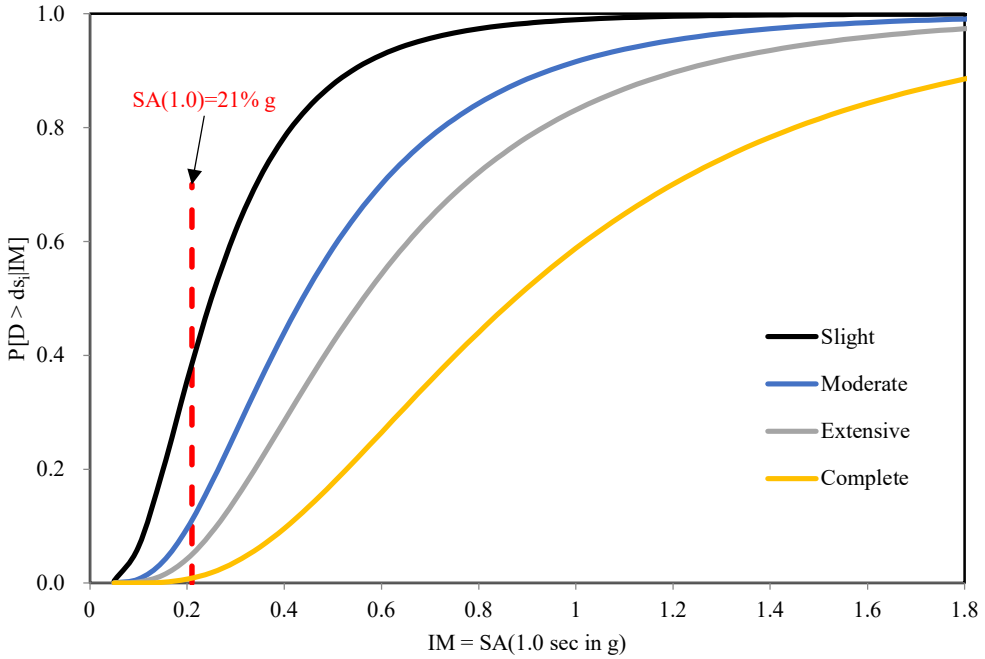

Figure 3.17. An example of fragility curves for an HWB5 reinforced concrete bridge class

Table 3.4. Variation of damage ratios defined by Hazus (slightly modified after Hazus)

Hazus Damage State	Best Estimate Damage Ratio (DR)	Range of Damage Ratios
None	0.00	0.00 to 0.01
Slight	0.03	0.01 to 0.03
Moderate	0.08	0.03 to 0.15
Extensive	0.25	0.15 to 0.40
Complete	1.0 if n<3 2/n if n≥3 n = number of spans	0.40 to 1.00

3.5.1 Fragility Analysis of the Bridges in Northern Cyprus

One of the future outcomes of this joint research study is to develop the analytical fragility curves of the bridges defined in our study region. This is done to increase the reliability of the loss calculation in Hazus as part of the general framework of the seismic risk assessment of the Northern Cyprus transportation network. The development of these curves under the umbrella of mobile SHM is as follows:

1. Data acquisition
2. Finite element modeling (FEM) and updating, and
3. Nonlinear time history analysis

The steps defined above each include a great deal of data collection and computational efforts to cover all the bridges. As such, for the current development of this thesis, the analytical fragility curves to be developed in the future will not be used in Hazus. However, to introduce the framework of our methodology, we will summarize the steps taken to achieve a calibrated and precise measure of the fragility curves for the current 20 identified bridges in the region.

3.5.1.1 Data Acquisition System

One of the most critical parts of SHM implementations is the data collection step. The efforts have been shifted toward the transition from the stationary sensors on the bridges to mobiles sensors such as smartphones or Unmanned Aerial Vehicle (UAV) [83]. The ideal direction for the current SHM studies is to achieve and integrate crowdsourcing platforms by using citizens' smartphones as a way to collect critical structural data such as acceleration from the embedded accelerometers. The proof of concept of this approach has already been carried out by our research team in the past [84]–[86]. The aim now is to extend this 'Citizen sensors for SHM' concept and bring it to the network level.

In accordance with the above explanation, to implement the SHM part of the study, we, therefore, use our smartphones, namely Samsung Galaxy S8 and LG G6 Plus, with a maximum of 500 Hz and 400 Hz sampling rates, respectively, to measure the acceleration response of the bridges. We used the Sensor Kinetics Pro Android application [87] to measure and transfer the acceleration data. A total of eight tests are performed for each bridge for precisely 22 minutes for verification purposes. The initial five tests require setting up on the phone exactly on the mid-span of the longest slab of the bridge. The 6^{th} test is such that one phone will be set at the quarter span length, and the other is kept in the mid-span. This is done to identify and catch the higher modes of the bridge, if applicable. To further verify the measurements of the modal analysis, the last two tests require to impose direct impact forces on the bridge. This is achieved by jumping on the mid-span at a constant interval. Finally, using MATLAB, the modal analysis using signal processing techniques such as Power Spectral Density (PSD), Fast Fourier Transformation (FFT), Short Time Fourier Transformation (STFT) and Time-Frequency Power Spectrum are carried out to identify the natural frequency of each bridge and to further verify it using the aforementioned techniques. Furthermore, for each 20 bridge, structural layout drawings (both 2D and 3D) using Tekla Structures software are developed to ease the creation of the FEMs in later stages. As an example, the 2D drawing of the steel bridge KK000005 (see Table 5.7 for details) is shown in Figure 3.18 (the figures are reproduced from the work of one of our research members who is currently working on the SHM aspect of the study titled "Finite Element Model Updating of Bridges with Mobile and Smart Technologies for Infrastructure-Related Decision-Making" [88])

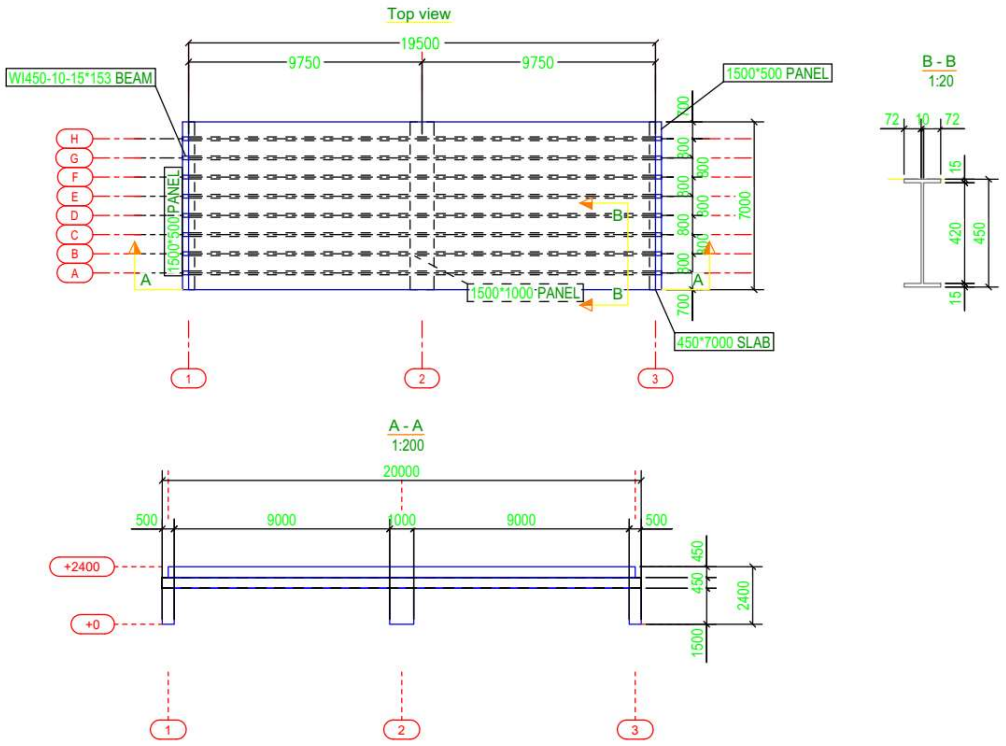

Figure 3.18. 2D structural drawing of bridge KK000005

3.5.1.2 FEM Updating

The Open System for Earthquake Engineering Simulation (OpenSees) software [89] is used to create the FEM for each bridge. The parametric analysis of bridges is interfaced with MATLAB in an iterative optimization process to achieve the desired modulus of elasticity and the moment of inertia. These two metrics indicate the changes in the structural properties of the selected bridge, respectively. In addition, moment-curvature analysis is carried out using SAP2000 software to find the characteristics of the plastic hinge to be used in the studied bridge. The plastic hinge is then set on the specified bridge and modeled in OpenSees, resulting in the determination of yielding moment. If the yielding moment is exceeded from the shaking induced from an earthquake event, the ductility demand factor would then be used to show the damage level in the bridge. Therefore, for the four damage states previously defined by Hazus, four different ductility demand factors will be assigned to identify the damages at each state [88].

3.5.1.3 OpenSees Nonlinear Time History Analysis

To develop the fragility curves, OpenSees is used again to carry out the nonlinear time history analysis from the historical severe earthquake records as well as the regional less severe events. In order to observe damages, especially from the small earthquake magnitude records, ground motion scaling procedure with the help SeismoArtif application is used. Lastly,

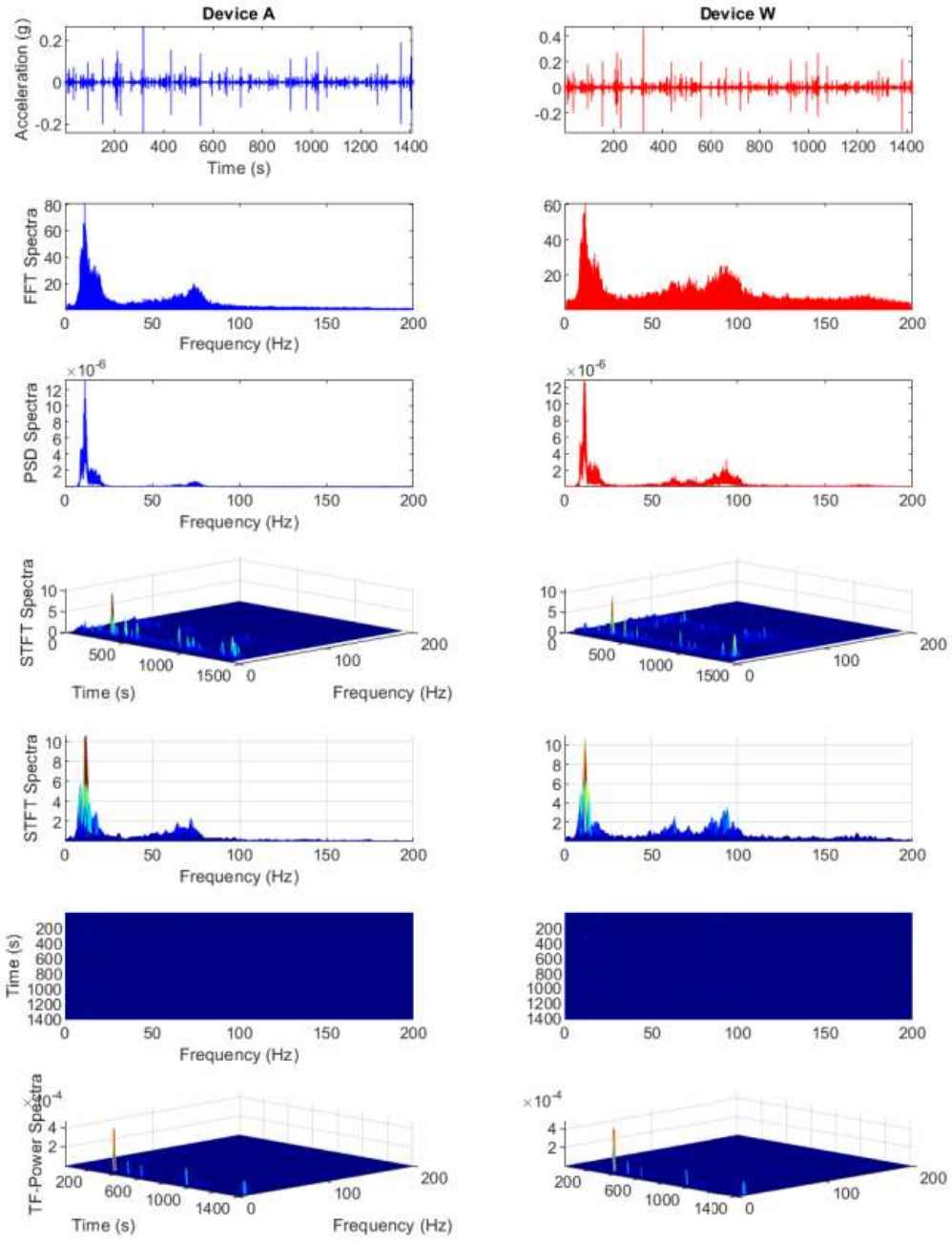

Figure 3.19. Bridge KK000005 ambient natural frequency result from test 1 procedure [88]

fragility curves are ideally developed to see at which earthquake event or intensity measure the bridge would result in damage.

To this time, the data collection and signal processing part of the SHM application have been completed. The FEM updating and OpenSees nonlinear analysis are currently underway. The results will be published in the thesis study by our research member [88] and will be integrated into this study in the future. To demonstrate the data collection and signal processing

part, an example of bridge KK000005 is shown in Figure 3.19. Looking at acceleration plots of devices A and W, both smartphones match in response. As a result, PSD, FFT, STFT, and Time-Frequency Power Spectrum show that the natural frequency of bridge KK000005 from test 1 is approximately 11 Hz (natural frequency is found from the first peak).

3.6 Chapter Summary

This chapter presented the seismic hazard analysis and the preliminary risk assessment of the Northern Cyprus transportation network. As one of the core aspects of this thesis, we explained the seismicity of Cyprus and identified the regions that are most prone to earthquakes. Additionally, a detailed overview of the probabilistic seismic hazard analysis of the region with comprehensive examples was presented. By doing so, we derived at the stage of developing deterministic seismic hazard maps using ShakeMap software developed by USGS. The data from ShakeMap is then transferred to Hazus to perform the risk assessment of the Northern Cyprus transportation network for scenarios defined in ShakeMap. Furthermore, as part of the overall objective of this research project, we introduce a novel method in determining the fragility curves of the bridges in Northern Cyprus using mobile SHM whose foundation is set for fragility assessment with calibrated bridge models. We precisely laid out the procedures that are currently undertaken to achieve a more precise loss estimation model in Hazus. A summary of the chapter is shown in Figure 3.20

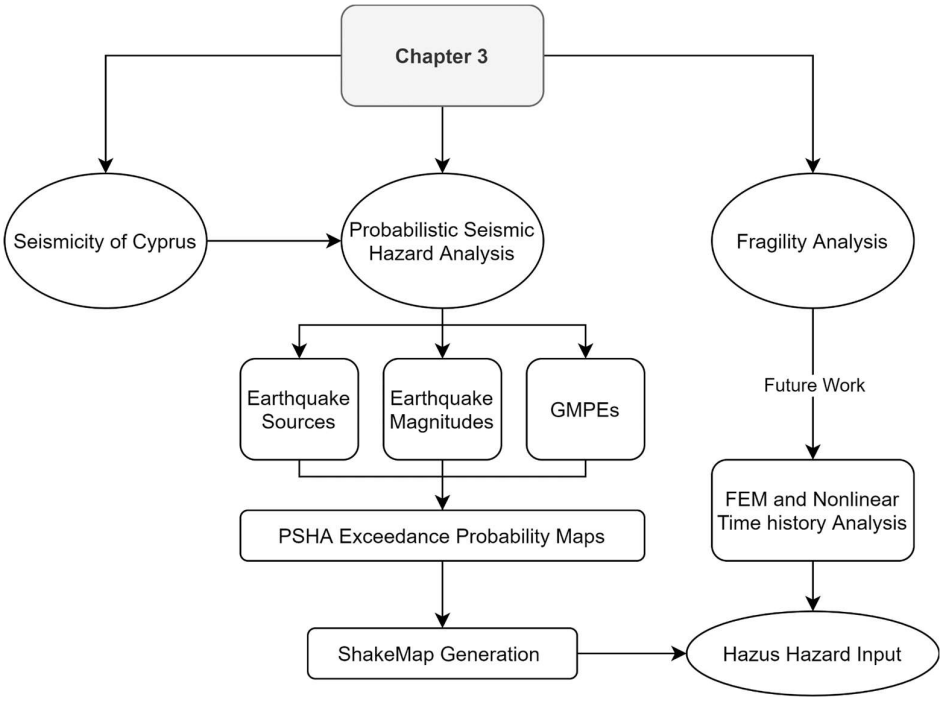

Figure 3.20. Chapter 3 summary chart

CHAPTER 4

THE TRANSPORTATION NETWORK OF NORTHERN CYPRUS

4.1 Introduction

Bridges are vital components and vulnerable elements in any transportation network [90]. Not only the failure of such high-risk critical components during an extreme event can lead to significant direct damage to the bridge, but it also affects the crucial lifelines connecting the epicenters to other locations. Such indirect damage to the road network can easily lead to congestion and long queues. The precautions taken in light of the modeled behavior, i.e. performance of the transportation network can help enormously reduce these indirect losses. Moreover, the consequences of such an event can sometimes be more prominent compared to the actual damage on bridges. Here, the serviceability of the road network becomes a metric that is needed to be carefully examined in three different categories, 1) travel time delay, 2) network flow capacity and overflow, and 3) the connectivity of the network. It is, therefore, important that the vulnerability of the road network is considered, reflecting the consequences in terms of the performance criteria mentioned above. In this chapter, we try to analyze the Northern Cyprus road network in terms of its topology, spatial distribution of its components, and the dynamic model of the traffic assignment.

4.2 Network Reliability and Vulnerability

Transportation networks are diverse and sparse. They are considered as interconnected systems where a failure on any link would result in cascaded degradation on the upstream and downstream parts of the network. Here, network connectivity and travel time reliability are the measures that network reliability studies usually consider to evaluate the performance of urban road networks [91]. Reliability, in general, is defined as the quality of service that a

system offers typically with regards to its degree of stability [92]. Considering rural areas, however, at the regional and national strategic level, reliability measure is often replaced by vulnerability analysis. As an example, consider enhancing the reliability of an urban road network by introducing effective measures to increase the capacity or by creating an alternative route to lessen the burden on a given link. However, considering these selective additions at a provincial level would not necessarily help to increase reliability. The vulnerability of the network becomes more important than the reliability in rural regions as any degradation, no matter how imminent a link failure is, would result in catastrophic impacts on the community. These two performance measures are related, but fundamentally, vulnerability analysis becomes an important subject in seismic performance assessment of transportation networks as reliability measures themselves can become vulnerable in severe events.

4.3 Topological Vulnerability Analysis Using Graph Theory

Network analysis, sometimes referred to as graph theory, plays an essential role in determining the efficiency of transportation networks [93]. Graph theory deals with understanding the properties of a set of linked vertices (nodes) V through edges (links) E. A graph $G = (V, E)$ is a simple structural representation of a 2D planar of a real network as illustrated in Figure 4.1. 'Graph' is undirected, i.e., movement in both ways are permitted (bidirectional), whereas a 'Digraph', is unidirectional. It is assumed, for the sake of simplicity in modeling the Northern Cyprus network, that the connections are bidirectional.

One of the first use of network modeling is measuring network properties [94]. Here we attempt to determine the structural measure – one of many network properties of Northern Cyprus. In our study region, the transportation network is consisting of 134 edges and 98 nodes with a total length of about $L = 124\ \mathrm{km}$. The network properties are defined for the abstract, i.e. graph version of the network. The Northern Cyprus Transportation network, in comparison to other research studies, is less complicated. The intention was to select the most critical nodes such that the network could be kept as simple as possible for future analysis without sacrificing the quality of the results. More in-depth analysis can be performed at the community level, but it is out of the scope of this study.

4.3.1 Structural Measures at Network Level

Measuring performance at the network level can enable the analysis of the network and to compare and show the evolution of the transportation network. The following sections provide additional measures alongside the basic description of the network in terms of its number of

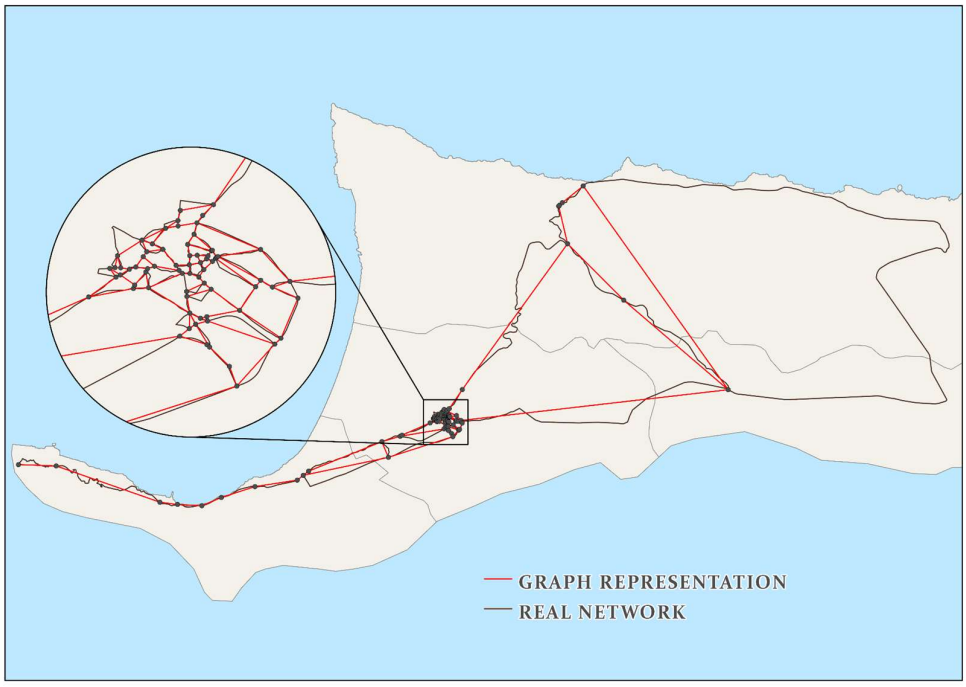

Figure 4.1. 2D graph representation of the study region's real transportation network

nodes, edges, total length, and traffic. Many of the formulations in this section are derived by Kansky [95], [96].

4.3.1.1 Diameter d

The diameter of the network shows the length of the largest shortest path. A higher δ indicates less linked a network tends to be.

$$\delta(G) = \max d(u, v) \ \ for \ u \neq v \tag{4.1}$$

where $d(u, v)$ shows the length of the shortest path from vertex u to vertex v.

4.3.1.2 Number of Cycles μ

The graph cycle shows the maximum number of independent cycles in a graph. A higher u is an indication of the complexity of the transport system. Index p indicates the number of sub-graphs, usually taken as one.

$$\mu = e - v + p \tag{4.2}$$

4.3.2 Structural Indices at Network Level

Different indices can be derived to show the complexity of a transportation network and the changes in the structural measures overtime. We only discuss the topological indices for this study. These indices are defined as ratios expressing a relation between two values.

4.3.2.1 The relation between elements in the network

Alpha (α), beta (β), and gamma (γ) indices express the relations between elements of a network. α index indicates a measure of connectivity in terms of cycles in a graph. With the increasing number of links, the ratio will approach to 1, i.e., a fully connected network

$$\alpha = \frac{\mu}{2v - 5} \tag{4.3}$$

β index measures the connectivity in a graph by expressing the ratio of the number of links to nodes. A high β index in complex networks indicates a surplus of link in the network

$$\beta = \frac{e}{v} \tag{4.4}$$

γ index measures the connectivity in terms of the number of observed links and the number of possible links. Similar to α index, γ index approaching one shows a fully connected network.

$$\gamma = \frac{e}{3(v - 2)} \tag{4.5}$$

Eta (η) and Phi (π) indices express the relations between the network and one of its elements. η index or the measure of average edge shows that with the addition of nodes, e.g., intersections in the network, the shorter the average edge length becomes, thus decreasing the maximum flow q in the network.

$$\eta = \frac{L(G)}{e} \tag{4.6}$$

π index shows the relation between the total length of a graph and its diameter. A higher length of the network tends to show a more complicated transportation network; therefore, a higher π index reflects higher degrees of development. It roughly indicates the shape of the network.

$$\pi = \frac{L(G)}{\delta(G)} \tag{4.7}$$

The above structural measures and indices often do not reveal the internal structures of a highly complex interconnected transportation network. For this reason, performance measures should be carried out at the node or link level. It becomes of utmost importance while carrying out vulnerability analysis to have a better understanding of what might happen if a node or link becomes either completely unusable or with less carrying capacity, i.e., reduction in serviceability of the transportation network. Imagine a link that carries the shortest path between point A and point B. In case of the complete failure or reduced capacity, this could

drastically affect the network and incur costs (travel time delay or queues) or complete inaccessibility to the other side of the network if there are no detours.

4.3.2.2 Network Level Based Indices Results

We defined the structural indices in 4.3.1, here we list the results of the pre-event assessment of the transportation network in Table 4.1. Once we determined the post-event effects on the network, we will compare them with the values given in the table to illustrate the loss of the structure indices in the transportation network.

Table 4.1. Pre-earthquake network level-based indices

Index	Results	Bound
$\delta(G)$	47 km	0 to ∞
μ	37	0 to ∞
α	0.19	0 to 1
β	1.36	1 to 3 (2D planer Graph)
γ	0.47	0 to 1
η	0.93 km	0 to ∞
π	2.64	1 to ∞

4.3.3 Structural Measures and Node and Edge Level

The abstract network G, with physical connections to the real network, can be evaluated based on system-based vulnerability analysis at the node and edge level [97], giving a better representation of the actual network performance considering the importance of a node in local or global scale and the effect of weighted links (e.g., length: the shortest path $d(u, v)$). Local measures are only interested in finding the metrics with respect to the neighboring nodes, whereas, considering a node's situation in the whole network, the global measure can better highlight the overall performance. In this section, we discuss some of the structural (topological) vulnerability metrics. The analyses are performed utilizing three different applications: Urban Network Analysis Toolbox for ArcGIS developed by City Form Lab [98], SANET (Spatial Analysis along Network) Standalone Tool V1.0 Beta [99], and Python 3.7 with NetworkX library [100].

4.3.3.1 Degree of Centrality C_D

The degree or order of a node in a network simply shows the summation of all its edges. A higher degree indicates the importance of that node. The magnitude of C_d is partly a function of the size of the network [101]. For a vertex v, the degree is defined below where Figure 4.2 shows the degrees of the centrality of our study region's transportation network

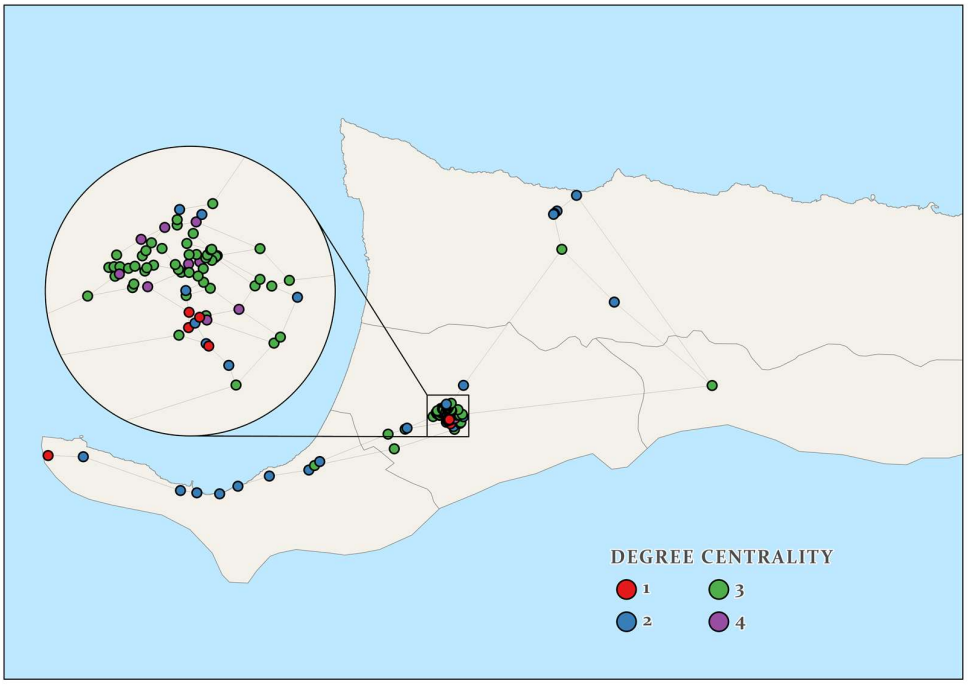

Figure 4.2. The abstract representation of the degree of centrality, C_D

$$C_D(v) = \sum_{j=1}^{n} G(v, j) \tag{4.8}$$

4.3.3.2 Betweenness Centrality C_B

C_B computes the shortest path betweenness for nodes or edges. It finds the fraction of the total number of the shortest path passing through a node v or an edge e. Given a pair of source and target node $V(s,t)$, the betweenness centrality is calculated as:

$$C_B(v) = \sum_{s,t \in V} \frac{\sigma(s,t|v)}{\sigma(s,t)} \tag{4.9}$$

$$C_B(e) = \sum_{s,t \in V} \frac{\sigma(s,t|e)}{\sigma(s,t)} \tag{4.10}$$

where $\sigma(s,t|v)$, and $\sigma(s,t|v)$ indicate the number of paths passing through some node v and some edge e, respectively. Similarly, $\sigma(s,t)$ is the number of shortest paths between (s,t)-path. Figure 4.3 and Figure 4.4 shows the node betweenness centrality and edge betweenness centrality of the study region's transportation network.

4.3.3.3 Closeness Centrality C_C

C_C indicates how close is a node to all other nodes in the network. It computes the reciprocal of the average shortest path distance to a node. It is defined for a node u as:

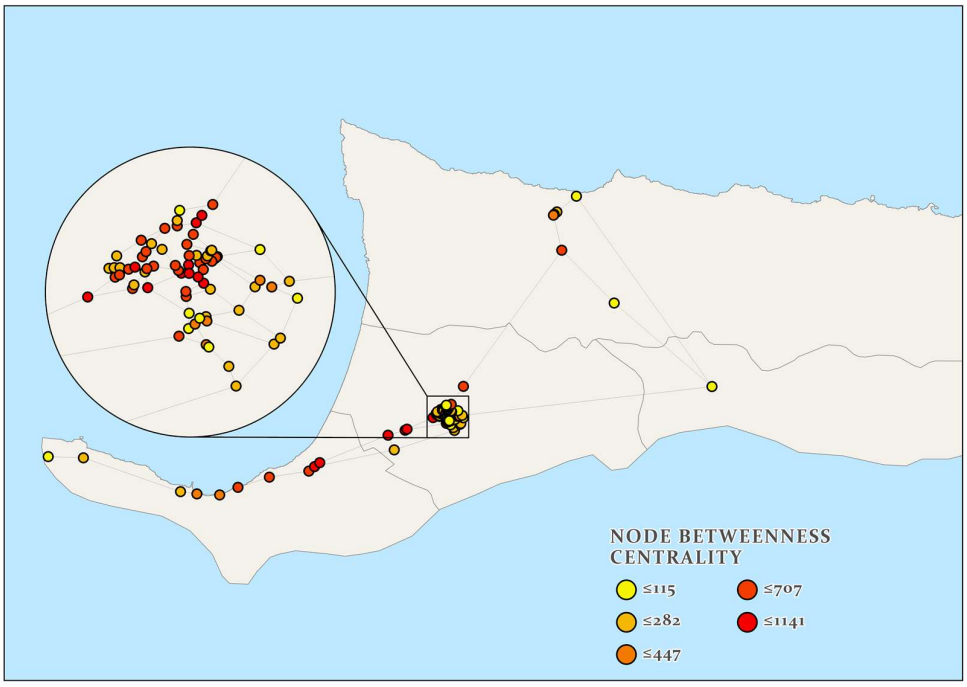

Figure 4.3. The abstract representation of node betweenness centrality, $C_B(v)$

$$C_C(u) = \frac{n-1}{\sum_{v=1}^{n-1} d(u,v)} \tag{4.11}$$

where n is the number of nodes reachable by u. Figure 4.5 shows the closeness centrality of the study region's transportation network. Higher C_C indicate higher centrality. It should be noted that NetworkX algorithms for calculating C_C is normalized according to:

$$\frac{n-1}{|\overline{G}|-1} \tag{4.12}$$

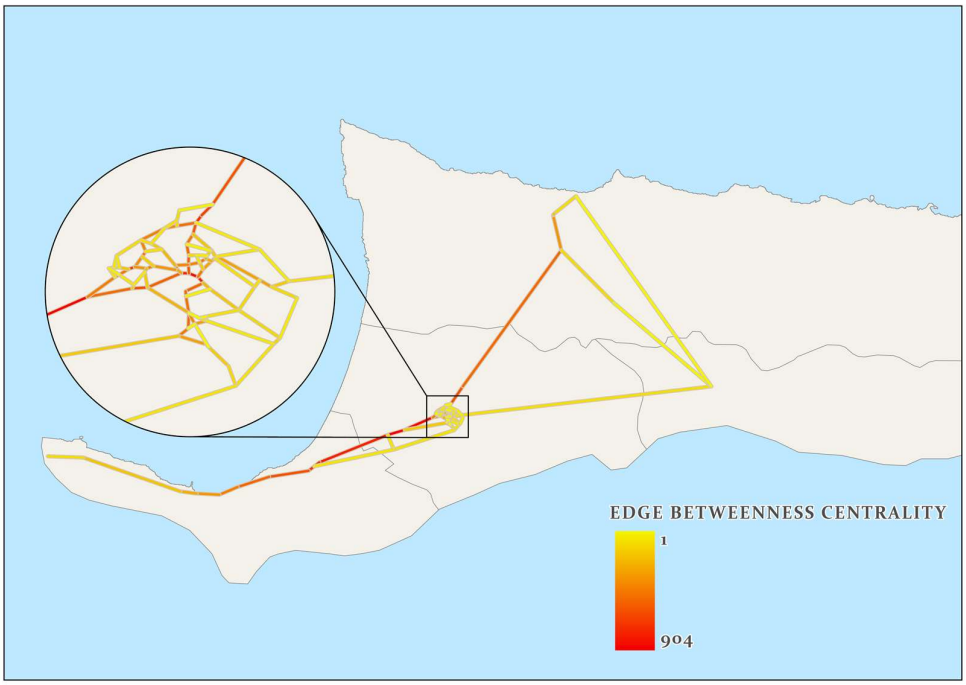

Figure 4.4. The abstract representation of edge betweenness centrality, $C_B(e)$

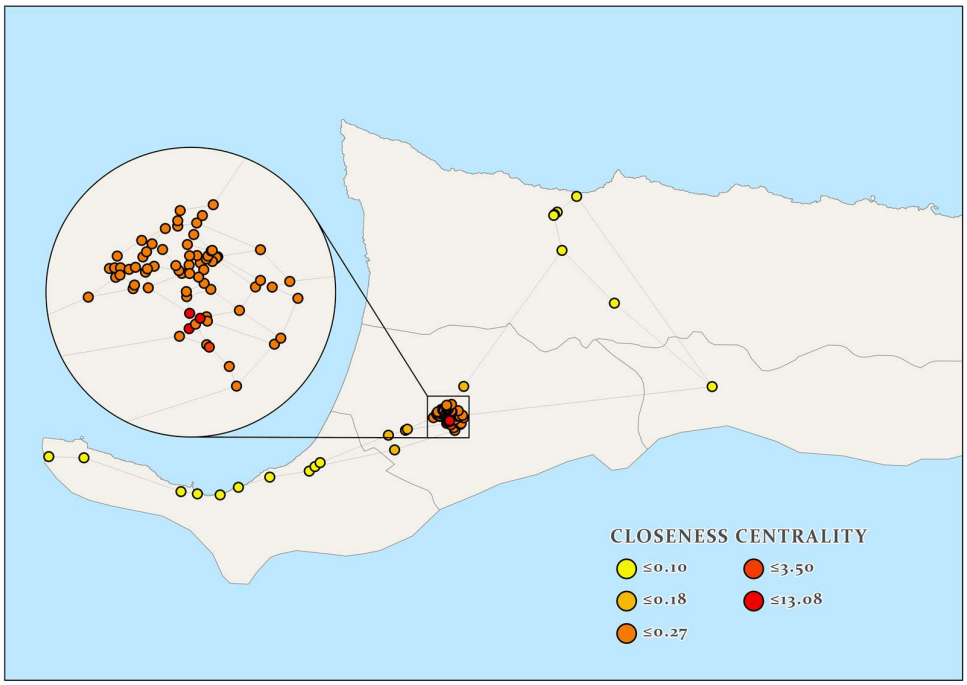

Figure 4.5. The abstract representation of closeness centrality, C_C

4.3.3.4 Gravity Index

Gravity measure takes into account the additional factors in the spatial impedance, such as length or other measures [102]. It is primarily used by urban planners to better understand the dynamics and the development of a region. Its primary function is to determine the attractiveness of an area in terms of its accessibility to the other nodes in the network. This index may not mainly be a measure of the performance of a transportation network for the context of this study. Nevertheless, it can still be used as a way to show how the network can be affected if the vulnerable nodes or links are removed from the network. Gravity index (GI) of a node i with respect to destination j within the graph G given a search radius r is defined as:

$$GI[i]^r = \sum_{\substack{j \in G-\{i\}, \\ d[i,j] \leq r}} \frac{W[j]}{e^{\beta . d[i,j]}} \tag{4.13}$$

The exponential decay e^{β} can be controlled based on the calibration carried out for the specific impedance metric. The exponent β is defined as 0.00217 for the impedance unit in meters [103]. Figure 4.6 shows the gravity measure of the study's regional transportation network.

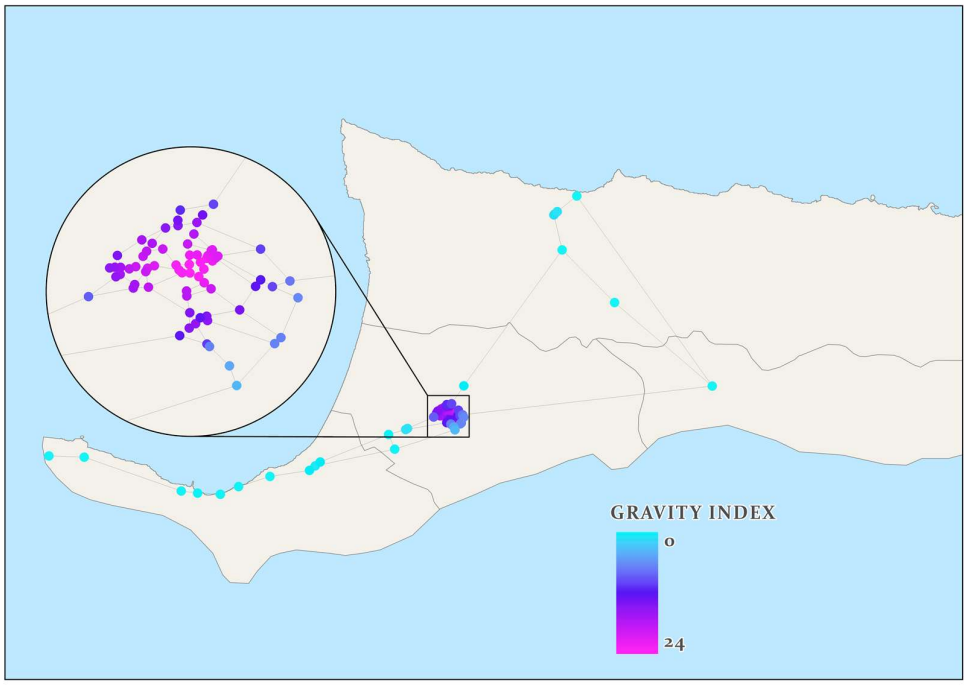

Figure 4.6. The abstract representation of gravity index, *GI*

4.3.3.5 Kernel Density Estimation

Hotspot analysis of events distributed over a network is one of the fundamental concepts in spatial analysis [104]. One of the most frequently used methods for analyzing distributed points on a network is to estimate the density of the points [105]. Kernel Density Estimation, KDE, is one of the most common techniques in discovering hotspots of point-events [106]. Ordinary KDE models such as 2-D Planer KDE are not useful in analyzing the linear road networks. Hence, an extension to the ordinary KDE, Network KDE (NKDE) was developed [107] such that:

$$\lambda_s = \sum_{i=1}^{n} \frac{1}{r} k(\frac{d_{is}}{r}) \tag{4.14}$$

where λ_s represents the density in location s, and r (bandwidth) indicates the search radius. k, the kernel function defines the distance decay effects or the weight of the distance of a point i to the location s. Therefore, the longer the distance, the less weight is applied to calculate the overall density. k can be defined with different models, such as Gaussian, Quadratic, Conic, and many others [107]. Instead of analyzing point-events on a network (e.g., crash zones, crime zones) as it the case for most of the kernel-based analysis, we try to estimate the density of the bridges and intersections for our study region. This way, we can get kernel classes for the whole network that could give a better overall view of the vulnerability of the network when a node (i.e., bridge) is removed from the network after the seismic assessment is performed. Generally, the NKDE analysis is performed over the real network, but to keep the flow consistent, we decided to use the abstract model, i.e., the graph. To perform the NKDE analysis, we used the SANET Standalone tool. The formulation of the NKDE in SANET is very similar to the previous equation; however, the kernel function k is defined differently as [105]:

$$K_y(x) = \begin{cases} k(x), & \text{for } -h \le x \le 2d-h \\ k(x) - \dfrac{n-2}{n} k(2d-x), & \text{for } 2d-h \le x \le d \\ \dfrac{2}{n} k(x), & \text{for } d \le x \le h \end{cases} \tag{4.15}$$

where $k(x)$ is the basic kernel function, and y is the center of the kernel for a point x in the network. The bandwidth h of the kernel function denotes how closely the points should be to match the distribution. Here d refers to the shortest path between x and y, and n denotes the node degree as defined earlier (C_d). Integrating the above system of equation will estimate the unbiased kernel density at origin O in the network [105].

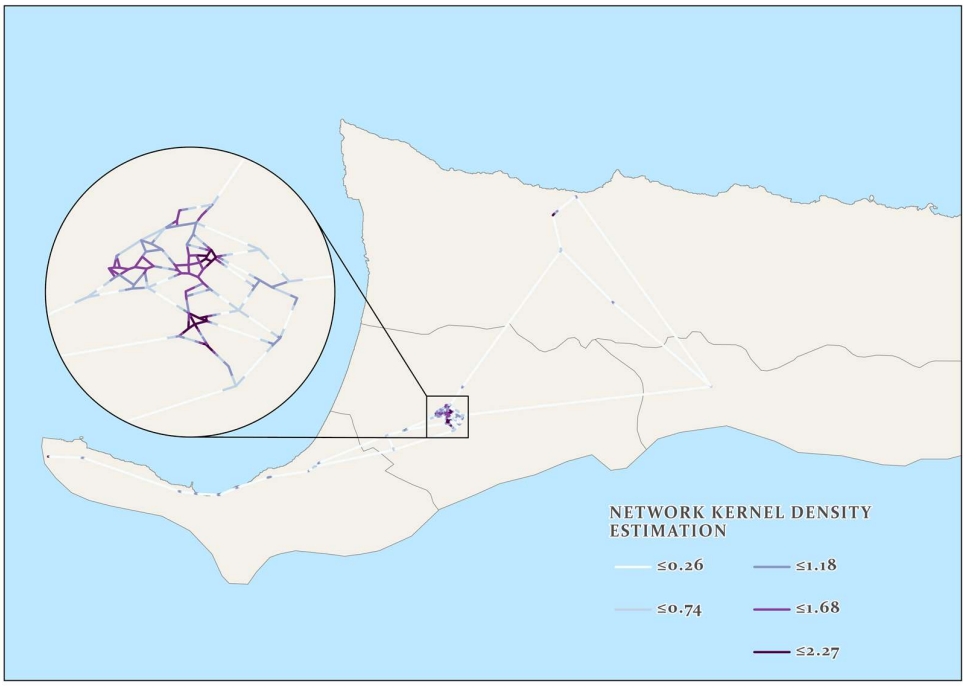

Figure 4.7. The abstract representation of NKDE, λ_s

$$D(O) = \int_{-h}^{2d-h} k(x)\,dx + \int_{2d-h}^{d} \left[k(x) - \frac{n-2}{n} k(2d-x)\right] dx + (n-1)\frac{2}{n} \int_{d}^{h} k(x)\,dx \tag{4.16}$$

It was recommended by the authors of the program to set the bandwidth as 200 m as to have a shorter computation runtime. Figure 4.7 depicts the NKDE of our study region in 5 kernel classes based on the Natural Break method. As it is evident, the district of Gulzelyurt shows higher kernel density compared to the other regions. The vulnerability of the bridges in the region that are located on the boundaries of the district show how vulnerable the densely populated network is in case of failures.

4.4 Link Performance Measures

In the previous sections, we talked about the reachability or the connectivity of the transportation network by analyzing the abstract representation of the study region through different metrics from graph theory. We determined the performance from the structural perspective. However, the real elements on the networks, i.e., the flowing traffic, could also play an important role in the overall network performance before and after an event. By looking at the travel demand and through network flow theory models as well as traffic assignments, we can quantitatively measure the impacts of travel time delay and queues. One area of conflict is that pre-event and post-event traffic demand that can be assumed the same or different. Depending on the choice of demand application, the cost could vary significantly.

In the sections below, we discuss travel demand modeling of our study region and show how the traffic assignment on the network is modeled.

4.4.1 4-Step Travel Demand Model

The traditional approach in estimating travel demand is the 4-step travel demand model that includes:

1) Trip Generation
2) Trip Distribution
3) Mode Choice
4) Trip Assignment

By estimating the four sequential steps above, one can approximate the travel demand for a network. Below we will discuss the steps necessary to implement the travel demand modeling of our study region.

4.4.1.1 Trip Generation

Starting with Trip Generation, the task is to identify sets of zones, called Traffic Analysis Zone (TAZ), where trips are generated from one zone to another based on the type of trip (working, social, etc.) or the activities (eating, lunch, visiting, etc.). The "classic three" purposes of generating trips are home-based work, home-based non-work, and non-home based [108]. To generate such trips, an extensive amount of data is needed. Surveys are to be designed carefully and distributed to the community, which could take years to collect and process. Usually, such information is available in census data at TAZ levels. For our case, however, this data is not available, nor the collection and processing of such data are feasible given the limited time and the scope of the research. Therefore, in order to achieve this section of the study, we assumed reasonable values for each TAZ trip production and attraction based on our intuition and engineering judgment of the traffic demand in the study region.

Another way to generate trips, other than relying on production/attraction from a TAZ, is by activity-based travel demand estimation (behaviorally-oriented activity-based approach). 4-step modeling does not include the interrelation between the trips – assume a home-based trip to two different work zones with one car. This is impossible to implement using the traditional 4-step modeling, but by using the activity-based approach, such modeling is achievable. However, given the scope of the study and availability of data, in addition to the complexity of implementing an activity-based model over the trip-based model, we opted for the trip-based model for analyzing the link performance of the transportation network. The traditional TAZ definition allocation was modified for our case to fit the generalized network model. Figure 4.8 illustrates the distribution of TAZ. The majority of the zones are defined for the

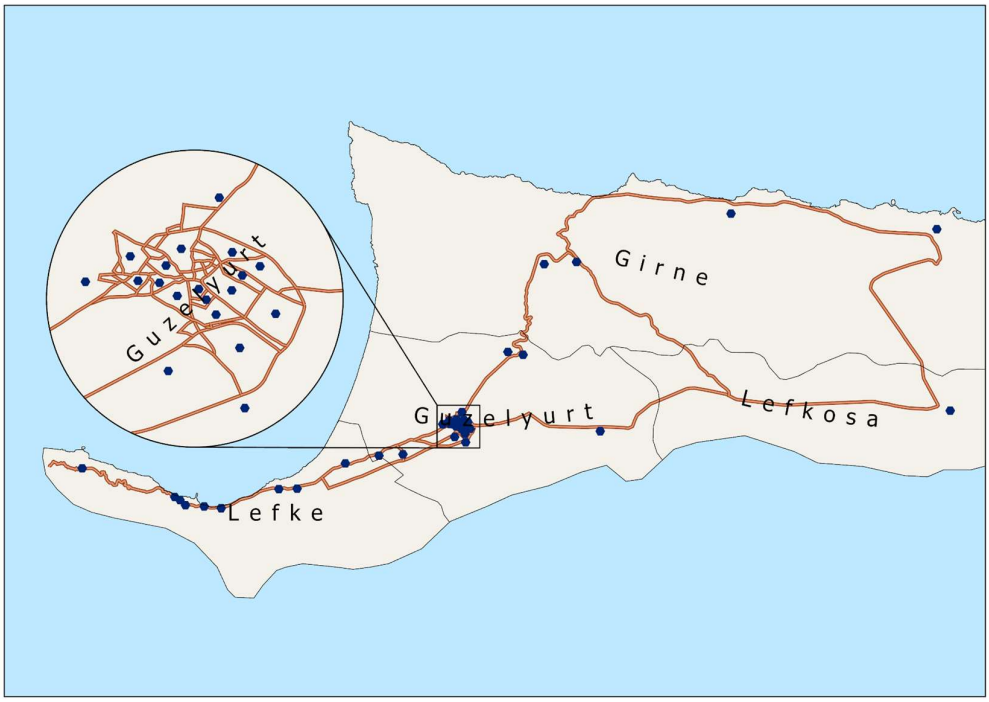

Figure 4.8. Distribution of the TAZs (circles represent the centroid of polygons enclosing a populated region)

Guzelyurt region acting as a hub connecting the central districts, Girne and Lefkosia, to the west, the district of Lefke.

4.4.1.2 Trip Distribution

The second step, Trip Distribution, as the name suggests, distributes the generated trips from zones. It generates Origin-destination (O-D) matrix and identifies the impedance parameters (e.g., travel time) for every zone in the network. There are three general ways to generate the distribution matrix. O-D matrix survey is the first choice, which is typically produced at the same time as collecting data in the trip generation step. Such surveys are typically used for small-scale regions but tend to be biased. The growth factor method and gravity model are the two other approaches in estimating the distributions of the trips. The gravity model is preferred as it utilizes the attributes of the transportation system [109]. The model is analogous to Newton's Gravitational Law, such that:

$$F = \frac{GM_1M_2}{d} \vdash T_{ij} = \frac{CO_iD_j}{c_{ij^n}} \tag{4.17}$$

where O_i and D_j indicate the amount of trips origination in zone i and the number of trips ending in zone j, respectively with travel cost c_{ij^n} between the OD pairs. A more generalized version of the gravity model ensures the number of trips from the OD pairs is balanced. To keep the zonal inputs balanced for the origin with the factor A_i, and for the destination with

the factor B_j, and considering the better representation of the deterrence cost between two zones, we can rewrite the equation such that:

$$T_{ij} = A_i O_i B_j D_j f(c_{ij}) \tag{4.18}$$

where $f(c_{ij})$ represents the generalized travel cost function or the deterrence function to de-incentivize travel based on time or distance. The doubly constraint formulation above ensures the zonal production and attraction are preserved. Singly constraint version of the gravity model can also be achieved by setting one of the balancing factors to 1. The deterrence function can be modeled as linear, negative exponential, power, and gamma functions [108]. If, however, the network is modeled via travel modeling software capable of dynamically finding the shortest-path between the zones, a variation of the above functions can be used after the Trip Assignment step is done to feed back the relevant deterrence parameters. That is one of the reasons why these two steps are combined typically while modeling the travel demand.

4.4.1.3 Trip Assignment

For the scope of this study, we do not consider the choice of transportation mode (modal split of OD matrix) as we are not interested in public transportation and other modes (walking, cycling, train, etc.) given the nature of the study. Although it should be noted that for microscopic traffic modeling, this step is necessary. Therefore, the final step is to allocate distributed trips to the transportation system. Trip assignment simulates vehicular movement through the network given the travel demand and zonal constraints, as well as overall network characteristics (e.g., signalized intersection, link speed, capacity). By doing so, we can estimate the traffic demand between zones and identify the congestions, travel patterns, effects of link/node removal, and many other measures. Typically trip assignments work by simulating the minimum path between OD pairs such that a traveler would always minimize the travel time. Travel time on a network (a measure of link performance) is typically defined by the power function developed by the Bureau of Public Roads (BPR) [110] as:

$$t = t_0 \left[1 + \alpha \left(\frac{V}{C}\right)^{\beta}\right] \tag{4.19}$$

where t indicates the travel time on the network; V and C are the volume and the capacity of the link, respectively, and α and β are coefficients calibrated for different free-flow speed. In general, $\alpha = 0.15$, and $\beta = 4$. The free-flow travel time t_0 is defined as:

$$t_0 = L/v_0 \tag{4.20}$$

where L is the length of the link, and v_0 is the free-flow speed. In order to realize the performance of the network for the current and future scenarios, the vehicular flow patterns

are simulated either by Static Traffic Assignment (STA) or Dynamic Traffic Assignment (DTA) models.

4.4.2 Static vs. Dynamic Traffic Assignment

Traditionally link performance was analyzed by STA methods. In the 4-step transportation planning, STA forms the last step of the process, and as its name suggests, it is only capable of static roadway condition modeling. It does not consider dynamic routing (time-varying travel conditions), congestion, queue buildup, and spillovers [111], [112]. STA does put a limit on the actual flow on the road as it distributes the traffic on the network at the same time. Therefore, the traffic demand would, in some cases, exceed the capacity of the links resulting in inaccurate estimation of the network performance. DTA, on the other hand, takes into account the fundamental relation between flow, capacity, and density, which in turn provides a more realistic traffic flow pattern. Incorporating the interactions of the road users with the network characteristics, allow for far better travel time reliability estimation for the vulnerable links on the network. For analyzing our study region's link performance, we incorporated NeXTA DTALite (Network Explorer for Traffic Analysis, Light-weight Dynamic Traffic Assignment Engine) [113]. NeXTA DTALite is a queue-based mesoscopic traffic simulator for travel modeling. Mesoscopic models are typically a middle level between macroscopic and microscopic models. They are used to bridge inconsistencies between the two mentioned models. No matter the method of trip assignment, in almost all applications User Equilibrium (UE) method is used to optimize the traffic assignment.

4.4.2.1 User Equilibrium

The definition of UE comes from Wardrop's first principle, which states, "*the journey times in all routes actually used are equal and less than those which would be experienced by a single vehicle on any unused route"* [114]. According to Wardrop, users (drivers) are selfish (non-cooperative) and have complete knowledge about the network (the path cost). To satisfy the user equilibrium through iterations, the following conditions/assumptions are to be made:

1) No user can reduce his/her path cost by switching routes, and
2) The route used between the OD pairs have equal and minimum cost (shortest path); the rest of the unused route has greater or equal cost compared to the used path cost.

The UE concept is utilized in STA. However, as discussed previously, with the shortcomings of STA, the UE model has to be modified based on the assumptions of the DTA. Therefore, Dynamic UE (DUE) was developed as a core function of DTA. In NeXTA DTALite, DUE is generalized as a nonlinear minimization problem via gap functions and solved through iterations until a user equilibrium is reached. The analysis of DUE is out of the

scope of this study, interested readers, are therefore recommended to check the detail of the process in [115].

In order to achieve a precise DTA model in NeXTA DTALite, we require extensive knowledge of the transportation network, including availability to sets of data that are not available or infeasible to collect. Therefore, to simplify our task while keeping the necessary level of detail for this study, some of the parameters in the program were kept as the default values. This is because a very accurate model requires a high level of understating of the network and different inputs from the department of transportation, which for the current scope of the study, is not achievable.

4.5 Inventory and Traffic Data Collection

In the previous sections, we defined the concepts behind the vulnerability analysis of the transportation network in addition to the traffic demand modeling. In order to be able to carry out the analysis, we need to collect the necessary inventory and traffic data for our study region. This is a demanding task, as we have to visit every bridge to collect the necessary traffic flow data on the associated link in order to calculate some traffic parameters needed for the DTA.

For this study, we counted the traffic flowing on the bridges for 1 hour at 15-min interval during the peak hours. This allows us to estimate the Peak Hour Volume (PHV) and Average Annual Daily Traffic (AADT). Counting was done during the weekdays in Fall and Spring at random intervals; however, we also observed the weekend traffic and concluded that during the weekend, the traffic is almost half of the weekday traffic. Some of the bridges are located on parts of the roadways that do not accommodate traffic often. The links associated with these bridges are not studied unless the links are part of the network that could allow traffic to pass in case of the failures of adjacent links. It should also be noted that manual counting of the traffic is not as reliable as the automatic methods. Nevertheless, it gives us a general idea of the flow of traffic in the network. Augmenting the counting methods for transportation networks by utilizing ITS devices can produce and more reliable results for long term monitoring of the traffic.

The majority of the road network in our study region are two-lane highways, i.e., one lane in each direction. While counting the traffic, we included both directions, as suggested in the Highway Capacity Manual (HCM) [116]. As most of the bridges are located on a stretch of one road and are closely spaced, we observe different traffic patterns on different days. In order to perform capacity analysis with simplification, we used the two-lane highway section of HCM (volume 2, chapter 15). We assigned the majority of the roadways as Class III two-

lane highways defined in HCM. If the parameters necessary for capacity calculation are unknown, we used the default values defined in HCM. The first step is to calculate the Free-Flow Speed (FFS) as:

$$FFS\ (mi/hr) = BFFS - f_{LS} - f_A \tag{4.21}$$

where $BFFS$ is the base free-flow speed; f_{LS} is the adjustment for lane and shoulder width (mi/h), and f_A is the adjustment for access-point density (mi/h). f_{LS} and f_A are taken as 5 and 3, respectively. A rough estimate of $BFFS$ is calculated from the posted speed limit plus 10 mi/h. Except for the freeways, the posted speed limit on almost all of the road network is 65 km/h (40 mi/hr). Therefore, FFS for the links associated with the bridges is estimated to be 42 mi/hr.

The second step is to find the demand adjustment for Average Travel Speed (ATS). The demand volumes in both directions are converted to the flow rates under equivalent base conditions with:

$$v_{i,ATS}(pc/hr) = \frac{V_i}{PHF \times f_{g,ATS} \times f_{HV,ATS}} \tag{4.22}$$

where $v_{i,ATS}$ is the demand flow rate for the ATS estimation in passenger car per hour (pc/h). V_i is the demand volume for analysis (d) and opposing (o) direction. $f_{g,ATS}$, $f_{HV,A}$ indicate the grade adjustment and heavy vehicle adjustment factors, respectively. $f_{g,AT}$ is taken as 1 and $f_{HV,ATS}$ is calculated as 0.96. PHF refers to the peak hour factor that is the variations in traffic flow within analysis hour. Since the demand is calculated as peak hourly factor (volume), PHF is set equal to 1. The decision to count the traffic for 1 hour in a 15-min interval is that estimation of PHF requires the maximum volume during the peak 15-min of the 1-hour analysis period as:

$$PHF = \frac{V}{4 \times V_{m15}} \tag{4.23}$$

where V is the hourly volume in both directions (veh/hr), and it is calculated by summing the four 15-min volume. V_{m15} is the maximum observed volume during the peak 15-min of the analysis period. Table 4.2 shows the observed 15-min counting of the traffic for 1 hour on the links associated with the 20 bridges (see Table 5.7 for bridge details). As mentioned before, we do not consider the links that experience negligible traffic unless the link is essential in detouring if the neighboring links fail. Accordingly, we assumed PHF of 0.60 and AADT of 500 veh/day for the link associated with bridge number 3 as it is one of the essential detour links in case of failure of the adjacent bridge number 2. Some of the results of PHF and PHV

may be underestimated or overestimated as the counting was done during random intervals once for every bridge in the period of 6 months.

It is also of interest, since the PHV is known, to roughly estimate the AADT such that:

$$PHV(veh/day) \cong (12-15)\% \times AADT \tag{4.24}$$

Moreover, assuming 50/50 directional split (%), D factor, and the proportion of AADT occurring at peak hour, K factor, we can also find the Directional Design-Hour Volume (DDHV) which shows the proportion of AADT in the peak hour in the predominant direction of traffic flow as:

$$DDHV(veh/hr/lane) = AADT \times K \times D \tag{4.25}$$

By calibrating the D factor and the percent of PHV for AADT, we found AADT is 12% of PHV and D as 0.12. In step three, we can now estimate the ATS in the analysis direction as:

$$ATS_d(mi/hr) = FFS - 0.00776(v_{d,ATS} + v_{o,ATS}) - f_{np,ATS} \tag{4.26}$$

where, $f_{np,AT}$ indicates the adjustment factor for ATS determination for the percentage of no-passing zones in the analysis direction, and it is found from the Exhibit 15-15 provided in HCM. Since we are assuming 50/50 percent distribution split, $v_{d,ATS}$ and $v_{o,ATS}$ are essentially equal.

The next step is to calculate the Estimate Percent of Free-Flow Speed (PPFS) as:

$$PFFS = \frac{ATS_d}{FFS} \tag{4.27}$$

Capacity measurements are evaluated based on the Level-of-Service (LOS), which is a qualitative measure of traffic service to a given flow. HCM proposes six LOS letters, namely, A, B, C, D, E in the descending order of quality of service. For Class III two-lane highways, HCM provides the following LOS for different ranges of PFFS, as shown in Table 4.3.

Table 4.2. Traffic flow for 1 hour with 15-min counting

Bridge	15-min counting (veh/0.25hr)				PHV (veh/hr)	PHF	AADT (veh/day)	DDHV (veh/hr/l)
	15'	30'	45'	60'				
B1	89	100	81	103	373	0.91	3108	187
B2	100	110	95	91	396	0.90	3300	198
B3	**Negligible Traffic (Important Link)**				**-**	**0.60***	**500***	**30***
B4	48	45	34	32	159	0.83	1325	80
B5	69	70	99	73	311	0.79	2592	160
B6	113	145	137	127	522	0.90	4350	261
B7	129	148	111	130	518	0.88	4317	259
B8	101	108	125	115	449	0.90	3742	225
B9	115	128	118	122	483	0.94	4025	242
B10	68	72	61	59	260	0.90	2167	130
B11	58	50	46	42	196	0.84	1633	98
B12	No Traffic				-	-	-	-
B13	80	74	70	81	305	0.94	2542	153
B14	**Negligible Traffic**				**-**	**0.60***	**400***	**12***
B15	83	97	84	100	364	0.91	3033	182
B16	44	65	35	41	185	0.71	1542	93
B17	80	74	69	70	293	0.92	2442	147
B18	71	82	65	75	293	0.89	2442	147
B19	66	69	72	59	266	0.92	2217	133
B20	No Traffic				-	-	-	-

Table 4.3. LOS for Class III two-lane highways

LOS	Class III Highways PFFS (%)
A	>91.7
B	>83.3-91.7
C	>75.0-83.3
D	>66.7-75.0
E	≤66.7

The base capacity defined for two-lane highways is 1700 pc/h. If $v_{i,ATS}$ is found to be less than 900 veh/hr, the directional capacity becomes the base capacity of the highway; otherwise, the capacity will be reduced as:

$$c_{dATS} = 1700 \times f_{g,ATS} \times f_{HV,ATS} \tag{4.28}$$

where, c_{dATS} is the capacity in the analysis direction under prevailing conditions based on ATS. The limit of the capacity in two directions is 3200 veh/hr. If the calculated capacity is found to be more than the limit, c_{dATS} would be calculated as:

$$c_{dATS} = \frac{3200}{2} \times f_{g,ATS} \times f_{HV,ATS} \tag{4.29}$$

To simplify the capacity calculation, we decided to use a more straightforward approach for the other rural 2-way highways where traffic counting was not performed. We used the NCHRP 387 Method [117] to calculate the capacity as:

$$Capacity\ (vph) = Ideal\ Cap \times N \times F_W \times F_{HV} \times PHF \times F_{dir} \times F_{nopass} \tag{4.30}$$

where, Ideal Cap is assumed to be 1400; the number of lanes N is set equal to 1; F_W indicates the lane width and lateral clearance factor and it is taken as 0.8; F_{HV} is assumed to be 0.90 based on HCM; PHF is taken as 0.9; the directional adjustment factor F_{dir}, and no-passing zone factor F_{nopass} are calculated as 0.97 and 0.93, respectively.

Similarly, for freeways using the NCHRP 387 Method [117], the following equation is used to find the capacity in a single direction as:

$$Capacity\ (vph) = Ideal\ Cap \times N \times f_{HV} \times PHF \tag{4.31}$$

where Ideal Cap is assumed to be 2200 for ~100 km/h free-flow speed according to HCM; N is set equal to 2 (2 lanes in each direction); f_{HW} is calculated as 0.98 [117], and PHF is assumed as 0.9.

In the end, following the equations shown above, we can determine the capacity of the transportation network. Table 4.4 shows the capacity of the links associated with the bridges, and Figure 4.9 shows the capacity of the whole network. Since the directional splits are set equal to 50/50 percent, the capacity in both directions would exceed the 3200 veh/hr limit. Therefore, the capacity for all the links associated with bridges is estimated as 1536 veh/hr.

Table 4.4. The capacity of the links associated with 20 bridges

Bridge	$v_{i,ATS}$ (pc/hr)	$f_{np,ATS}$	ATS_d (mi/hr)	PFFS	LOS	c_{dATS} (veh/hr)	c_{dATS}^{Actual} (veh/hr)
B1	194.27	0.90	38.08	0.91	B	1632	1536
B2	206.25	0.90	37.90	0.90	B	1632	1536
B3	-	-	-	-	-	-	1536
B4	82.81	0.10	40.61	0.97	A	1632	1536
B5	161.98	0.50	38.99	0.93	A	1632	1536
B6	271.88	0.90	36.88	0.88	B	1632	1536
B7	269.79	0.90	36.91	0.88	B	1632	1536
B8	233.85	0.90	37.47	0.89	B	1632	1536
B9	251.56	0.90	37.20	0.89	B	1632	1536
B10	135.42	0.40	39.50	0.94	A	1632	1536
B11	102.08	0.10	40.32	0.96	A	1632	1536
B12	-	-	-	-	-	-	1536
B13	158.85	0.50	39.03	0.93	A	1632	1536
B14	-	-	-	-	-	-	1536
B15	189.58	0.80	38.26	0.91	B	1632	1536
B16	96.35	0.10	40.40	0.96	A	1632	1536
B17	152.60	0.50	39.13	0.93	A	1632	1536
B18	152.60	0.50	39.13	0.93	A	1632	1536
B19	138.54	0.40	39.45	0.94	A	1632	1536
B20	-	-	-	-	-	-	1536

4.6 Dynamic Traffic Simulation

After we collect and calculate the necessary information to create the transportation network of our study region, we can now proceed to model the DTA in NeXTA DTALite simulation software. To make the task easier, we assigned the necessary attributes (e.g., capacity, speed limit, number of lanes) of the transportation network in ArcGIS. We then used the 'GIS-Import_Export_Tool' bundled with software to make the conversion from the ArcGIS network to the required data format used by the software. It should be noted that NeXTA DTALite input files are in .CSV format, and in order to convert the data to readable format in the software, we constructed the Network Dataset of the road network in ArcGIS. This creates the Cost OD Matrix, which in turn outputs the road network in terms of 'From Node" and "To Node" format, that is required by the software. After the conversion, we created the TAZs with the precise locations as discussed previously in section 4.4.1.1. Figure

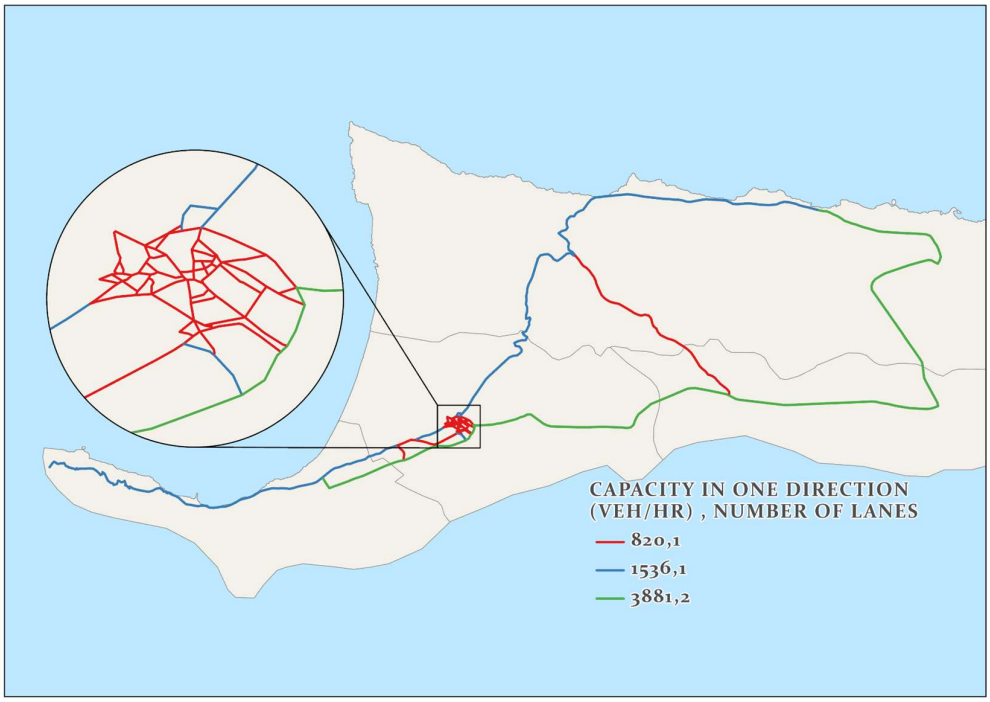

Figure 4.9. Transportation network link capacities distribution

4.10 depicts the transportation read network of our study region in NeXTA DTALite simulation software.

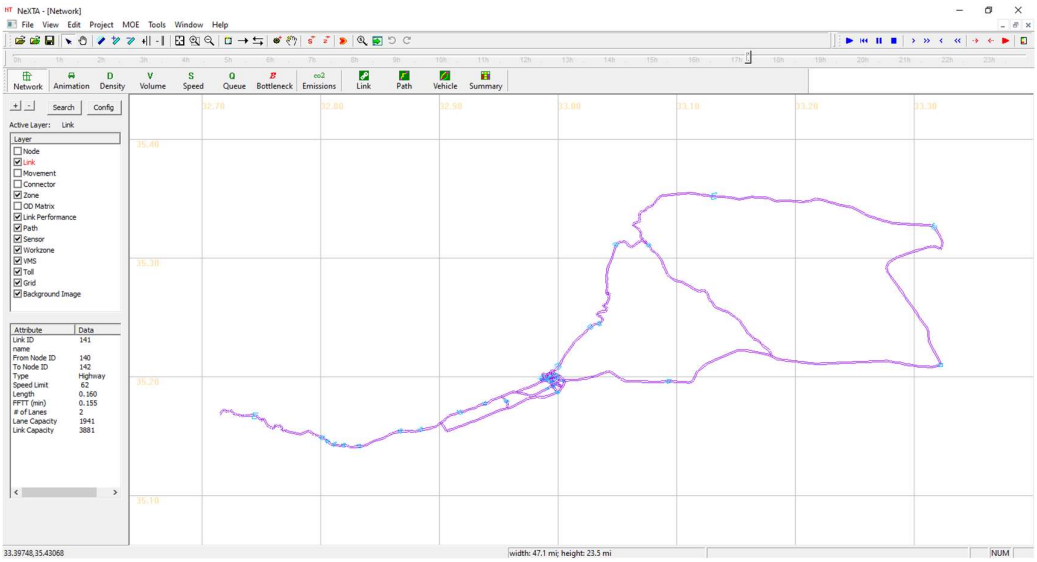

Figure 4.10. The simulated road network in NeXTA DTALite software

As explained before, since the current traffic data of all the links are not available, we, therefore, assumed the TAZ production and attraction values. By using the gravity model, we created the OD matrix between the zones and distributed the trips according to the production and attraction of each zones. Table 4.5 provides TAZ attraction and production attributes in

Table 4.5. TAZ attraction and production attributes (pcu)

Zone ID	Production	Attraction	Zone ID	Production	Attraction
28	200	500	**287**	200	200
64	350	150	**312**	100	100
66	350	150	**351**	200	200
69	350	150	**366**	100	100
72	500	400	**376**	100	100
77	1000	1800	**384**	100	100
92	300	150	**385**	100	100
100	300	150	**391**	100	100
124	300	150	**397**	100	100
141	500	500	**419**	100	100
157	300	150	**444**	1000	1800
196	200	200	**453**	500	500
208	200	200	**492**	300	300
229	200	200	**537**	300	300
242	200	200	**564**	200	200
249	200	200	**617**	1500	1500
256	200	200	**828**	3500	3500
257	200	200	**841**	4500	4500
284	200	200			

items of passenger car units (pcu). Zones 28 to 114 are located in the district of Lefke, zones 141 to 453 and zone 564 belongs to the district of Guzelyurt. Zones 492, 537, 617, and 828 are located in the district of Girne, and finally, zone 841 represents the district of Lefkosia. To add, Zone 77 and Zone 444 are representing the European University of Lefke, and METU NCC, respectively. Zone 828 and 841 shows the generation or trips that take place from Girne and Lefkosia, to Guzelyurt and Lefke, respectively. It should be noted that this represents a baseline of what can be used, albeit with slight modification (e.g., demand multiplier) to represents the daily trip generation between the designated zones. Without access to the complete data, we cannot produce real values of zonal production and attraction. However, to calibrate and to make traffic volume more realistic, we incorporated AADT for the bridge-links in which the 1-hr peak daily flow is available. We also applied demand multiplication until we observe a realistic volume of traffic.

In a recent Federal Highway Administration (FHWA) report on utilizing DTA in modeling, it was explained in great detail the process, framework, and the data requirement as well as model development and calibration techniques to achieve DTA in the analysis of modeling the routing behavior of drivers in a transportation network [118]. The variability in traffic distribution is a challenging task to predict as it differs based on the regional characteristic, dynamic environmental parameters, and more. DTA aims to predict such changes and variabilities for the long-term behavior of traveler's adaptation to experienced congestion on the rods. Therefore, the demand distribution or demand profile with congestion periods can

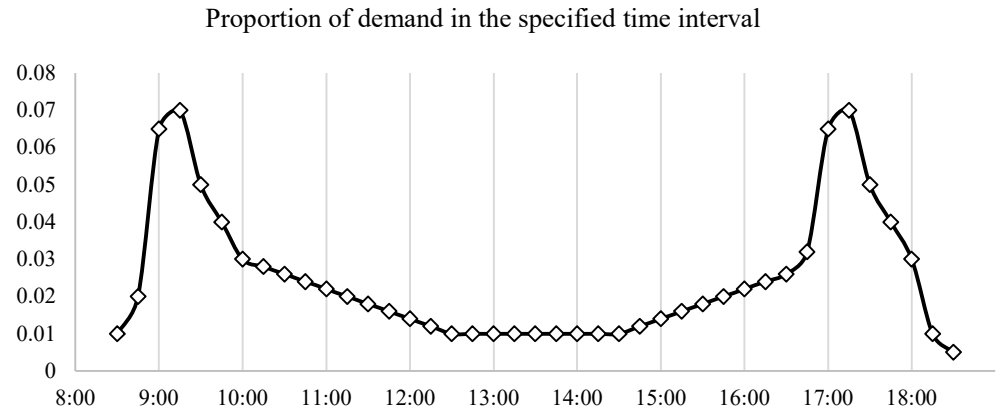

Figure 4.11. 9:00 to 18:00 daily traffic demand

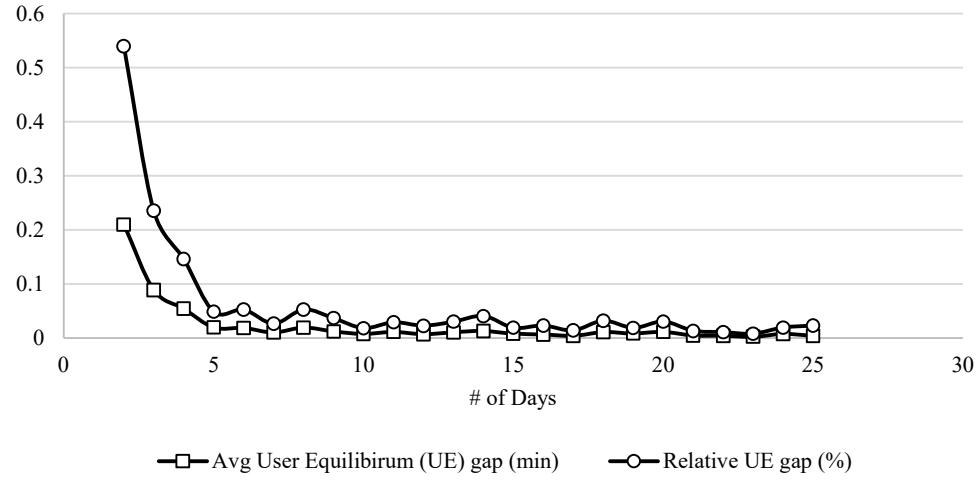

Figure 4.12. UE convergence after simulating for 25 consecutive days

vary per each link. The demand profile usually shows two peaks, one in the morning and the other in the afternoon. Such distribution examples can be seen from several sources such as [118], [119]. To get a better picture of the demand for a region, we would require long-term data collection of the traffic. This, however, cannot be achieved as the current transportation infrastructure of Northern Cyprus has not yet transitioned to the long-term travel forecasting stage by using traffic counting tools or modeling software. Therefore, to analyze the transportation network for the scope of this study, certain assumptions based on perceived demand and supply of the region and engineering judgments and intuition were made. We distributed the daily traffic demand in the network, as shown in Figure 4.11.

We assumed that the peak traffic would happen during 9-10:00 in the morning and 17-18:00 in the evening. We applied a 10-fold increase in the demand to meet the actual volume of the traffic in the network. We verified this for the bridge-links according to their designated AADT. We simulated the traffic flow for 25 days – 10 days to reach UE and 15 days to

optimize the OD Matrix Estimation (ODME) using the known flow volumes of the bridge-links. The traffic simulation was run from 9:00 in the morning until 6:00 in the afternoon, with 30 minutes before and after to smooth the distribution. Figure 4.12 shows the UE convergence of the simulated network after 25 days. To verify the simulated volumes, we can observe the link associated with bridge 6 which has an AADT of about 4317 veh/day (see Table 4.2), and the simulated number of vehicles passing through the link is estimated as 4147 veh/day for the whole duration of the simulation, as shown in Figure 4.13. Moreover, in the same figure, the simulated traffic volume on the same link follows the defined traffic pattern of Figure 4.11.

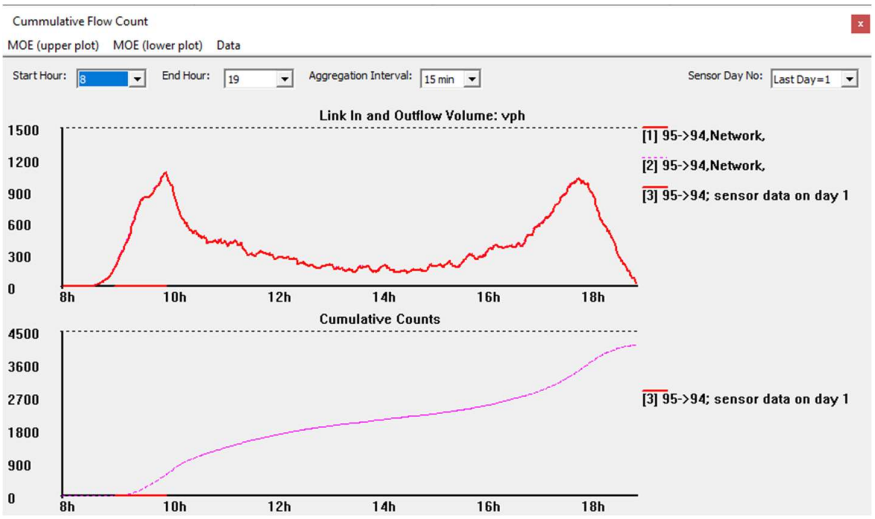

Figure 4.13. Simulated link capacity of Bridge 6

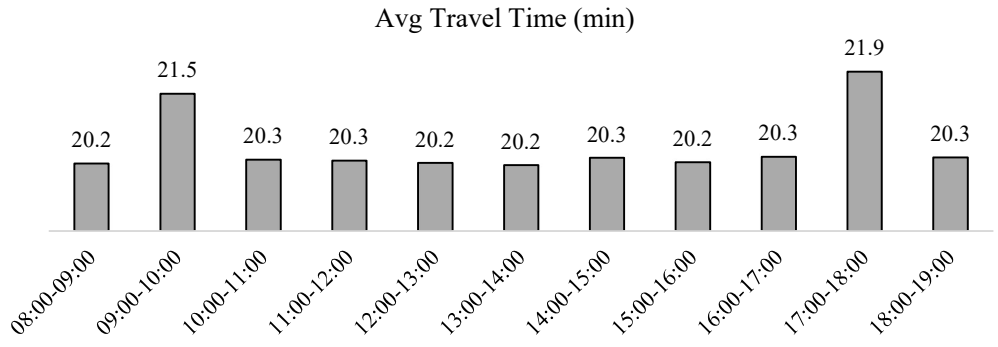

Figure 4.14. Average travel time for the shortest path from METU NCC to European University of Lefke

In summary, 19,110 vehicles were simulated in this analysis, with a total travel time of 5.5 thousand minutes and an average travel time of 29 minutes between the OD pairs. To give a perspective, traveling from METU NCC to the European University of Lefke would result in the following estimated travel time and network density/volume contour map shown in Figure 4.14 and Figure 4.15, respectively. Some of the results above might be overestimated due to a

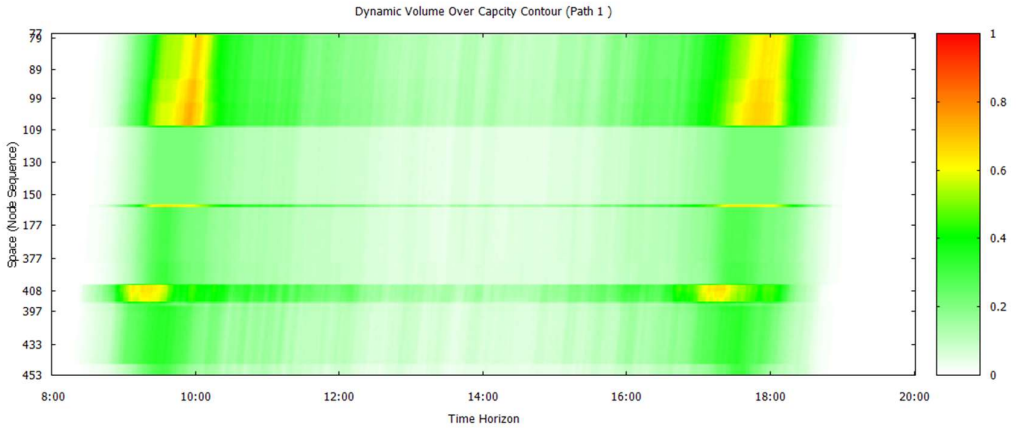

Figure 4.15. Volume/capacity contour map for the shortest path from METU NCC to European University of Lefke

lack of knowledge on the travel pattern and detailed traffic flow, and the estimated values might not reflect reality. However, such a model can still be used as a baseline to compare with post-event effects for evaluating the performance of the transportation network.

4.7 Chapter Summary

The failure of bridges can have significant impacts on the transportation network. The reduced serviceability or complete failure of a bridge can negatively impact the travel time and increase the distance to travel between pairs of ODs. In this chapter, we introduced the reliability and vulnerability of the transportation network. To quantify the vulnerability metrics, we incorporated graph theory to extend the topological vulnerability analysis. We performed several network-based structural measures as well as evaluation of the performance of the network based on a system-based vulnerability analysis at the node and edge level, incorporating three different software.

Additionally, after discussing the reachability or the connectivity of the transportation network, we introduced the link performance measure. Here, we showed that in the real network, analysis of the traffic would play an essential role in determining the overall effectiveness of the network. To analyze the traffic, we implemented the ubiquitous 4-step travel model (excluding the mode choice) to determine the travel time. After generating the trips from OD pairs and distributing the trips by gravity model, we employed a dynamic traffic assignment simulation software to analyze the traffic and considered this as our baseline; the pre-event traffic performance of the transportation network. Having concluded the hazard analysis, the next chapter explains the adaptation of Hazus for our study region. Figure 4.16 highlights the important parts of this chapter.

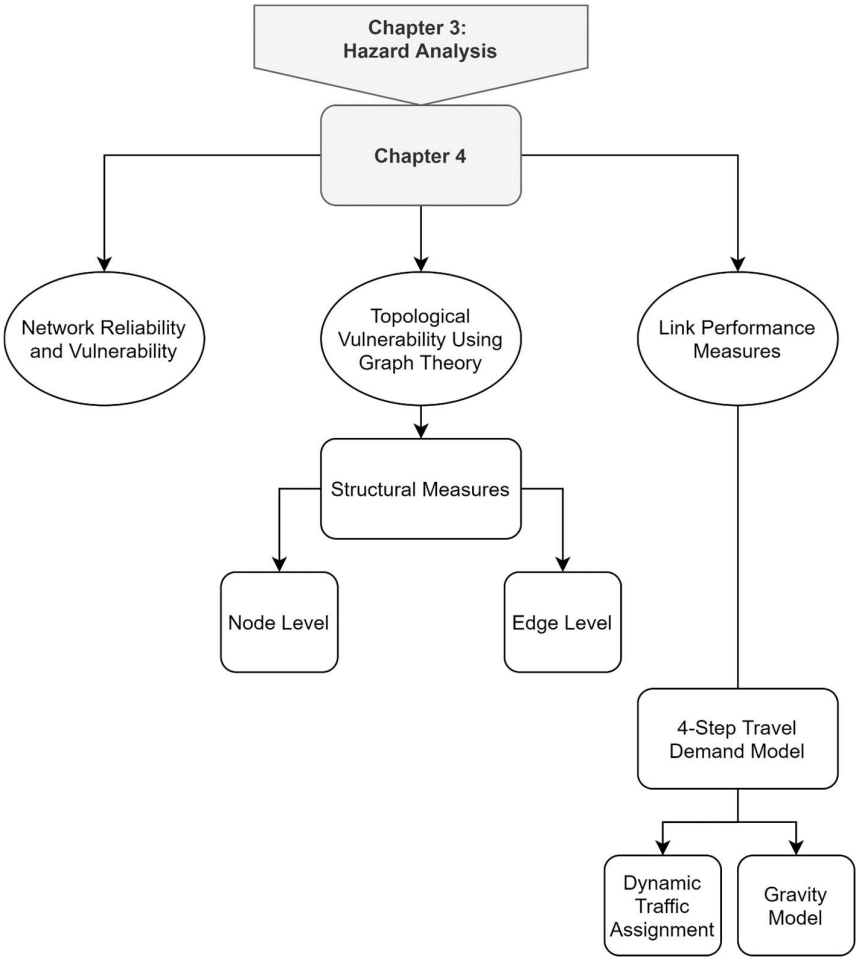

Figure 4.16. Chapter 4 summary chart

CHAPTER 5

NORTHERN CYPRUS ADAPTATION FOR HAZUS EARTHQUAKE MODELING

5.1 Introduction

Hazus provides a risk assessment tool for the communities throughout the U.S. The models and parameters, as well as the building stock, are all U.S.-centric. However, as a general risk assessment tool in locations where a standardized risk assessment methodology is not yet developed, Hazus can be used as a way to conduct a detailed hazard analysis, granted that an accurate database could be created for such locations. With the most recent version of Hazus 4.2 and the transition from ESRI Personal Geodatabase (pGDB) .mdb format to more versatile SQL Server spatial format, under the effort of modernizing Hazus since 2014, some of the hurdles of developing an international Hazus model in the past have been overcome. Although a significant effort in developing and adapting Hazus for non-U.S. countries is still required, however, the reward is also valuable. It should, however, be noted that the default Hazus U.S. inventory is detailed down to small parameters that are not feasible for other regions to collect. This includes utility systems, essential facilities (school, police stations, etc.), high potential loss facilities (dams, military facilities, nuclear facilities, and more), building construction practices, and population demographics. Even if such data exist, they are most probably not in geospatial format.

Hazus is capable of analyzing various levels of geographic scale with small or large details. In general, as depicted in Figure 5.1, there are four geographical scales that Hazus can run its risk analysis. Generally, the lower the level of geographical division is used, the better accuracy of the Hazus model. Census Block is the smallest geographic unit used by the United States Census Bureau that refers to a boundary bounded by visible features such as roads,

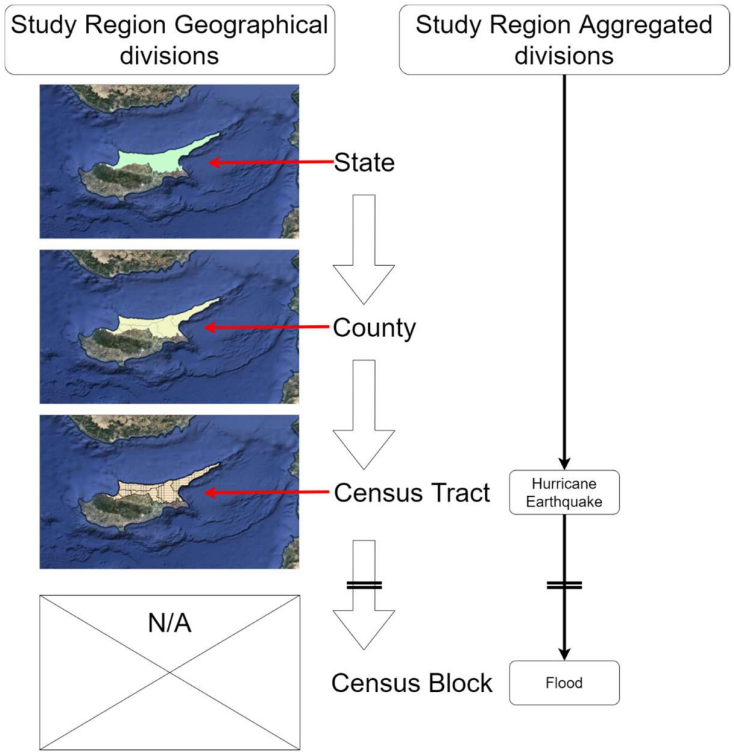

Figure 5.1. Cyprus geographical division according to Hazus schema

streams, and nonvisible features such as property lines, school districts. In Northern Cyprus, such designation is not used and therefore, will not be considered for developing the study region's inventory. Additionally, Census Blocks are required for flood risk assessment which is out of the scope of this study.

There are two ways to collect the necessary information needed to construct a database of a country, 1) regional or national scale approach, 2) community or local scale approach. In this study, due to the nature of our work, unavailability of geospatial data at the community level, and the challenges in collecting detailed building stock, the national approach is chosen as it provides more globally consistent information throughout the region. However, an effort was taken to collect local datasets such as bridges by visiting them one by one and taking notes of their structural characteristics.

5.2 LandScan Grid and Administrative Boundary

To define our study region as a polygonal grid, population exposure datasets are used to develop and to divide the region into grids as local geospatial data are unavailable. Different datasets with distinctive features are available for global use. Gridded Population of the World (GPW) by NASA [120], Global Exposure Dataset (GED) by UNISDR (United Nations International Strategy for Disaster Reduction) [121], and LandScan [122] are some of the

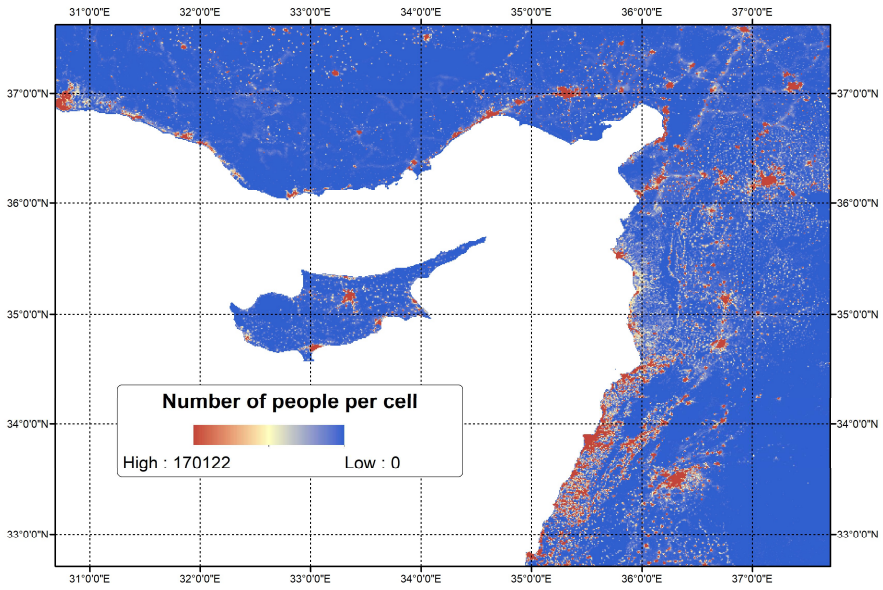

Figure 5.2. Population distribution of Cyprus according to 2018 LandScan gridded population data

standard population exposure datasets available for risk assessment analysis considering different scenarios. GPW and GED provide more in-depth information about demographics and building stocks. At the same time. LandScan is considered to be an up-to-date source of global population distribution at a 1 km spatial resolution with no additional demographic or built environment data. Since our region is limited to Level 1 analysis only on the transportation network scale, we, therefore, utilized the LandScan gridding approach. Although the cost of population loss is not the aim of this study, for future-proofing our work in case of expansion of seismic risk assessment of Northern Cyprus, LandScan is a feasible option given its fine resolution and current population database. LandScan was developed by the Department of Energy's Oak Ridge National Laboratory (ORNL) as an effort to introduce an industry-standard global population distribution with high resolution in a GIS raster format. In this study, the latest available version of LandScan Global 2018 with geographic projection as WGS 1984 is used. Figure 5.2 shows the 2018 population distribution of Cyprus as modeled by LandScan. This gridded population will be used later in developing syHazus database for syTract feature class. The procedure is explained in the subsequent sections.

The Admin 0 boundary of Northern Cyprus is downloaded from GDAM, a spatial database of the world's administrative boundaries [123]. The Level 1 (first sub-division) of the Northern Cyprus boundary provided by GDAM, does not include the District of Lefke. The reason for this is that the Lefke region was part of the district of Guzelyurt before Dec. 2016 and the group at GDAM have not yet updated their database. Therefore, the district of Lefke had to be

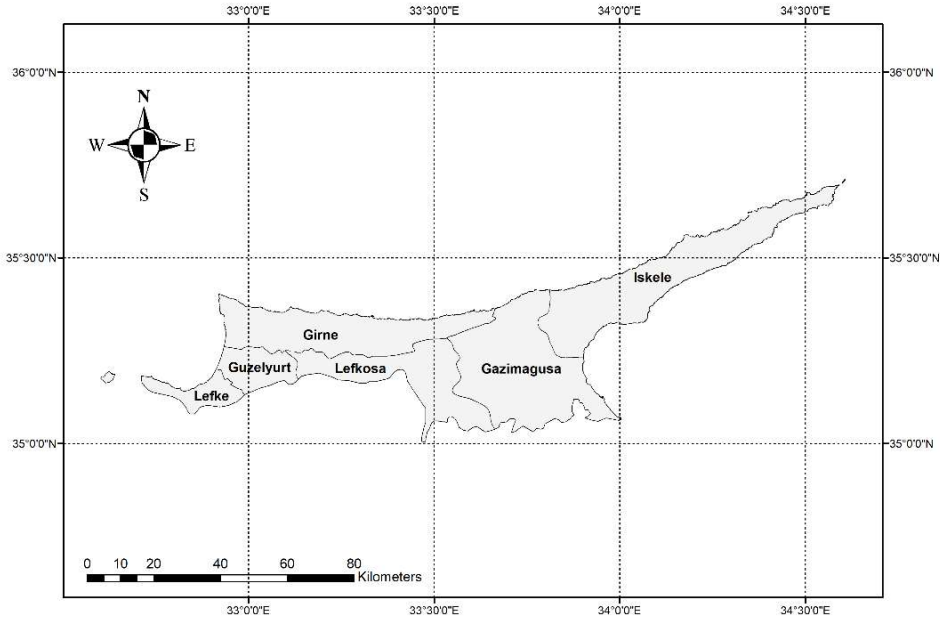

Figure 5.3. Northern Cyprus district divisions

added manually to the map. Figure 5.3 shows the six districts of Northern Cyprus. This study is limited to the risk assessment of bridges located in Lefke, Guzelyurt, and part of Girne.

5.3 Hazus Database

Hazus is comprised of two databases that are needed to be correctly formatted to the desired region's characteristics.

- syHazus.mdb
- Hazus_State.mdb

syHazus holds the required information for defining the GIS boundary information relative to states, counties, and census tracts. Whereas Hazus_State contains GIS boundary information for counties, census tracts, and census blocks. Additionally, it includes the necessary aggregated data about the demographic, building information, and structure exposures. The required input data for our case study are shown in Table 5.1. Hazus_State contains many different features classes, but it is limited to bridges and roads for this study only.

The sections below will explain the procedure of collecting and developing each database and the required fields to be inputted.

Table 5.1. Hazus required input database

Hazus Inventory Geodatabase	Object	Description
syHazus.mdb	syState	Northern Cyprus state boundary
	syCounty	Northern Cyprus counties (districts)
	syTract	Northern Cyprus census tracts
Hazus_State.mdb	hzHighwayBridge	Geometry (point features) and all-hazards information of highway bridges
	eqHighwayBridge	Earthquake specific information for highway bridges
	eqHighwaySegment	Earthquake specific information for highway segments
	hzHighwaySegment	Geometry (line features) and all-hazards information highways
	hzTract	A state extent boundaries feature

5.3.1 syHazus Database

A full explanation for the required input data for each feature class in the syHazus database is explained in [124]. Unless otherwise mentioned, except for the information listed below, the rest of the fields are kept as default or empty. In developing the syHazus database, some of the fields are dependent on the other feature classes for the necessary entries. County or tract designation and the number of tracts are the examples of such a case.

5.3.1.1 Feature Class: syState

This feature class provides state boundary information. This basically defines the country borders and the necessary identification parameters. The required fields to populate are:

1. StateFips: 79 (Federal Information Processing Standard (FIPS) state code)
2. StateID: KK (Kuzey Kibris/Northern Cyprus)
3. State Name: KKTC
4. NumCounties: 6 (Number of counties/districts)

5.3.1.2 Feature Class: syCounty

This feature class provides the county/district boundary information. The required fields to populate are shown in Table 5.2

Table 5.2. Required syCounty fields in Hazus

CountyFips	CountyFips3	CountyName	State	StateFips	NumTracts
79001	1	Gazimagusa	KK	79	67
79002	2	Girne	KK	79	49
79003	3	Guzelyurt	KK	79	13
79004	4	Iskele	KK	79	69
79005	5	Lefke	KK	79	18
79006	6	Lefkosa	KK	79	39

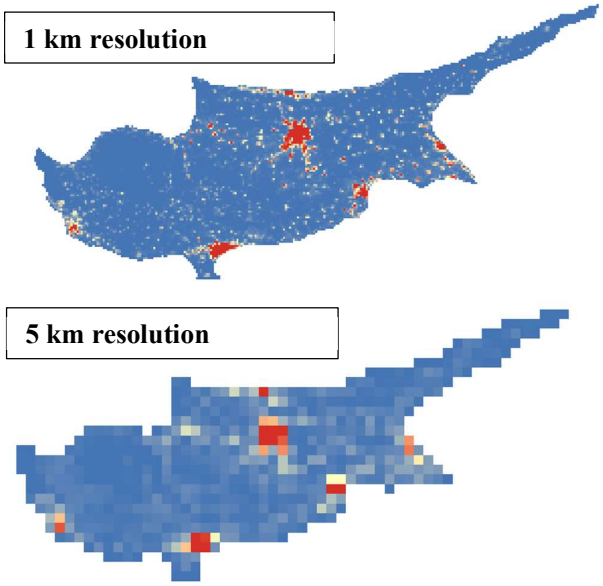

Figure 5.4. 1 km and 5 km aggregated population gridded dataset of Northern Cyprus

The number of tracts (NumTracts) is found from the syTract feature class. Since our study is limited to one region, State and StateFips would, therefore, refer to one state designation with the information listed in the previous section.

5.3.1.3 Feature Class: syTract

This feature class provides the census tract boundary information. Census tracts in the US are small, relatively permanent statistical subdivisions of a county. They comprise of 4,000 (1,200 min, 8,000 max) inhabitants. As such, designations are not available geospatially. To create Northern Cyprus gridded datasets to develop census tracts, the LandScan population exposure dataset is used. As explained before, LandScan uses 1 km grids cell distribution. However, for this study and to make sure that HAZUS can run analysis quickly, it was decided to aggregate the 1 km raster file to a grid cell of 5 km. In theory, higher resolution is used for areas where population density is comparatively high, and when the risk analysis is performed at a community scale, which is usually the case for a flood. Figure 5.4 shows how aggregated grid cell changes the resolution of population exposure.

Using the aggregated gridded exposure at 5 km, converting the raster file into features with point geometry, and using Thiessen Polygons analysis in ArcGIS, we can create the regional grid dataset. Figure 5.5 shows the combined process of generating the grids, and Figure 5.6 depicts the Northern Cyprus grid dataset at 5 km resolution using the LandScan population exposure dataset. In total, 255 grids were generated. Table 5.3 shows the first 10 fields that are either generated (area and centroid) or populated based on the syCounty or syState information. Here, CountyFips refers to the county/district where the grid is located at.

Table 5.3. syTract required fields in Hazus

Tract	CountyFips	Tract6	TractArea	CenLongit	CenLat
79001000001	79001	1	17.539898	33.561459	35.139053
79001000002	79001	2	9.052102	33.682214	35.064329
79001000003	79001	3	17.540815	33.603126	35.139053
79001000004	79001	4	17.549788	33.644792	35.097387
79001000005	79001	5	17.540631	33.644792	35.139053
79001000006	79001	6	17.549645	33.686459	35.097387
79001000007	79001	7	0.151725	33.765481	35.033794
79001000008	79001	8	0.439714	33.713594	35.032864
79001000009	79001	9	16.334262	33.769647	35.057119
79001000010	79001	10	17.549856	33.728126	35.097387

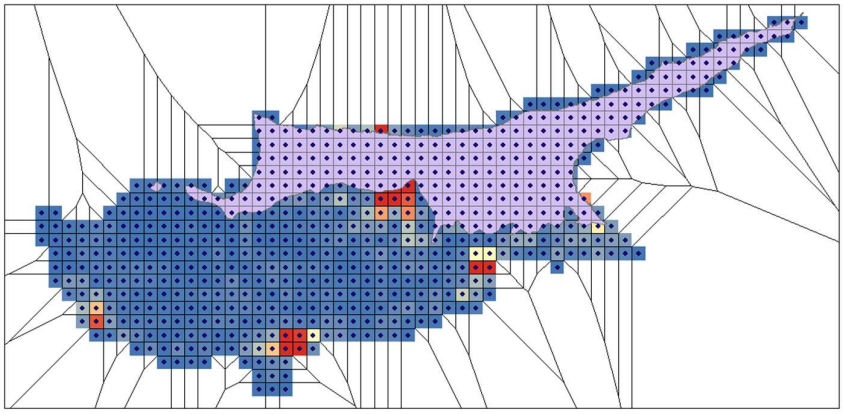

Figure 5.5. Grid generation with Thiessen Polygons analysis

TractArea, CentLongit, and CenLat refer to the area of the census tract, census tract longitude (centroid), and census tract latitude (centroid), respectively. At this point, SyHazus database is completed. The feature classes are converted to a personal geodatabase named syHazus.mdb.

5.3.2 Hazus_State Database

This database contains the features classes with demographic and building inventory profiles aggregated at the census block and census tract levels. They comprise of fields that are relevant to all hazards and specific tables for earthquake and flood models. The geographical domain of the Hazus_State database is the state; hence for each state, there exists one database. As explained before, since this study only considers the transportation network

Figure 5.6. Northern Cyprus grid dataset at 5 km resolution

for seismic risk assessment, the only required features classes for this database are bridges and roads.

5.3.2.1 Feature Class: hzHighwayBridge

This feature class provides the geometry of highway bridges. In our study region, which consists of all the major bridges located on the main roads in the western part of Northern Cyprus, there exist 20 bridges. We do not take into account culverts (there are ten culverts in the same geographical domain) for this study. Analysis of culvert is typically done on a multi hazard-based basis, or flood-only hazard as they are considered a hydraulic system. Figure 5.7 shows the distribution of bridges in the western part of Northern Cyprus with the majority of the bridges (nine to be exact) being in the district of Lefke.

Hazus bridge classification system is by far the most comprehensive document in grouping similar bridges based on their seismic risk vulnerability. The grouping incorporates many parameters that are used in fragility analysis. The bridge classification scheme of Hazus [76] is depicted in Figure 5.8. Hazus requires to classify the brides from the 28 available Highway

Figure 5.7. Bridge distributions in the Western part of Northern Cyprus

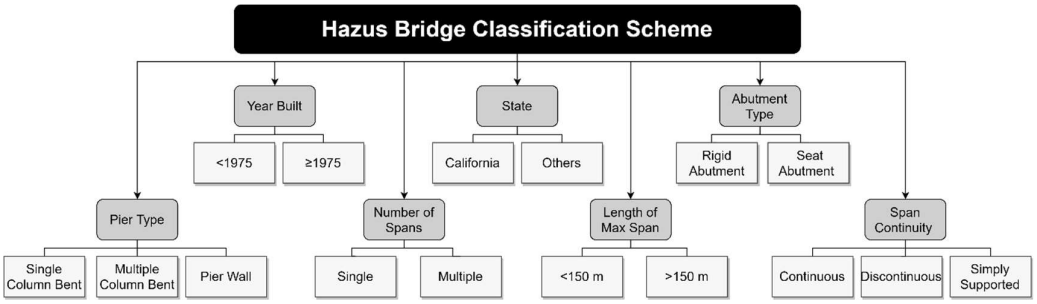

Figure 5.8 Hazus Bridge classification Scheme

Bridge (HWB1-HWB28) classes. The description of each 28 Bridges is shown in Table 5.4 [125].

In our region, which comprises all the bridges in the districts of Gulzelyurt, Lefke, and part of Girne (before Karsiyaka village), we have identified 20 potential bridges. Every 20 bridges were visited one by one, and a detailed structural description of each one was noted down. Figure 5.9 shows a close-up of the bridges in our study region, and Table 5.7 shows the collected data for the Hazus bridge methodology and classification scheme. It should be noted that, in Hazus, the ESRI field data type for the necessary information to be entered is of the type long integer. Therefore, the collected values from bridges are rounded to the nearest integer.

Some of the identified bridges cannot be classified with the current Hazus methodology (HWB28). These bridges are old or did not follow a strict design guideline. Furthermore, there are unusual bridges where a reinforced concrete bridge has been added to the existing masonry arc bridge without demolishing the existing structure. As such, all these bridges were assigned as HWB28.

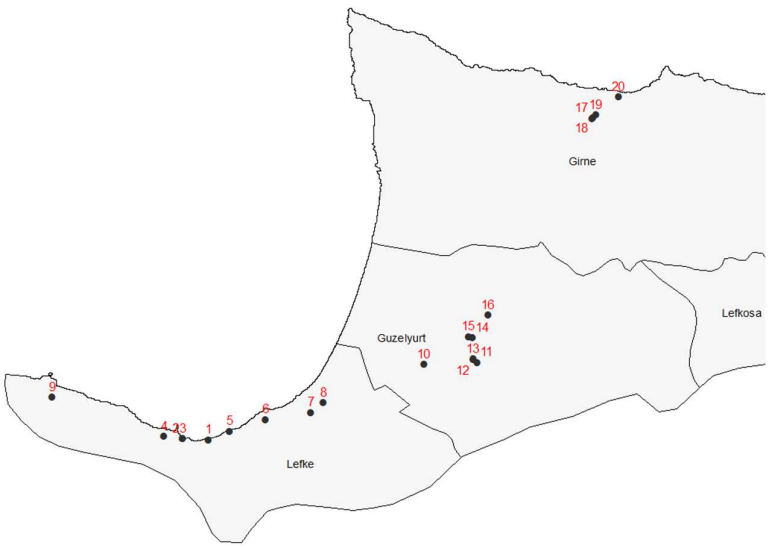

Figure 5.9. The bridge numbering scheme for bridge class identification (labeled based Object ID of Table 5.7)

Table 5.4. 28 Bridge classes defined by Hazus methodology

Class	Category	Description
HDFLT	Highway	Default Bridge
HWB1	Highway	Major Bridge - Length > 150m (Conventional Design)
HWB2	Highway	Major Bridge - Length > 150m (Seismic Design)
HWB3	Highway	Single Span – (Not HWB1 or HWB2) (Conventional Design)
HWB4	Highway	Single Span – (Not HWB1 or HWB2) (Seismic Design)
HWB5	Highway	Concrete, Multi-Column Bent, Simple Support (Conventional Design), Non California (Non-CA)
HWB6	Highway	Concrete, Multi-Column Bent, Simple Support (Conventional Design), California (CA)
HWB7	Highway	Concrete, Multi-Column Bent, Simple Support (Seismic Design)
HWB8	Highway	Continuous Concrete, Single Column, Box Girder (Conventional Design)
HWB9	Highway	Continuous Concrete, Single Column, Box Girder (Seismic Design)
HWB10	Highway	Continuous Concrete, (Not HWB8 or HWB9) (Conventional Design)
HWB11	Highway	Continuous Concrete, (Not HWB8 or HWB9) (Seismic Design)
HWB12	Highway	Steel, Multi-Column Bent, Simple Support (Conventional Design), Non California (Non-CA)
HWB13	Highway	Steel, Multi-Column Bent, Simple Support (Conventional Design), California (CA)
HWB14	Highway	Steel, Multi-Column Bent, Simple Support (Seismic Design)
HWB15	Highway	Continuous Steel (Conventional Design)
HWB16	Highway	Continuous Steel (Seismic Design)
HWB17	Highway	PS Concrete Multi-Column Bent, Simple Support - (Conventional Design), Non-California
HWB18	Highway	PS Concrete, Multi-Column Bent, Simple Support (Conventional Design), California (CA)
HWB19	Highway	PS Concrete, Multi-Column Bent, Simple Support (Seismic Design)
HWB20	Highway	PS Concrete, Single Column, Box Girder (Conventional Design)
HWB21	Highway	PS Concrete, Single Column, Box Girder (Seismic Design)
HWB22	Highway	Continuous Concrete, (Not HWB20/HWB21) (Conventional Design)
HWB23	Highway	Continuous Concrete, (Not HWB20/HWB21) (Seismic Design)
HWB24	Highway	Same definition as HWB12 except that the bridge length is less than 20 meters
HWB25	Highway	Same definition as HWB13 except that the bridge length is less than 20 meters
HWB26	Highway	Same definition as HWB15 except that the bridge length is less than 20 meters and Non-CA
HWB27	Highway	Same definition as HWB16 except that the bridge length is less than 20 meters and in CA
HWB28	Highway	All other bridges that are not classified (including wooden bridges)

5.3.2.2 Feature Class: eqHighwayBridge

This feature class provides Earthquake Model-specific information on highway bridges. The most critical parameter in this feature class is soil condition. Building Seismic Safety Council of the National Institute of Building Sciences (NIBS) recommends soil classifications based on in-situ tests carried out to determine shear wave velocity of soils to 30 m depth (Vs30). NIBS established the Building Seismic Safety Council (BSSC), which itself established the National Earthquake Hazards Reduction Program (NEHRP) site classification

system, which is currently used by Hazus. Therefore, accurate soil classification of Northern Cyprus based on NEHRP is required. The regional site classification of Northern Cyprus was carried out by Cagnan et al. [126] in 2012. In their work, they characterized soil conditions using surface seismic (MASW) and standard penetration tests (SPT). They classified the site condition based on NEHRP and Eurocode 8 on 14 different stations. Table 5.5 summarizes the NEHRP global soil classification system and the list of 14 Northern Cyprus sites where soil classes were defined. Hazus soil classification is based on the NEHRP-MASW technique. As can be observed from the table, the majority of Northern Cyprus is classified as Soil Class C. It should be noted that the discrepancies between the two NEHRP approaches are unavoidable due to basics limitations inherent in the application of MASW and SPT [126]. Additionally, as it can be noticed, there was no reported site class for Kalkanli station in the MASW method. Therefore, we assumed Soil Class C for Kalkanli as determined by SPT and as agreed by most of the locations. Table 5.6 shows the required parameters for the bridges in the study region, including the soil type, and Figure 5.10 depicts the NEHRP soil classification for our study region. In this study, liquefaction and landslide susceptibility are not considered, and hence their parameters are not shown in the table.

Table 5.5. NEHRP global soil classification system of Northern Cyprus

Soil Profile Classification System Used by NEHRP						
Soil Class	A	B	C	D	E	F*
V_{s30}	> 1500	760 < V_s ≤ 1500	360 < V_s ≤ 760	180 < V_s ≤ 360	≤ 180	-
Description	Hard Rock	Rock	Very Dense Soil and Soft Rock	Stiff Soils	Soft Soils	Soils requiring site-specific evaluations
List of Soil Classes in Northern Cyprus [126]						
Town	**Lat**	**Long**	**V_{s30} (m/s)**	**NEHRP (MASW)**	**NEHRP (SPT)**	**Eurocode 8 (MASW)**
Lefke	35.13	32.83	592	C	C	B
Guzelyurt	35.19	32.99	310	D	C	C
Kalkanli	35.25	33.02	-	-	C	-
Sadrazamkoy	35.39	32.95	473	C	C	B
Girne	35.34	33.32	571	C	C	B
Esentepe	35.35	33.6	732	C	C	B
Yenierenkoy	35.53	34.18	637	C	C	B
Tuzla	35.17	33.91	304	D	E	C
Magosa	35.13	33.93	449	C	C	B
Beyarmudu	35.04	33.71	554	C	D	B
Haspolat	35.22	33.42	510	C	C	B
Lefkosa	35.18	33.37	344	D	D	C
Gonyeli	35.21	33.32	570	C	C	B
Magosa	35.12	33.94	560	C	D	B

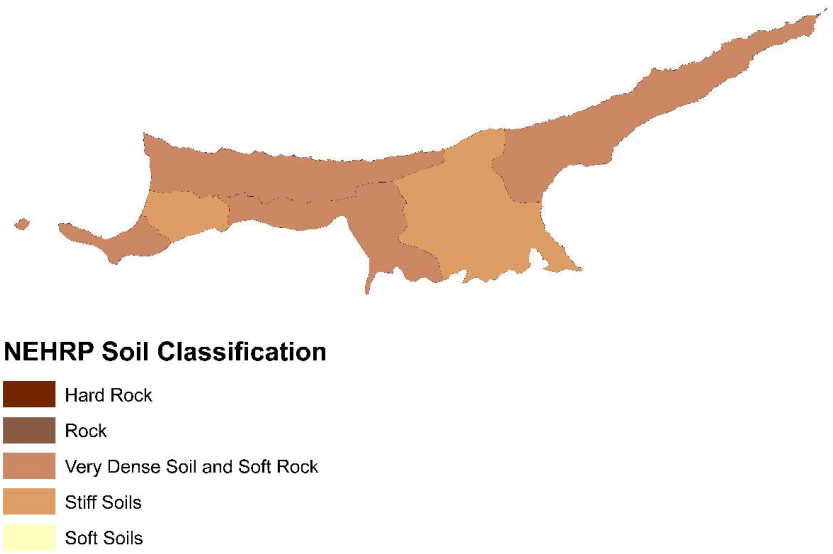

Figure 5.10 NEHRP soil classification of Northern Cyprus

Table 5.6. Required input fields for bridge soil classification in Hazus

Highway Bridge Id	Soil Type	Highway Bridge Id	Soil Type
KK000001	C	KK000011	D
KK000002	C	KK000012	D
KK000003	C	KK000013	D
KK000004	C	KK000014	D
KK000005	C	KK000015	D
KK000006	C	KK000016	D
KK000007	C	KK000017	C
KK000008	C	KK000018	C
KK000009	C	KK000019	C
KK000010	D	KK000020	C

5.3.2.3 Feature Class: hzHighwaySegment

This feature class provides the geometry of highway roads. To create the road network of Northern Cyprus, opensource OpenStreetMap (OSM) data was used. OSM creates and distributes free crowdsourced geographic data. We use the latest OSM shapefiles that are updated at least daily by Geofabrik Co. [127] offering a variety of services related to OSM (e.g., free shapefiles of the global road network). Figure 5.11 shows the latest road network of Northern Cyprus. In this figure, every road, street, or path class defined by OSM [128] is visible.

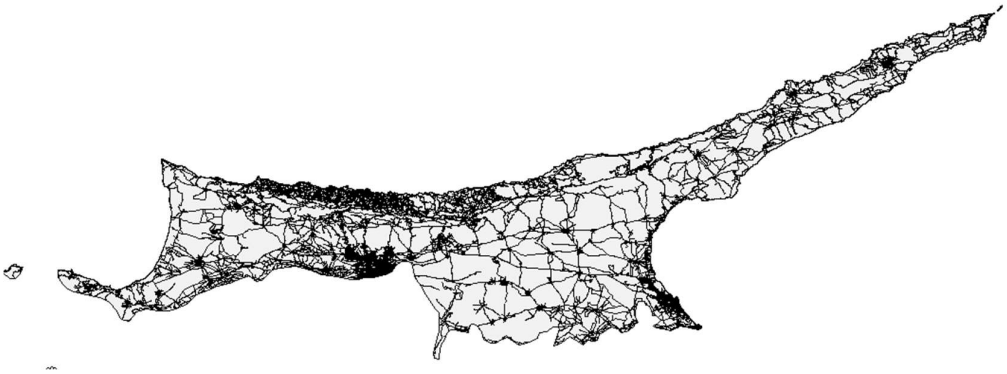

Figure 5.11. The complete transportation network of Northern Cyprus

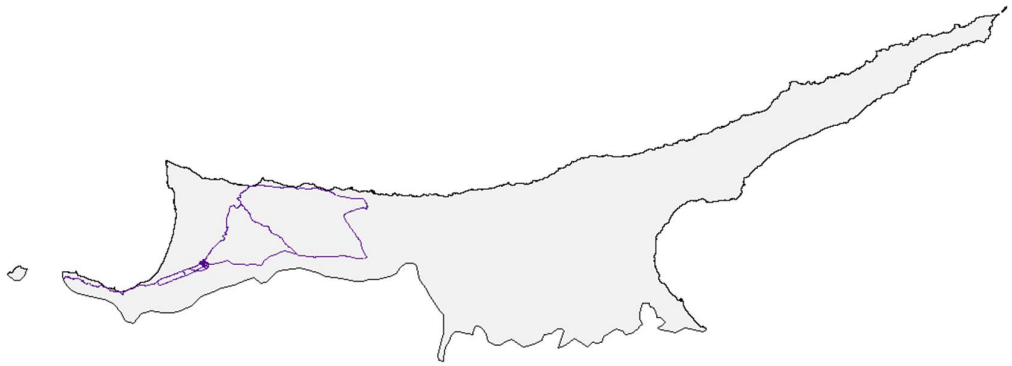

Figure 5.12. The reduced transportation network of the western part of Northern Cyprus

This part of the study is one of the most cumbersome portions of implementing the Northern Cyprus Hazus database as there are no free or available geospatial sources of the transportation network. The time-consuming part is to construct the necessary network suitable for this study where a large number of additions and deletions of the OSM data were necessary.

Google Street Map as a base map was overlaid on top of the study region, facilitating the complexities above. In this way, we determine the major roads connecting the bridges accurately and identify geographically misplaced bridges on the map. We have reduced the network down to the major roads that are connecting the bridges and can provide alternative routes in case of failures. Moreover, we have only included the roads suitable to drive on (e.g., asphalt roads) and roads that can accommodate the most cars in case of detours. The network is kept fully connected to ensure maximum flow on each road. Figure 5.12 shows the reduced transportation network of Northern Cyprus concerning the study region. Major roads in this study are defined as the links that connect two bridges as well as the highways. Urban roads are defined such that they do not connect two bridges in a given link and serve as detour roads if needed.

5.3.2.4 Feature Class: eqHighwaySegment

This feature class provides Earthquake Model-specific information on the highway roads. There is no vital explanation of this feature class as it only links the roads identified in the previous section for the estimation of hazards, damages, and loss of functionality.

5.3.2.5 Feature Class: hzTract

This features class is similar to syTract, with the only inclusion being to provide the extra details on the tract and aggregated blocks regarding the seismic design of buildings in each tract. This is required for Hazus to initialize the initial aggregation, though it would not be of importance for our case study as we do not consider census block.

5.3.3 Database Transfer via SQL and Python

After the initial database creation is done, the two newly created databases i.e., syHazus.mdb and Hazus_Database.mdb will be transferred to the Hazus inventory. The procedure requires Microsoft SQL Server Management Studio (SSMS) 18 and Python 2.7 (default installation with ESRI ArcGIS 10.5.1). Initially, a backup of the default syHazus database in SSMS is taken to make sure that any changes can be reverted in case of the addition or deletion of Northern Cyprus Inventory Data. To replace the Hazus inventory, a State dataset has to be selected first. From the datasets available on the Hazus-FEMA website [129], the state of Puerto Rico (PR) is selected because it is the smallest dataset available, which makes the replacement process much faster. The PR database is attached to the SQL server and renamed as the Northern Cyprus state name defined in sy_State.mdb, i.e., KK. The python script developed by Rozella [49] is used to transfer the inventory to Hazus. The script is available in Appendix A. With a slight modification to the code, if run successfully, upon creating a Hazus region at the state geographical level, “KKTC” should appear as the only available option, as shown in Figure 5.13.

Table 5.7. Full bridge description and class definition

OBJECT ID	Highway Bridge Id	Bridge Index Label	Bridge Class	Lat.	Long.	Num Spans	Max Span Length (m)	Length (m)	Width (m)	Skew Angle (°)	Pier Type	Abutment Type	Span Continuity	Material
1	KK000001	B9	HWB8	35.142	32.835	3	9	28	7	0	PW	R	C	RC
2	KK000002	B10	HWB3	35.142	32.819	1	4	4	9	27	-	S	C	RC
3	KK000003	B20	HWB28	35.142	32.819	1	3	3	4	0	-	S	C	RC
4	KK000004	B11	HWB8	35.144	32.808	2	6	17	9	27	PW	R	C	RC
5	KK000005	B8	HWB15	35.147	32.848	2	10	20	7	0	PW	S	SS	Steel
6	KK000006	B7	HWB28	35.154	32.870	2	8	13	7	0	PW	S	C	RC
7	KK000007	B6	HWB3	35.158	32.898	1	6	12	7	0	PW	R	C	RC
8	KK000008	B5	HWB28	35.164	32.905	9	9	65	8	0	PW	R	D	Masonry
9	KK000009	B12	HWB28	35.168	32.740	3	8	50	9	17	PW	R		RC
10	KK000010	B4	HWB3	35.188	32.966	1	3.5	4.3	9	0	-	R	C	RC
11	KK000011	B15	HWB3	35.189	32.999	1	5	5	7.2	50	-	S	C	RC
12	KK000012	B14	HWB3	35.190	32.996	1	5	5	11	40	-	R	C	RC
13	KK000013	B13	HWB8	35.191	32.996	2	4	8	12	31	PW	R	SS	RC
14	KK000014	B2	HWB8	35.204	32.996	10	10	101	11.5	0	PW	R	SS	RC
15	KK000015	B3	HWB8	35.204	32.994	8	3	26	13	20	PW	R	C	RC
16	KK000016	B1	HWB8	35.217	33.006	2	6	13	10	0	PW	R	SS	RC
17	KK000017	B16	HWB28	35.337	33.069	1	5	5	9	0	-	R	C	RC
18	KK000018	B17	HWB28	35.338	33.069	1	6	6	8	0	-	R	C	RC
19	KK000019	B18	HWB3	35.339	33.071	1	6	6	8	36	-	R	C	RC
20	KK000020	B19	HWB3	35.350	33.085	1	5	6	8	34	-	R	C	RC

Pier Type: PW (Pier Wall)
Abutment Type: S (Seated), R (Rigid)
Span Continuity: C (Continuous), SS (Simply Supported), D (Discontinuous)
Material: RC (Reinforced Concrete)

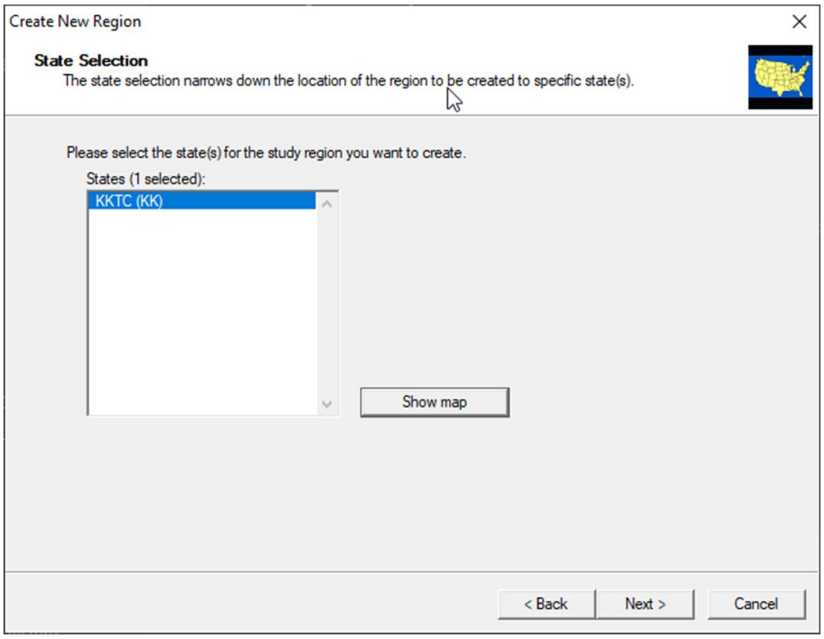

Figure 5.13. Creating a new region with Northern Cyprus as one of the options in Hazus

Upon creating the study region would, the Northern Cyprus boundary should appear in the interface. Figure 5.14 shows the completed database of Northern Cyprus and its transportation network inventory successfully initialized in Hazus.

5.4 Chapter Summary

In this chapter, we presented the exact procedures taken to adapt the Hazus inventory to our region. We outlined the necessary assumptions as well as the detailed analysis of the region in terms of its transportation network and site condition. The current inventory is created in such a way to accommodate future implementations of indirect cost and social loss estimation, e.g., population exposure. The necessary files, codes, and tools are uploaded online, as outlined in Appendix A.

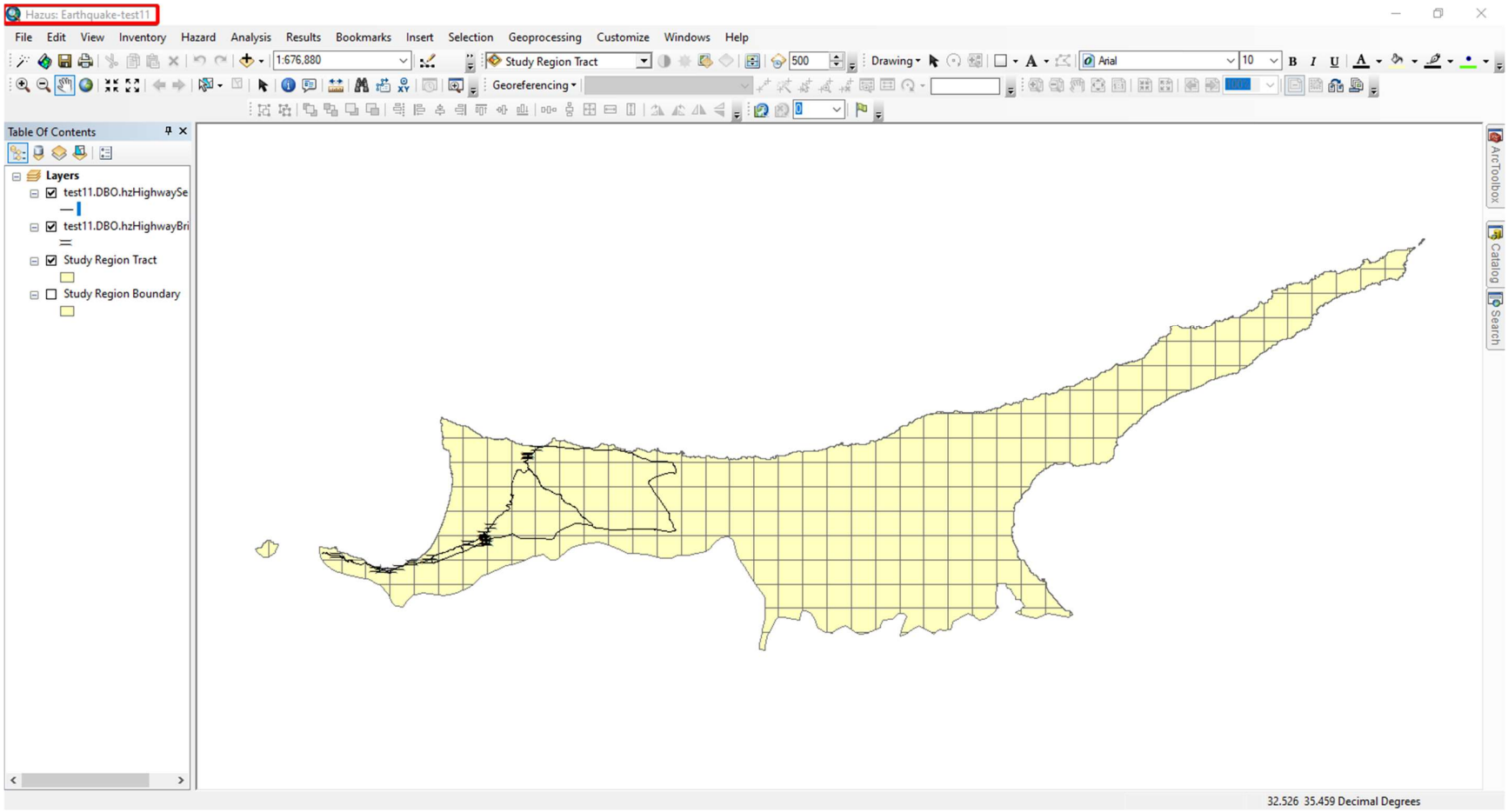

Figure 5.14. Hazus interface with Northern Cyprus as the study region boundary

CHAPTER 6

SEISMIC RISK ASSESSMENT OF NORTHERN CYPRUS TRANSPORTATION NETWORK

6.1 Introduction

After collecting the relevant transportation data and the hazard maps, scenario-based analysis of seismic risk assessment can be conducted. In this chapter, emphasis will be put on network performance and the functionality loss of the transportation system for different earthquake events. The selected region for this research is limited to the western part of Northern Cyprus. It was previously shown that (see Chapter 3) this part of the island can experience earthquake moment magnitudes of up to M7.4. The probability of such events, however, is extremely low as it was also proven in two separate studies; for 5% exceedance probability in 50-years, low PGA values are expected. However, due to uncertainties in PSHA analysis [130] and the fact that Cyprus has previously encountered devastating historical earthquakes outside our recorded history, e.g., 1222 Cyprus (~M7.0–7.5), the risk of experiencing sever events is high, as these events have return periods of 1000-2500 years. To realize different earthquake scenarios, we, therefore, opted for ShakeMap models for the seismic hazards input into Hazus. We will then use the output of Hazus, i.e., the component damage states of bridges for the transportation network, and incorporate the results for assessing the vulnerability of the network in terms of different performance indicators described in Chapter 4.

6.2 Earthquake Scenarios

The choice of the location for simulating different earthquake magnitudes and depths can significantly influence the loss estimation results. Given that the study region is quite large (approx. 50 x 50 km^2), for a very strong to a severe event (0.25-0.4g PGA), the structural loss can vary significantly. Area model simulation is one of the better approaches to reduce the inconsistency between the seismic events for large areas. This approach is the method used in PSHA. Since the bridges are distributed in three different districts, mainly on a stretch of one continuous link, we simulate three different scenarios using ShakeMap with the parameters specified in 3.4 and the same scenarios in Hazus' arbitrary hazard module. The latter is done for validation purposes. GMPE in Hazus hazard analysis is only limited to one model, and it is assigned as Boore and Atkinson [71]. The scenarios' parameter selection is shown in Table 6.1. The scenario in Lefke is the event illustrated in Figure 3.11 with the same parameters except for a higher magnitude (M7.4). An additional scenario is also tested for an event that is more likely to occur for the current region, i.e., Scenario 4.

Table 6.1. Earthquake scenarios information

Parameters	ShakeMap DSHA and Hazus Arbitrary Event			ShakeMap
	Scenario 1	Scenario 2	Scenario 3	Scenario 4
District	Lefke	Guzelyurt	Girne	Guzelyurt
Coordinate	35.121, 32.809	35.202, 32.976	35.330, 33.033	35.202, 32.976
Magnitude	7.4	7.0	6.5	5.5

The events listed in the table for the Scenario 1 is closely related to the 2475-year return period, Scenario 2 and 3 falls in 975-year return period; and finally, Scenario 4 shows an event with 475-year return period [57]. Seismic events with a 10% probability of exceedance in 50-years (i.e., 475-year return period) result in PGA of around 0.3g which is similar to previous studies. The PGA shaking intensity for such an example is depicted in Figure 6.1 (the epicenter is selected according to Scenario 2 at depth 30 km with magnitude M5.5). For most of the bridges, however, such moderate to strong shaking intensities would not result in severe failures. This is more evident for the bridges in Northern Cyprus that are typically short-span and exhibit a high modulus of elasticity. To simulate the worst-case scenario, we, therefore, rely on events that can produce at least 0.40g PGA. These events would likely fall in the 975-year return period or higher events [57]. It should be note that, magnitude is not the sole parameter of indicating damaging earthquakes. Evens with depths around 0-10 km for lower magnitudes can be destructing as well, if not more severe.

The IM shaking grids for all four scenarios are generated using the command line interface of the ShakeMap software. The results for each scenario are combined into one grid.xml file that will be used to input the hazard results into Hazus. The data sources and results of each

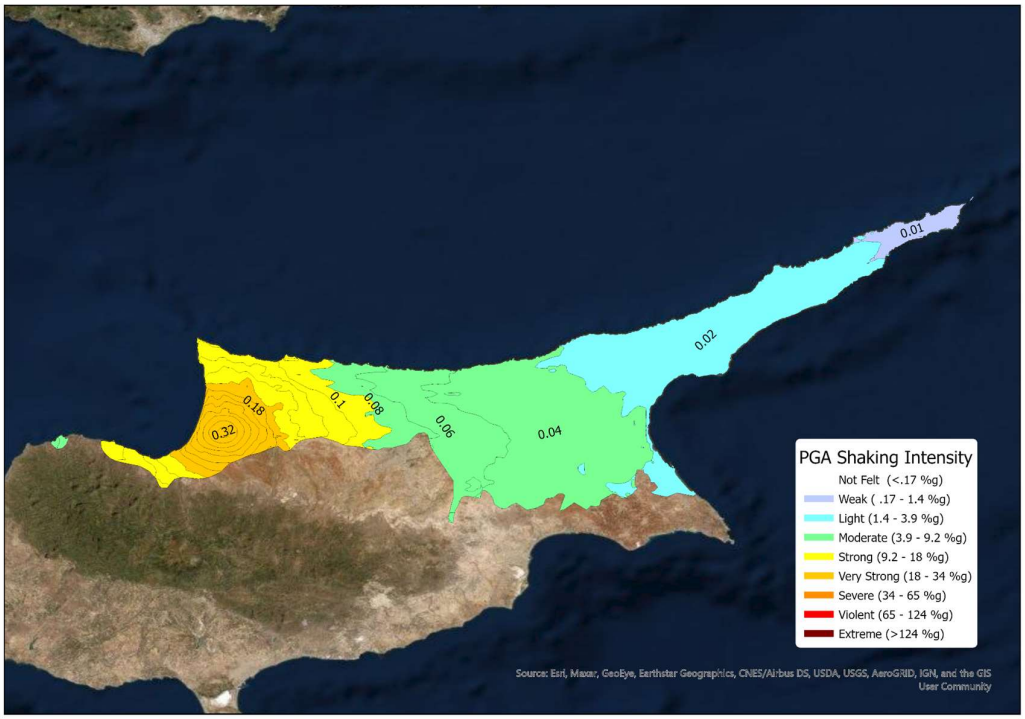

Figure 6.1. PGA shaking intensity maps for Scenario 4

hazard scenario are itemized in Appendix A and B. The results are bounded to the study region boundaries to reduce the time to import the grids into Hazus. Larger grids would take anywhere between 5-10 minutes or more.

6.3 Structural Loss Analysis

The following sections describe two methods of estimating structural losses from ShakeMap hazard maps and built-in Hazus deterministic arbitrary-event hazard analysis.

6.3.1 Structural Loss Estimation from ShakeMap Hazard Maps

From Table 3.4 for each best damage ratios (from now on, referred to as the mean damage ratio DR_{ds}) and for each range of DR_{ds} in the table, we can calculate the mean μ_m and the standard deviation σ_m of damage states for an event m per bridge as:

$$\mu_m = \sum_{k=1}^{4} P(DS = k|IM_m) DR_{ds_k} \tag{6.1}$$

$$\sigma_m = \sqrt{\sum_{k=1}^{4} P(DS = k|IM_m) \cdot [DR_{ds_k} - \mu_m]^2} \tag{6.2}$$

Table 6.2. Overall damage state description for Scenario 1

Bridge ID Number	Damage State $P(DS = k\|IM_m)$					Overall Damage		
	None	Slight	Moderate	Extensive	Complete	μ_1	σ_1	Mean Damage State
KK000001	0.321	0.161	0.132	0.206	0.181	0.188	0.219	Extensive
KK000002	0.913	0.036	0.025	0.02	0.006	0.014	0.084	Slight
KK000003	0.913	0.045	0.021	0.016	0.005	0.012	0.077	Slight
KK000004	0.448	0.128	0.125	0.174	0.125	0.182	0.298	Extensive
KK000005	0.939	0	0	0.047	0.015	0.027	0.129	Slight
KK000006	0.893	0.054	0.026	0.021	0.006	0.015	0.084	Slight
KK000007	0.856	0.068	0.035	0.031	0.01	0.023	0.106	Slight
KK000008	0.854	0.069	0.035	0.031	0.011	0.015	0.048	Slight
KK000009	0.94	0.031	0.015	0.011	0.003	0.007	0.045	None
KK000010	0.906	0.048	0.022	0.018	0.005	0.013	0.077	Slight
KK000011	0.922	0.001	0.035	0.032	0.011	0.022	0.111	Slight
KK000012	0.922	0.02	0.028	0.024	0.007	0.016	0.091	Slight
KK000013	0.516	0.113	0.117	0.154	0.099	0.150	0.274	Extensive
KK000014	0.52	0.16	0.109	0.134	0.077	0.062	0.080	Moderate
KK000015	0.527	0.141	0.111	0.139	0.082	0.068	0.087	Moderate
KK000016	0.541	0.158	0.105	0.127	0.07	0.115	0.242	Moderate
KK000017	0.996	0.003	0.001	0	0	0.000	0.003	None
KK000018	0.993	0.005	0.001	0.001	0	0.000	0.009	None
KK000019	0.993	0.003	0.002	0.001	0	0.001	0.009	None
KK000020	0.998	0.001	0.001	0	0	0.000	0.003	None

Equation (6.1) is a variation of Equation (3.27) where k indicates the bridge damage state. For these calculations, the "None" damage state is neglected. Table 6.2 shows the overall damage states for the bridges considering Scenario 1. Tables for damage state for other scenarios are provided in Appendix C. The results are also depicted in Figure 6.2. As it can be noticed from the figure, there seem to be large standard deviations for some bridges. This is mainly due to the algorithm used to calculate the damage states. Moreover, the fragility curves for some bridge categories are unrealistic; hence the standard deviation of damage state values for these types of bridges can be relatively high. The overall mean damage state for all four scenarios is depicted in Figure 6.3 - Figure 6.6.

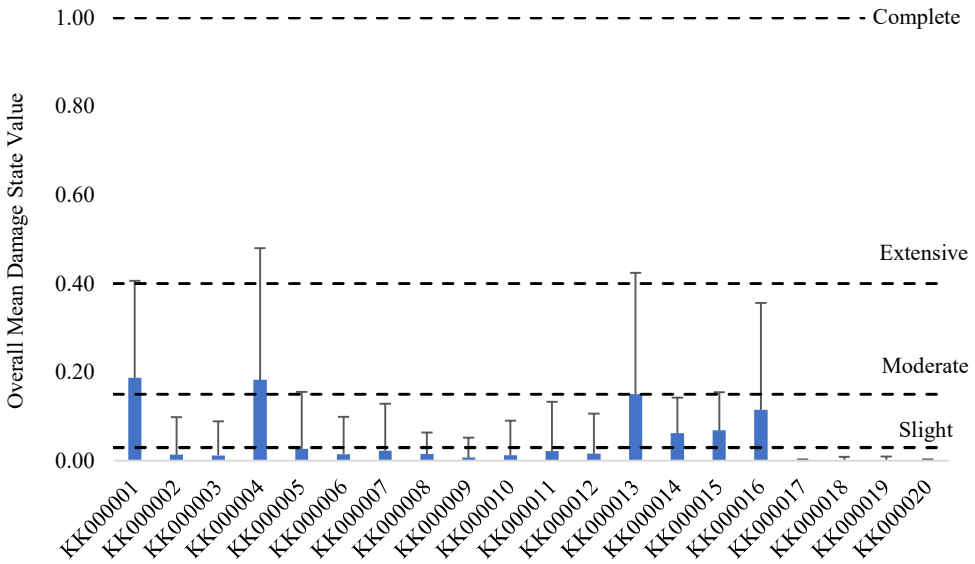

Figure 6.2. Overall mean and standard deviation bridge damage state values for Scenario 1 (M7.4)

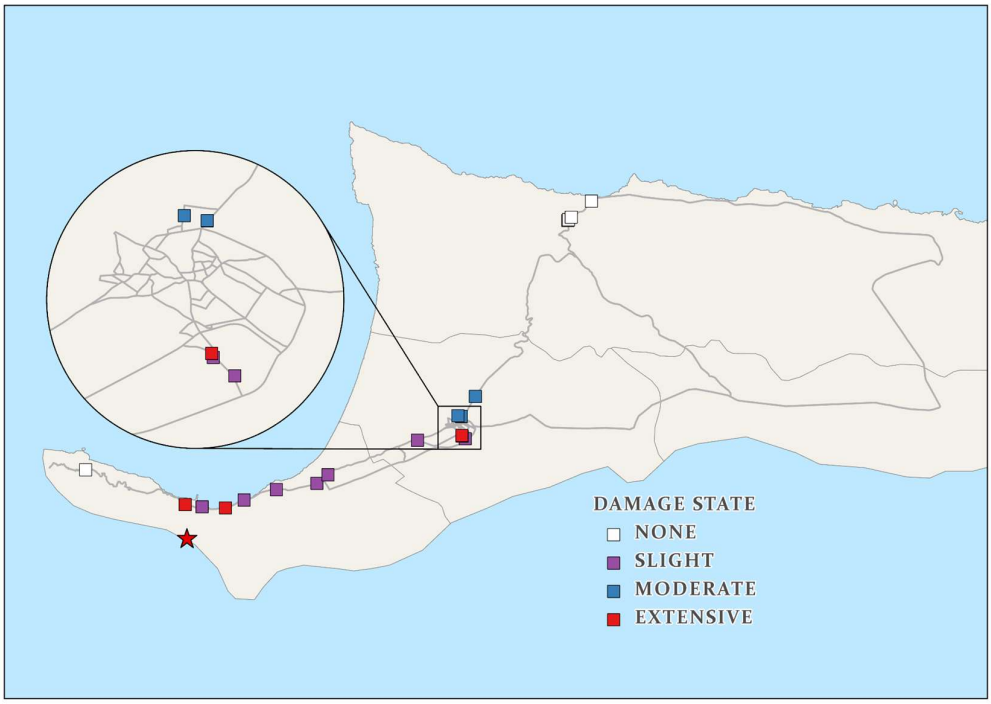

Figure 6.3. Scenario 1 overall damage state – Lefke M7.4

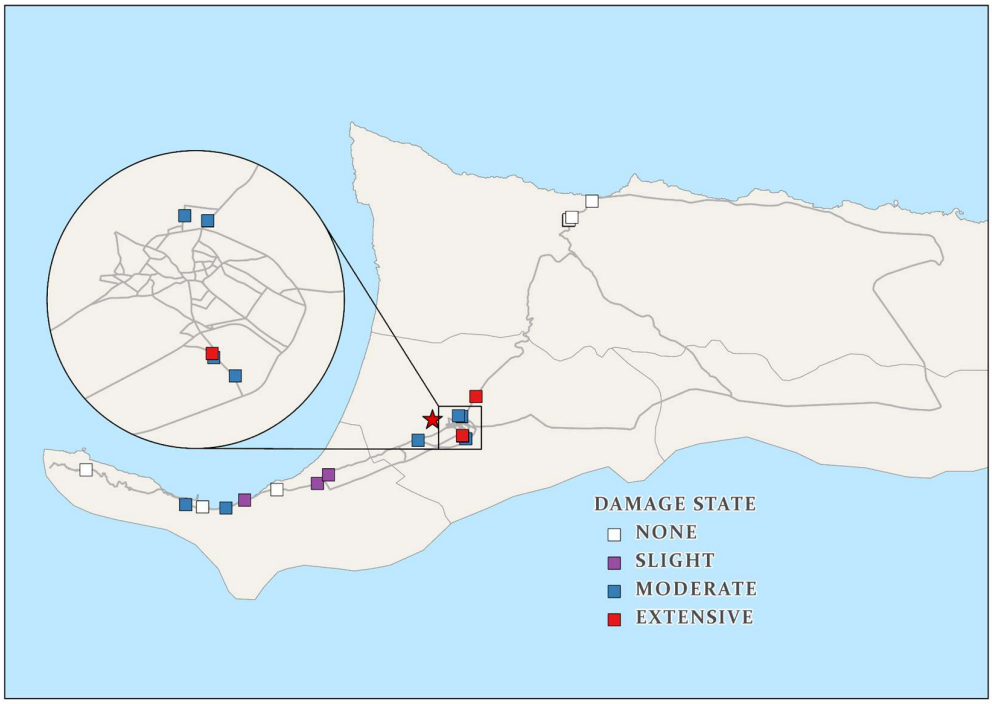

Figure 6.4. Scenario 2 overall damage state – Guzelyurt M7.0

Figure 6.5. Scenario 3 overall damage state – Girne M6.0

Figure 6.6. Scenario 4 overall damage state – Guzelyurt M5.5

We can observe that with an increase in the magnitude of an earthquake event and how close the bridges are to the epicenter, the possibility of the higher damage state. The only exception would be for Scenario 1 where bridges KK000001 and KK000004 experience extensive damage as it is expected due to how close they are located from the epicenter, whereas the other bridges in the vicinity experience slight damage state. These two particular bridges were assigned as HWB8 class, which shows more susceptibility to damage for any given IM. This is more evident by analyzing their fragility curves in Figure 6.7. As can be seen from the figure, the exceedance probabilities of HWB8 are higher than HWB3. Therefore, for the same level of IM (in this figure, IM = SA (1.0. sec in g) is depicted), HWB8 experiences higher damage state probability. We can have a better idea of how sensitive the fragility curves are once we obtain the actual damage state exceedance probabilities for all 20 bridges in the study region in the future (see 3.5.1).

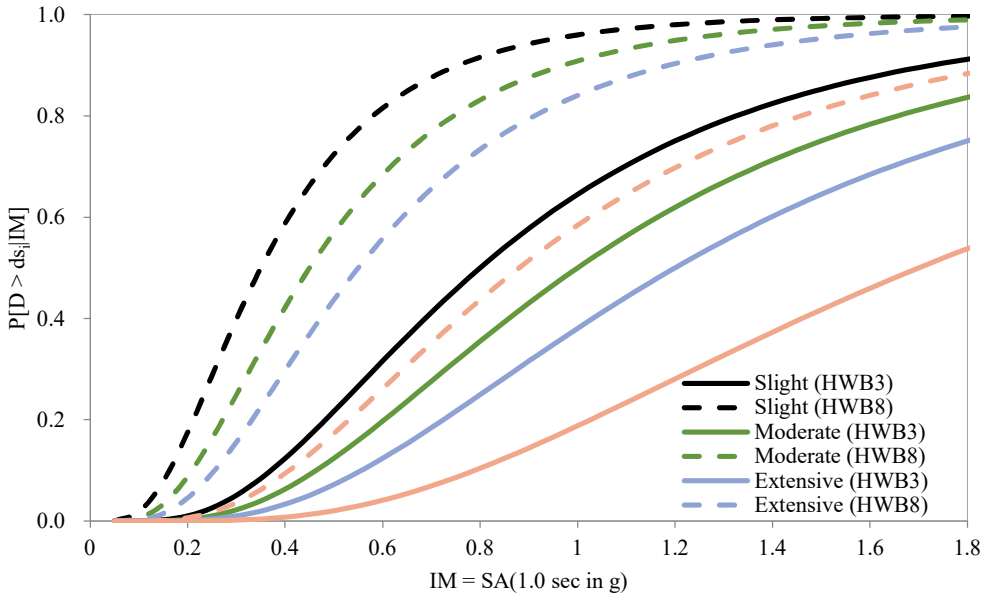

Figure 6.7. Comparison between HWB3 and HWB8 fragility curves

In general, we can summarize the distribution of damage states for the four bridges classes defined in the region in Table 6.3.

Table 6.3. Damage state distribution of all four scenarios

None Damage State				
Type	Scenario 1	Scenario 2	Scenario 3	Scenario 4
HWB3	2	3	7	8
HWB8	0	0	1	5
HWB15	0	0	1	1
HWB28	3	5	5	6
Total	5	8	14	20
Slight Damage State				
Type	Scenario 1	Scenario 2	Scenario 3	Scenario 4
HWB3	5	1	1	0
HWB8	0	0	0	0
HWB15	1	1	0	0
HWB28	3	1	1	0
Total	9	3	2	0
Moderate Damage State				
Type	Scenario 1	Scenario 2	Scenario 3	Scenario 4
HWB3	0	4	0	0
HWB8	3	3	4	0
HWB15	0	0	0	0
HWB28	0	0	0	0
Total	3	7	4	0
Extensive Damage State				
Type	Scenario 1	Scenario 2	Scenario 3	Scenario 4
HWB3	1	0	0	0

HWB8	2	2	0	0
HWB15	0	0	0	0
HWB28	0	0	0	0
Total	3	2	0	0

6.3.2 Structural Loss Estimation from Hazus Hazard Module

To validate and compare the structural loss obtained from ShakeMap hazard data, we perform the same analysis in Hazus built-in hazard module. In the deterministic hazard section of Hazus, "Arbitrary event" is selected with attenuation function set as Boore and Atkinson [70] Strike-Slip fault type. The fault parameters of the simulated scenarios are based on the fault located on the western coast of Northern Cyprus (see Figure 3.4 for location and http://diss.rm.ingv.it/share-edsf/sharedata/SHHTML/GRCS699INF.html for the fault information). Therefore, fault rupture orientation of 28° CW from N and 70° dip angle is selected for each of the four scenarios. Surface and subsurface rupture lengths are automatically calculated based on the magnitude using the empirical relationships described in [131].

The comparison between Hazus and ShakeMap damage estimates is illustrated in Figure 6.8. In Hazus arbitrary event module, the none damage state appears to be lower in number when compared to ShakeMap. This is more noticeable for higher earthquake magnitudes, i.e., Scenario 1 or 2. This means that there are more bridges, for each scenario, that experience at least slight damage. Looking at the graph for slight damage state, one can see that ShakeMap hazard estimates cause more slight damage for higher magnitudes than Hazus built-in hazard estimates. As the magnitude decreases, however, the reverse is true, at least up to a certain limiting magnitude (in Scenario 4, both methods result in no slight damage). For both moderate and extensive damage states, Hazus hazard module produces a higher number of damaged bridges associated with the damage states mentioned above. Therefore, from the first four damage states, we can draw a conclusion in which the ShakeMap hazard approach causes bridges to exhibit none or slight damage. In contrast, there are more damaged bridges related to moderate and extensive damage states in Hazus. Additionally, we can see complete damage to some bridges in Hazus hazard estimation, in which there was none for the ShakeMap model.

The apparent differences between the two approaches are probably due to two main reasons: different GMPEs and the assumptions made in ShakeMap that includes no fault/rupture definition and also, the default fault assignment in Hazus can contain high degrees of uncertainty, typically in the orientation, dip angle, and surface rupture length. This is more significant for high magnitudes of earthquakes. Sensitivity analysis is therefore needed to adjust the fault parameters inside Hazus. The Finite-rupture Approximation model used in

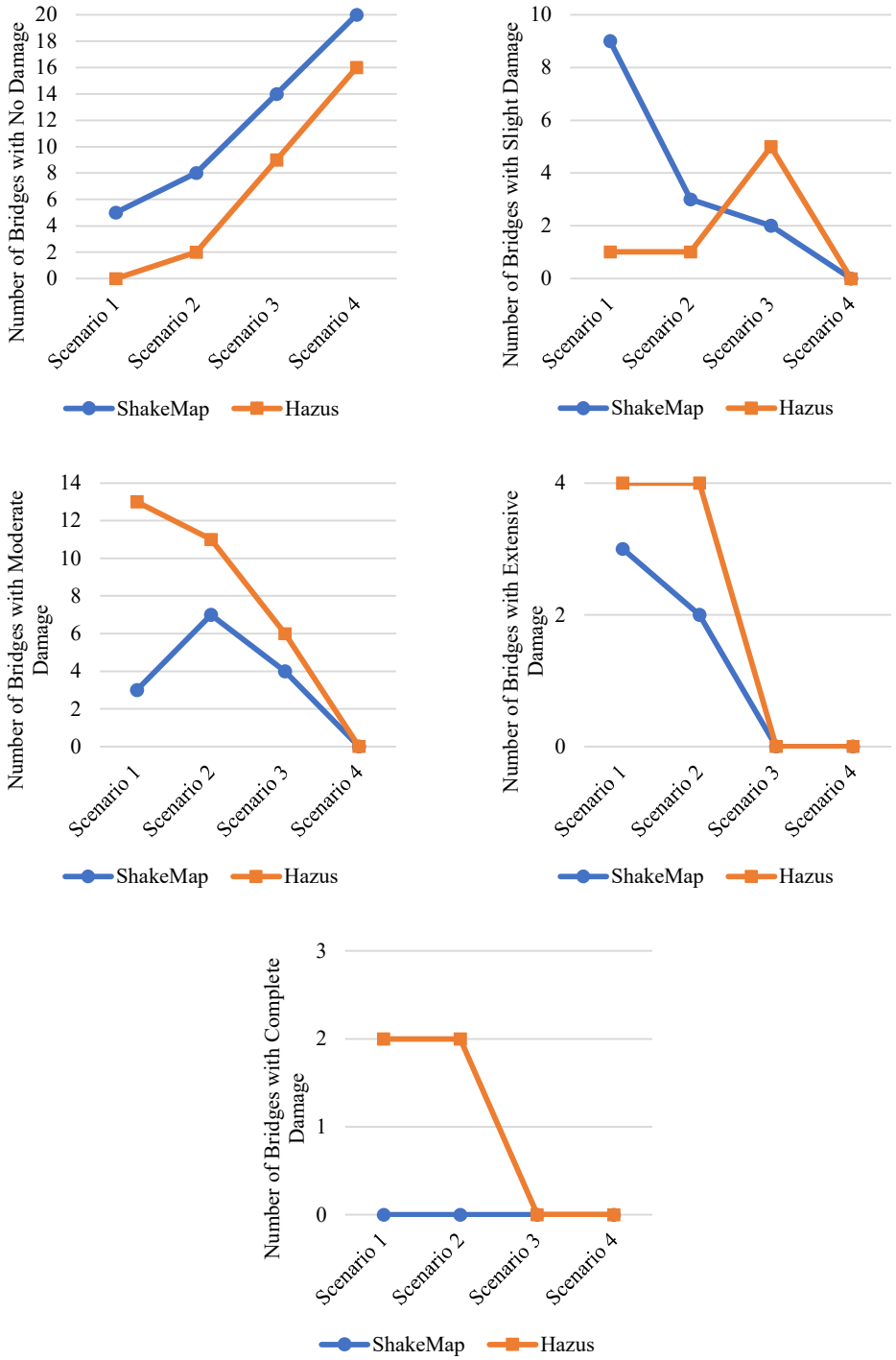

Figure 6.8. Comparison of estimates of number of bridges damaged based on ShakeMap and Hazus hazard analysis

ShakeMap [132] can adjust the uncertainties in the predicted ground motion where no rupture geometry and dimension is defined. This model also contains slight uncertainties when approximating rupture characteristics. In our future study, we will input the QuadRupture rupture model in ShakeMap to validate our analysis. As it stands now, the fragility curves in

Hazus with ShakeMap input will be used as the basis of the structural and operational loss estimation. With the incorporation of the actual fragility curves and adjustment to ShakeMap hazard analysis in the future, we can expect a better representation and estimation of the losses due to seismic events.

6.4 Estimation of Bridge Restoration Model

Depending on the overall level of the damage, we can roughly estimate the direct cost, or more precisely, the restoration cost of the bridges. As explained before, it is assumed that the repair cost is proportional to the replacement value. This relationship was described as damage ratios modified after Hazus. Using the following equation, we can determine bridge restoration cost C_{RPm} for an event m as:

$$C_{RPm} = \sum_{n=1}^{N} \mu_m C_n \tag{6.3}$$

where μ_m is the mean damage sate per bridge for event m and C_n is the replacement cost of bridge n. The replacement cost is calculated by multiplying the deck area by the unit area replacement cost. We assumed the replacement cost of the bridges, as indicated in Table 6.4.

Table 6.4 Replacement value per bridge class

Bridge Class	Unit Area Replacement Cost ($/m^2)
HWB3	850
HWB8	960
HWB15	1140
HWB28	800

The total structural loss for the four scenarios is shown in Figure 6.9. As can be observed from the figure, Scenario 2 incurs higher structural loss compared to a higher magnitude scenario (e.g., Scenario 1, M7.4 event) because there are more vulnerable bridges in the region, i.e., Guzelyurt. Moreover, HWB8 generates higher losses as expected. The exceedance probabilities of this class of bridges are higher, as previously described. The uncertainties in the derivation of the losses can vastly impact the strategy taken to mitigate such losses.

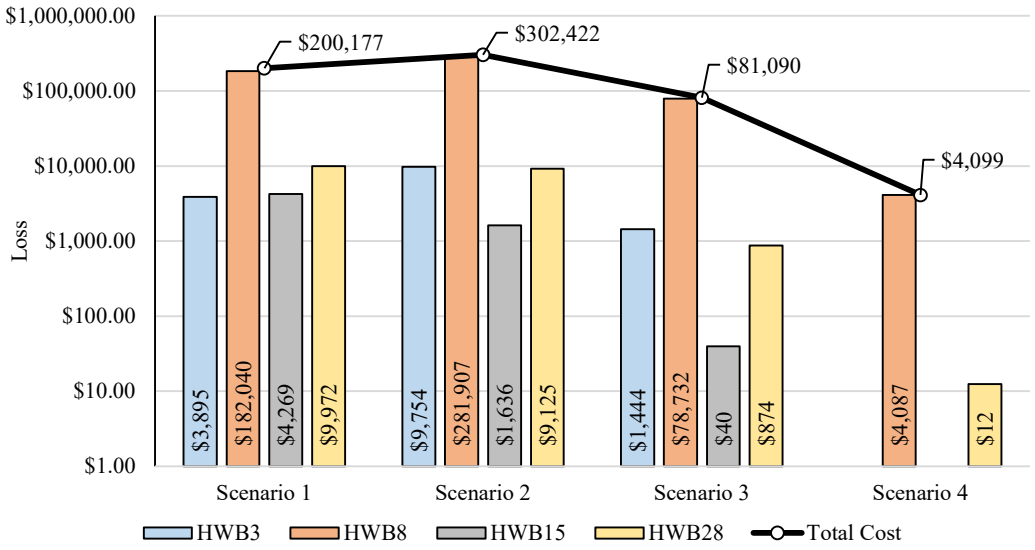

Figure 6.9. Total structural loss per bridge class

For mitigation scenarios, where retrofit strategy is applied for certain bridges, the retrofit cost C_R can be expressed as being proportional to the replacement value as:

$$C_{Rm} = \sum_{m=1}^{M} C_{RPm} r_m \tag{6.4}$$

where r_n is the retrofit cost ratio set equal to 20%. This is independent of the seismic event, and due to the complexity of the estimating retrofit value for each bridge, the ratio is assumed to be constant. Seismic retrofitting of bridges before earthquake events, assuming that it does not exceed the total repair cost of the bridge, can reduce the structural losses significantly. The reduction in the loss can be assigned as the benefit achieved from avoiding replacement costs. In the subsequent section, the cost-effectiveness of bridge retrofit, including the operational losses in terms of cost-benefit analysis, will be investigated.

The amount of time required to repair a damaged bridge depends on the state of the damage. The Hazus methodology assumes the bridge capacity starts to recover right after the event and increases following a CDF function. Moreover, the time it takes to 100% restoration follows the fact that the budget is unlimited, and therefore, the analysis becomes simple. However, the uncertainty in developing functions that include bridge characteristics, budget limitations, and other factors is complicated and is beyond the scope of this study. The Hazus CDF restoration model is expressed as:

$$R(t) = \Phi\left(\frac{t - m_{t,ds}}{\sigma_{t,ds}}\right) \tag{6.5}$$

where $m_{t,d}$ and $\sigma_{t,d}$ indicate mean and standard deviation of the restoration curve parameters for each of the damage state ds. Hazus provides the necessary parameters for developing restoration curves for each damage state, as shown in Table 6.5, resulting in restoration curves depicted in Figure 6.10.

Table 6.5. Parameters of Hazus restoration function

	Days to restore 100% functionality (days)	
Damage State	Mean	Standard Deviation
Slight	0.6	0.6
Moderate	2.5	2.7
Extensive	75	42
Complete	230	110

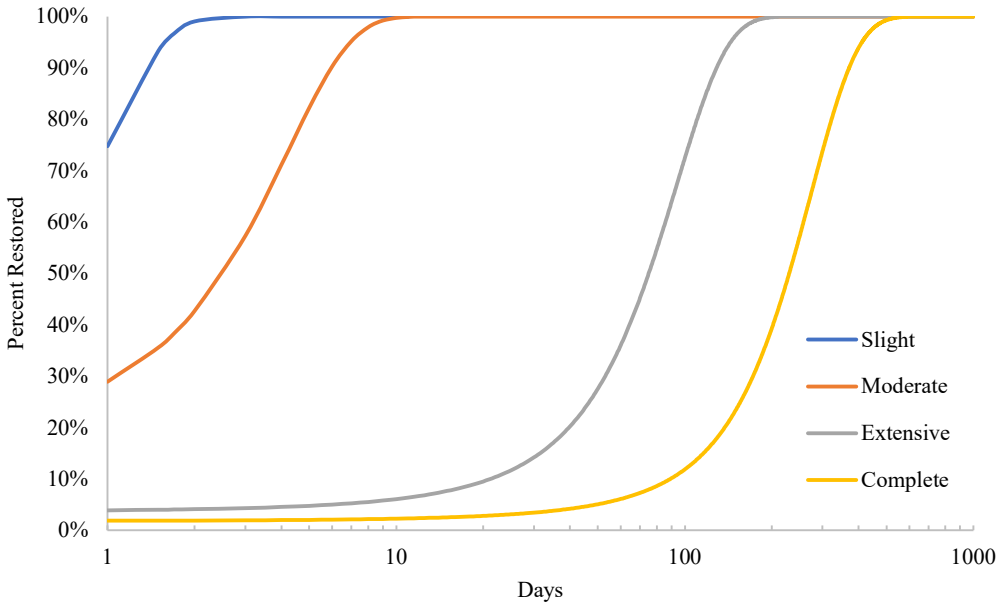

Figure 6.10. Restoration curves for highway bridges in Hazus methodology

6.5 Transportation Network Performance and Loss Analysis

In line with the structural loss analysis in the previous section, the following subsections try to estimate the transportation network performance loss in terms of the topological vulnerabilities and operational losses, e.g., travel time loss described in Chapter 4.

6.5.1 Post-earthquake Network Reliability Indices

For the scenarios tested in this study, the bridge network did not suffer from complete failure. To determine the post-earthquake network topological indicators, however, we need to assume temporary network failure for certain bridges. Therefore, based on restoration curves generated before (see Figure 6.10), we assume for the first couple of days after an earthquake, bridges that experience moderate to complete damages are non-functional. Therefore, for each scenario, these bridges and the links associated with these bridges are removed from the network. The results of the topological vulnerability analysis are shown in Table 6.6. In terms of reliability, Scenario 2 is the worst-case scenario. On average, however, the first three scenarios have shown a reduction in the network reliability indices. There was no change in Scenario 4 as expected.

Table 6.6. Transportation network reliability indicators before and after an earthquake

		Scenario 1	Scenario 2	Scenario 3	Scenario 4
Index	Before	After (% Change)	After (% Change)	After (% Change)	After (% Change)
V	98	90 (-8)	**86 (-12)**	93 (-5)	*No Change*
E	134	121 (-10)	**117 (-13)**	126 (-6)	
L	124 km	99 km (-20)	**96 km (-23)**	109 km (-12)	
$\delta(G)$	47 km	48 km (2)	49 km (4)	**62 km (32)**	
μ	37	33 (-11)	**32 (-14)**	34 (-8)	
α	0.19	0.19 (0)	0.19 (0)	0.19 (0)	
β	1.36	1.36 (0)	1.36 (0)	1.35 (-1)	
γ	0.47	0.46 (-2)	0.46 (-2)	0.46 (-2)	
η	0.93 km	**0.81 km (-13)**	0.82 km (-12)	0.87 km (-6)	
π	2.64	2.1 (-20)	1.95 (-26)	**1.75 (-34)**	

6.5.2 Post-earthquake Structural Loss at Node and Edge Level

We follow the steps we took in 4.3.3 to determine the post-earthquake structural loss. Instead of providing maps for each indicator, we will present percent changes in the average and maximum values for each indicator. Table 6.7 presents the results of the transportation network structural loss for the scenarios simulated in this study. Similar to Table 6.6, we can observe that Scenario 2 shows, on average, the maximum amount of network structural loss. The results above suggest that the District of Guzelyurt (Scenario 2) is more vulnerable to losses in the transportation network in terms of the indicators explained previously.

Table 6.7. Transportation network structural properties before and after an earthquake

Index	Before	Scenario 1	Scenario 2	Scenario 3	Scenario 4
		After (% Change)	After (% Change)	After (% Change)	After (% Change)
$^{max}C_D$	4	4 (0)	4 (0)	4 (0)	*No Change*
$^{avg}C_D$	2.73	2.75 (1)	2.76 (1)	**2.71 (-1)**	
$^{max}C_B(v)$	1141	**885 (-22)**	943 (-17)	1017 (-11)	
$^{avg}C_B(v)$	428	340 (-20)	**333 (-22)**	397 (-7)	
$^{max}C_B(e)$	904	703 (-22)	**694 (-23)**	842 (-7)	
$^{avg}C_B(e)$	284	222 (-22)	**217 (-24)**	266 (-6)	
$^{max}C_C$	13	13 (0)	13 (0)	13 (0)	
$^{avg}C_C$	0.72	0.77 (7)	0.71 (-1)	**0.7 (-3)**	
^{max}GI	24	23 (-3)	**23 (-4)**	23 (-3)	
^{avg}GI	12.9	**13.1 (3)**	13.1 (2)	12.6 (-2)	
$^{max}\lambda_s$	2.77	2.33 (3)	**2.92 (29)**	2.33 (3)	
$^{avg}\lambda_s$	0.2	**0.23 (15)**	**0.23 (15)**	0.21 (5)	

Following the outcomes in the direct loss estimation, i.e., the damage to bridges, we can see that combining the two analyses, the district of Guzelyurt, is in fact, in the risk of catastrophic failure. Scenario 2 is proven to be the worst outcome that can potentially result in total isolation of the district from the nearby districts, cities, and villages. To demonstrate this risk visually, in the case of similar events as in Scenario 2, we can expect a damaged transportation network, as shown in Figure 6.11. The outcome of this scenario is devastating as it will completely cut off fast access to nearby cities and villages for the first responders. To travel from METU NCC to Guzelyurt for example, the drivers have to make a circle around the island. The European University of Lefke will have no access to the nearest hospital or fire stations, nor can commute anywhere as they will be isolated. These are only some of the outcomes of this scenario.

To mitigate these catastrophic situations, there needs to be a policy change. Firstly, retrofitting of the vulnerable bridges in an optimal manner. Some bridges are already deteriorating due to weather, flood, and other hazards in the region. The analysis of this study does not consider deterioration effects; therefore, even the bridges that are undamaged or slightly damaged could be at serious risk of total collapse, even for smaller earthquake magnitudes. Secondly, mitigation strategies have to be put in place to accommodate emergency responders as fast as possible in case of network failure. This can be done by providing detour roads around vulnerable links. Doing so will keep the functionality of the network at a reasonable level. Loss in the functionality of the network will also incur other indirect costs to the city and ultimately the country. To avoid this, emergency response preparations must be coupled with other mitigations approaches that can help cities to protect themselves from extreme scenarios.

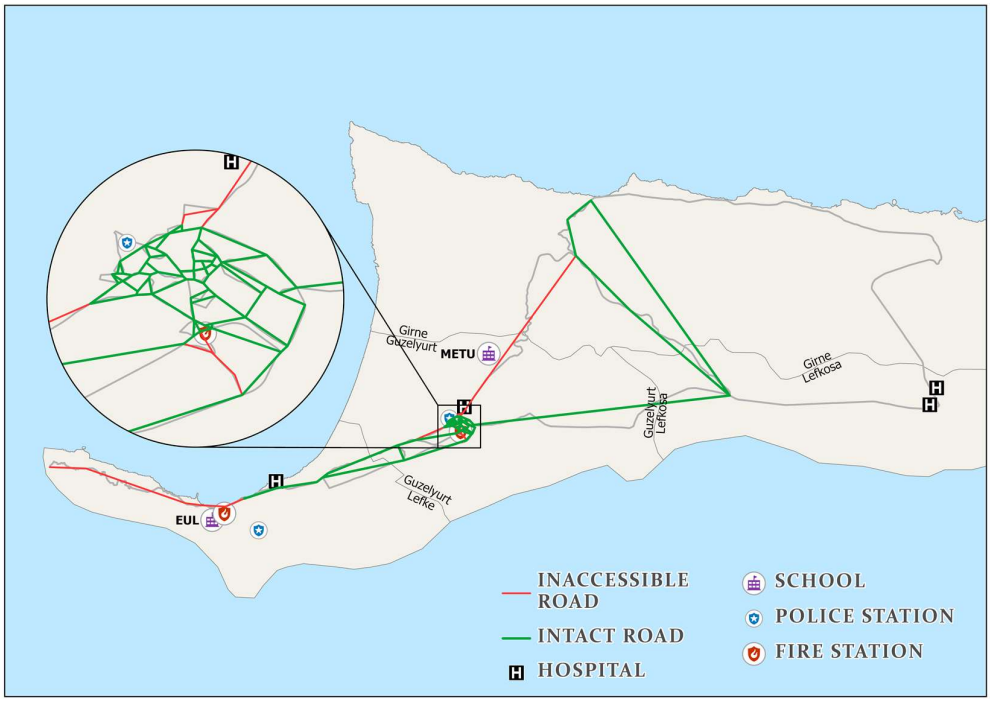

Figure 6.11. Scenario 2 transportation network

6.5.3 Travel Time Loss Estimation

To simulate the travel time loss of the transportation network, some assumptions have been made. We suppose that the post-event demand is the same as the pre-event to consider the worst-case. One reason is that robust and reliable OD reduction factors are hard to calculate and are not universal. Socio-economic characteristics and the culture of the region also play essential roles in determining OD changes. The second assumption is related to the reduction of road capacities. Damage to bridges has a proportional effect on the connecting links. A transportation network is designed in such a way that, detouring traffic through alternative roads can be possible in cases when one or more links become inaccessible in the network for some reason. Hence, all links can have residual capacities for each damage state that can accommodate a certain percent of traffic flowing in the network. Therefore, depending on the damage degree, the nominal capacities of the roads, as well as the free-flow speed, will be reduced by a residual percentage. We adopted the methodologies described in [133] and [134] for moderate residual link traffic carrying capacity and free flow speed reduction, respectively, as shown in Table 6.8.

Table 6.8. Residual traffic carrying capacity and free-flow speed reduction

Damage State	Residual Capacity (%)	Free-flow Speed (%)
None	100	100
Slight	100	100
Moderate	50	50
Extensive	25	50
Complete	0	0

DTALite was used again with the same parameters (see 4.6) to simulate day 0, i.e., immediately after an earthquake. The results are presented in Table 6.9. Here Scenario 1 is the worst-case event in terms of total travel time loss. The main reason is due to the heavy demand in Girne and Lefkosia districts (TAZ 821 and 848, see Table 4.5), where OD from these regions was found to be critical.

Table 6.9. Daily travel time loss before and after (day 0)

Scenario No:	Total Travel Time (hr.)	Average Travel Time (min)	Total Travel Time Loss (hr.)
Base	9248	29.02	-
1	12698	39.87	3450
2	9782	30.71	540
3	9368	29.41	126
4	Same as base		

We have previously shown an example of travel time for the shortest path between METU NCC and the European University of Lefke in 4.6 (see Figure 4.14) while performing the traffic assignment. Considering that as the base case, following the events in Scenario 1 (worst case), we can observe queues and long delays in the same path, as shown in Figure 6.12. During peak hours, we can expect up to 30 minutes of delays between the two locations. This could potentially hinder emergency responses during the event.

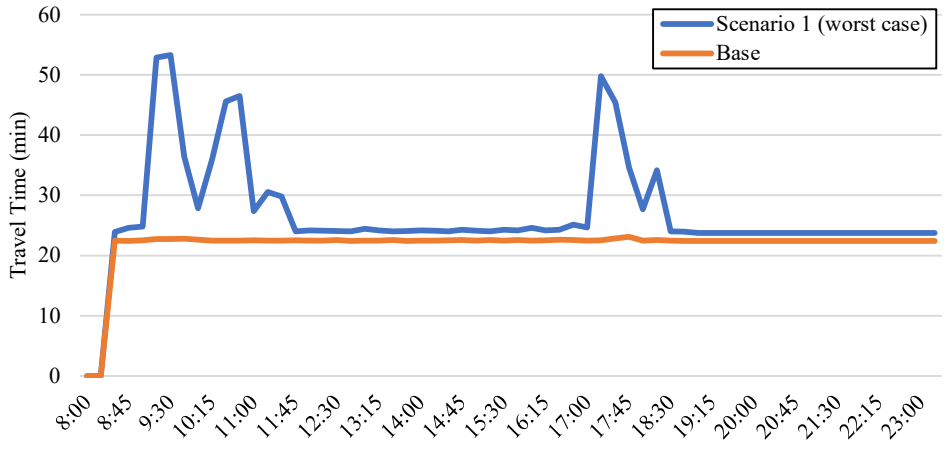

Figure 6.12. Travel time increase in the shortest path connecting METU NCC and EUL

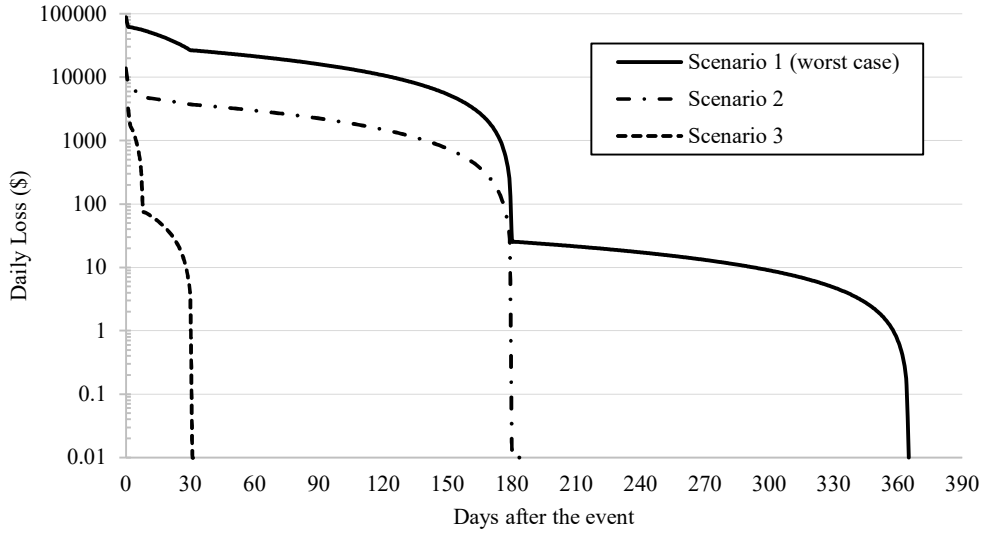

Figure 6.13. Change in operational cost overtime for the first three scenarios

The travel time loss in terms of monetary values, i.e., operational cost, can be calculated as the product of the Vehicle Car Occupancy (VCO), the value of time, and total travel time loss. OD demand is given in passenger car units. To estimate the number of passengers traveling in a single-car, an average occupancy factor is needed. We use VCO = 1.50 based on parameters presented in [135]. The value of time is based on the socio-economic profile of the region. Such studies have not been done before for Northern Cyprus. Therefore, we assume 17$/hr on average as the value of time. To estimate the total loss over time, we perform the same analysis for each scenario for 1, 7, 30, 180, and 365 days after the event has occurred. The recovery of the bridge functionality and its corresponding links follow the curve restoration curves in Figure 6.10. The discrete value of percent-restoration is found for each damage state. Assuming a linear decrease of the daily loss between the days as mentioned above, we can construct a plot showing the operational daily loss overtime for the first three scenarios. Hence, the total operational loss for each scenario is computed by integrating the curves in Figure 6.13 (there is no operational loss in Scenario 4)

From the plot, we can observe that Scenario 1 produces the largest operational loss until all the bridges in the network return to 100% functionality, which could take up to a year. This results in a total indirect cost of $3,439,478. Scenarios 2 and 3 result in $433,296 and $10,481, respectively. Interestingly enough, the operational loss well exceeds the structural loss for each scenario. This is particularly important as it is often ignored by the relevant authorities while deciding the course of actions to be taken after the risk assessment is performed. Although, it should be noted that we assumed a fixed demand case, which sometimes does not reflect the reality for some regions. The study in [90] showed that variable travel demand could decrease

the total travel time loss by almost a factor of 10^{-4}, which is quite large. Moreover, the traffic analysis in this study only considered commuter traffic delays. Although lower in number, freight and truck traffics can have a profound impact on the total indirect cost. The value of time of truck drivers and the value of the cargo can sometimes be five or six-fold more than that of public commuters [135], [136].

6.6 Operational and Structural Loss Aggregation, Economic Analysis of Bridge Retrofitting

Before any mitigation strategies such as seismic bridge retrofit, the total operational and structural losses are summed to estimate the total seismic loss for each event. The operational loss is the crucial changing factor in determining the best policy to be implemented to reduce the overall losses incurred by a region. Though, given the limited number of bridges in the study region (20 bridges in total), and the uncertainties in the damage state bridges experience, we still believe that indirect costs are significant and should not be ignored. The aggregated losses for three different scenarios are shown in Figure 6.14 (the total loss in Scenario 4 is almost zero; therefore, it is not shown in the figure)

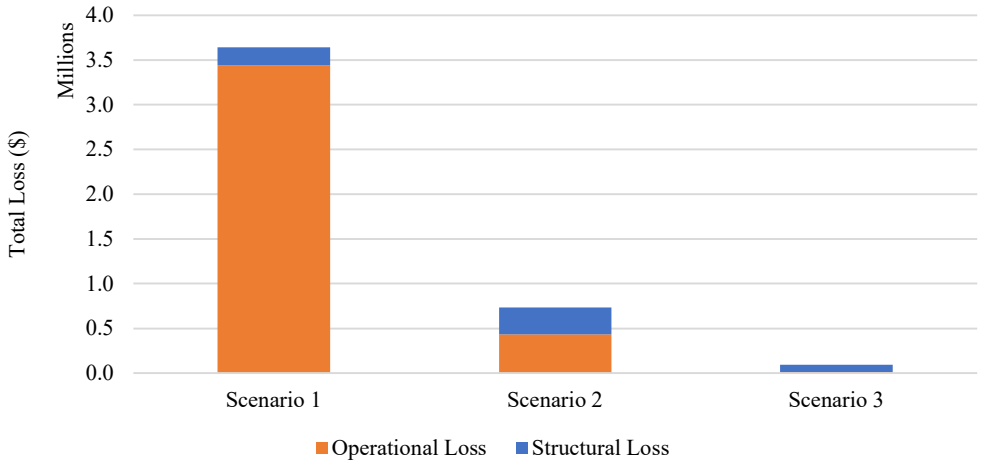

Figure 6.14. Total loss for three different scenarios

After applying the seismic retrofitting of bridges before the event, we expect to have reductions in the total seismic loss, including the structural and the operational losses. This reduction is considered as the benefit achieved by avoiding these losses. The model below is presented in [137] and slightly modified to fit our analysis. Hence, the cost avoided for the repair/restoration cost for an event m can be modeled as:

$$\overline{B}_{SLm} = C^{0}_{RPm} - C^{R}_{RPm} \tag{6.6}$$

where $\overline{B}_{SLm}$ is the expected benefit from cost avoided from structural loss; C^0_{RPm}, and C^R_{RPm} are the system restoration cost with and without retrofitting. Since detailed computational work is required to find new damage state probabilities of the retrofitted bridges, for simplicity, we assume that retrofitting will ensure 90% cost saving for both the structural and operational losses, i.e. $C^R_{RPm} = 0.10 \times C^0_{RPm}$.

Similarly, the expected annual benefit from the avoided operational loss for an event m $\overline{B}_{OLm}$ is expressed as:

$$\overline{B}_{OLm} = C^0_{OLm} - C^R_{OLm} \tag{6.7}$$

where, C^R_{OLm}, and C^o_{OLm} are the operational losses with and without retrofitting, respectively. Therefore, the annual benefit from retrofitting is calculated by adding the costs avoided in structural and operational losses as:

$$\overline{B} = \sum_{m=1}^{M} [\overline{B}_{OLm} + \overline{B}_{SLm}] p_m \tag{6.8}$$

where $\overline{B}$ is the annual benefit and p_m is the annual probability of event m, or simply its annual recurrence rate discussed in 3.3.5. To compute the total benefit over the residual service life T, and assuming uniformly distributed annual benefit through the period, the total present value of the benefit B_{PV} for an effective interest rate r for a time period T is expressed as:

$$\overline{B}_{PV} = \sum_{t=1}^{T} \frac{\overline{B}}{(1+r)^t} = \overline{B}\ \frac{(1+r)^T - 1}{r(1+r)^T} \tag{6.9}$$

The effective interest rate r is not easy to calculate, therefore to show the effect of different interest rates assuming $T = 50$ years, the total benefit-cost ratio $BCR = \sum_m^M B_{PVm}/C_{Rm}$ for a range of rates is shown in Figure 6.15. According to the figure, we can observe that for our study region until 4.25% discount rate, the retrofitting strategy is cost-effective. Seismic loss analysis is susceptible to bridge damage state and link residual capacities, in addition to the restoration functions. Therefore, future studies should incorporate the sensitivity analysis of the parameters assumed here. Moreover, the transportation network in this study only considered the main roadway links in the region. Local detour link analysis should be integrated into the analysis to determine the best possible alternative routes to reduce the residual capacities on the main links. Some of the bridges in Cyprus are historical and date back more than 50 years. Therefore, the service life of bridges will impact the analysis. Lower discount rates and higher bridge service life are more cost-effective. Finally, many of the bridges are already deteriorated, therefore, their capacity to withstand seismic loads are less. This study considered the nominal performance of each bridge, i.e., bridges are at their full

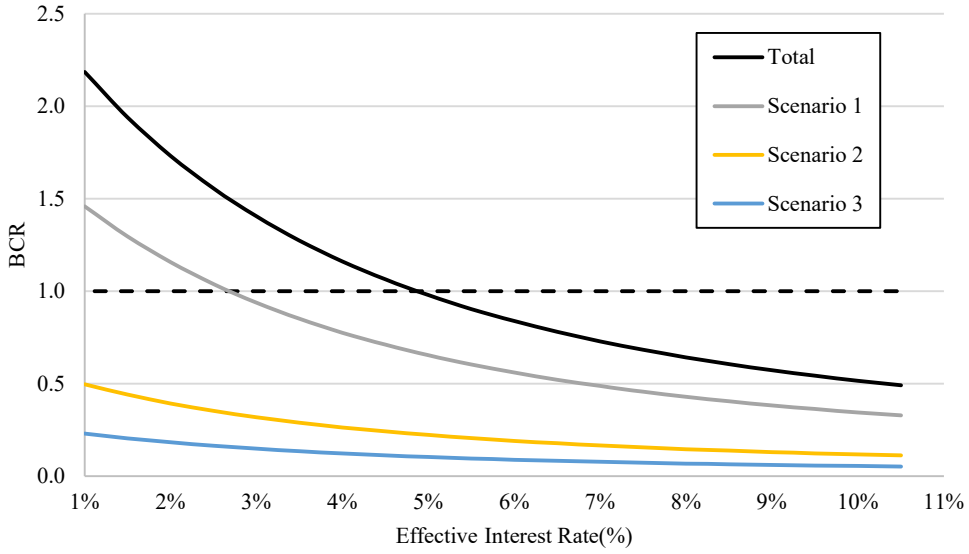

Figure 6.15. Total benefit/cost ratio for all three scenarios

capacity while performing seismic assessment. This leads to a more conservative loss estimation model and obscures the real loss incurred on a region; operational losses would be even more prominent.

Bridge seismic retrofit prioritization is a way to determine the most critical bridges in the network. Optimization algorithms based on network simplex models (e.g., minimum cost flow analysis) or maximum flow are typically solved as a mixed-integer linear program. The algorithms under a constraint retrofitting budget can find the most critical links and bridges. This allows the decision-makers to retrofit the most critical components only. Bridge retrofit prioritization is out of the scope of this study. However, to illustrate a simple case-study under a constraint budget, an example is provided in Appendix D.

As a general framework, therefore, bridge retrofit prioritization should be integrated with local detours and linked directly to seismic loss tools or analytical loss models with sensitivity assessments to calibrate for the best parameters to find the expected seismic loss and benefit for a region.

6.7 Chapter Summary

This chapter presented a case study for the seismic risk assessment of bridges in Northern Cyprus. We outlined the four earthquake scenarios that are simulated to estimate the structural and operational losses of the bridge transportation network. We incorporated the methodologies described in earlier chapters to find the structural losses from ShakeMap data and the built-in Hazus hazard module. We assumed the results from ShakeMap to derive the

bridge damage probabilities and translated the losses into a bridge restoration model. We found that Scenario 2 (M7.0 in Guzelyurt) produces the most significant loss following Scenarios 1, 3, and 4, respectively. Furthermore, operational loss analysis considering the network's reliability as well as the structural integrity was carried out. In terms of the indices from the graph theory and network analysis, Scenario 2 was found again to be more vulnerable when critical nodes and links are removed from the network.

We also examined the travel time loss estimation from the dynamic traffic simulation program. When compared to the baseline, Scenario 1 resulted in a total of 3,450 hr of travel time loss for the day following the event. To compute the annual loss until the system is restored to the initial state, we followed a system restoration function for each damage state and found the total annual cost due to operational loss for each scenario. We discovered that operational loss in Scenario 1 (the worst case) is far more significant than its structural loss counterpart. Finally, both losses were aggregated to rank the worst-case scenario. A simple retrofit economic analysis was carried out to find the cost-effectiveness of bridge seismic retrofitting. Up to 4.25% effective interest rate, it is cost-effective to retrofit the bridges. In the future, bridge retrofit prioritization based on network optimization algorithms will be studied.

CHAPTER 7

CONCLUSION

7.1 General Remarks and Contributions

This study aims to perform a seismic risk assessment of Northern Cyprus and lay the initial foundations to develop an innovative SHM system in conjunction with ITS. This integration offers earthquakes risk assessment by considering the state-of-the-art technologies by introducing a flexible decision platform system. Using modern tools and methodologies, the comprehensive analysis of the seismic hazards and the transportation network in this study enabled us to determine the best strategies reducing the overall losses for the scenarios tested here. The followings provide a general overview of our findings and conclusions for the objectives of this study.

Chapter 3 introduced the concept of probabilistic hazard analysis for Northern Cyprus with an emphasis on generating ShakeMap data for hazard analysis inside Hazus. Furthermore, the concept of fragility function and the algorithm used to find the exceedance probabilities of bridge damage states were also provided. Moreover, this chapter presented the framework of Mobile SHM patches for the fragility curves of the bridges in the region as a supplementary component for the state-of-the-art decision-making system.

Chapter 4 presented the transportation network of Northern Cyprus and computed its topological vulnerability indices as well as the structural integrity based on the graph theory and network analysis models. This chapter also applied dynamic traffic modeling for travel time estimation in the network. The accurate representation of the network and the travel demand modeling play a significant role in determining operational loss following an earthquake event.

Chapter 5 provided the detailed walkthrough on how a well-known risk assessment tool, Hazus, was adapted and how its inventory was modified to fit our region. The current inventory is created in such a way as to accommodate future implementations of indirect cost and social

loss estimation. The necessary tools and manuals for Hazus adaption are provided in Appendix A.

Chapter 6 presented a case-study for the western part of Northern Cyprus, consisting of 20 bridges, 98 nodes, and 134 bridges. We simulated three different scenarios for both the structural loss and the operational loss estimation using the standard methods and models described in the previous chapters. The results indicated that for the scenarios tested, Northern Cyprus is vulnerable to seismic risks for high shaking intensities. Given that the majority of the bridges are historical and not seismically designed to withstand high magnitudes, this study can help decision-makers to have an idea on the importance of the transportation network for emergency response preparedness following similar events. Moreover, the results can provide a simple understanding of which bridges are more vulnerable, and if seismic retrofitting can be a viable solution or not. Effectively, a simple retrofit economic analysis was shown to find the cost-effectiveness of bridge seismic retrofitting. We concluded that up to 4.25% effective interest rate, it is cost-effective to retrofit the bridges in the region.

The present research can provide many useful information and data to the responsible agencies in the hope that the results of this study can be used to reduce the risk of earthquake in the future. Therefore, we suggest the following proactive measures assembled from the findings of our study:

1. Developing a real-time seismic hazard and risk assessment.
2. Initiating a localized hazard assessment of the critical regions. e.g. District of Lefke and Gazimagusa.
3. Gathering a comprehensive transportation network data including the road characteristics, travel time estimation and socioeconomic parameters taken from detailed surveys.
4. Retrofitting vulnerable links and bridges as identified in this study especially the ones categorized as HWB8.
5. Providing detour links in the areas where the risk of bridge failure is high, especially in the District of Lefke where no detour links exist.

With improvements in this study and conducting assessment of the whole island, we believe Northern Cyprus can be better prepared for potential hazards in the future.

7.2 Limitation and Future Work

This study cannot represent the actual losses incurred by the region following an earthquake event in full detail. Although we investigated and modeled our assumptions in such a way as to illustrate the risks associated with the region with a certain degree of confidence, numerous

limitations and assumptions were inevitable. Therefore, in the future, we will explore new ways to overcome the shortcoming of the thesis.

7.2.1 Limitations of the Thesis

Below we outline the assumptions and limitations for the current thesis, specifically:

- In Chapter 3, the ShakeMap data and Hazus built-in hazard module do not include the fault information of the region. Therefore, the hazard maps generated for the three different scenarios in ShakeMap and Hazus are slightly overestimated. Moreover, the fragility curves assumed for the bridges in the study region follow the default Hazus fragility function. The damage functions are aggregated in 28 highway bridge classes defined in Hazus for U.S. bridges. This can result in underestimation or overestimation of some bridges' damage state functions for a given IM. Therefore, to represent the actual fragility curves, a detailed analysis is required. This research can also include damages to other network components such as culverts, roadway segments, and tunnels.
- In Chapter 4, the vulnerability parameters only considered the network as a whole and ignored some essential components in urbanization, such as the evolution over time in hazard exposure and community vulnerability exposure. As urbanization increases, the model complexity increases with the same rate. This results in the degradation of the network over time. Therefore, time-dependent factors should be incorporated into future studies. In terms of the link performance measure, some significant portion of this section had to be assumed as data availability is either limited or non-existent. Data such as the actual demand of the network, the road network capacity, and the traffic were mostly assumed. Therefore, by updating our inventory, we can expect a more realistic analysis in the future.
- In Chapter 6, the simulation and parameters used in the analysis are uncertain. The earthquake scenarios evaluated are limited in number and variety. The spatial correlation in ground shaking of these scenarios is another factor that can significantly influence the hazard modeling of the study. Moreover, the cost variables in cost estimation of the structural loss and operational loss are assumed for the region. Future studies are, therefore, required to calibrate these values through sensitivity analysis. Furthermore, one significant aspect of suggesting cost-effective mitigations strategies is to develop bridge retrofit prioritization models. In this way, under a constraint budget, we can retrofit those bridges

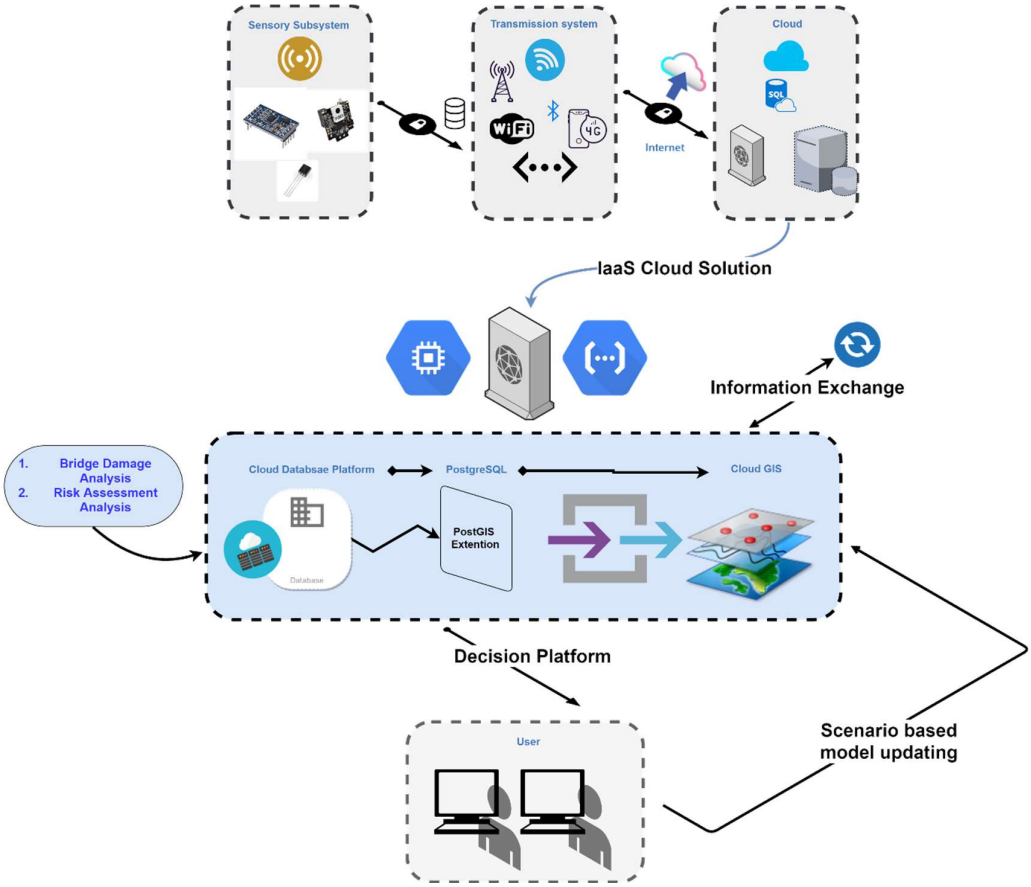

Figure 7.1. An idealized cloud-based SHM-GIS decision-making support system for real-time bridge monitoring

which are vital in keeping the transportation network at a reasonable functionality level.

7.2.2 Future Research

As mentioned before, to determine the actual fragility curves through mobile sensing, the current thesis can be extended towards state-of-the-art mobile SHM. The initial work is already laid out, and we aim to include the results in our future work. Additionally, we plan to develop a more seamless and integrated decision-making system considering both SHM and ITS into one unified platform. Under the umbrella of a synergistic combination of an intelligent SHM-GIS cloud-based bridge monitoring system, we believe the system architecture presented in our paper [138], as shown in Figure 7.1, is cost-effective, efficient, and sustainable solution in bridge prognosis and diagnosis. The capability of this system can be further enhanced by utilizing machine learning techniques in addition to drone assisted SHM [139]. This system can also be linked to an ITS platform for better integration into smart city paradigm under SHM-informed-ITS models.

The new paradigm shift in the incorporation of new and innovative technologies for bridge seismic risk assessment can offer many prospects in this field. Notably, we can expect to see a real-time bridge assessment immediately after an event. In case of damage or total collapse of a bridge, in order to keep the performance of the transportation network at high levels to ensure a fast emergency response to reduce other the socials cost, ITS can come into play to suggest alternative routes or provide real-time traffic information to reduce operational costs. The opportunities in this field are vast, and as time goes by, with the increase in complexity of the transportation network, the need to change to a better decision-making system becomes more critical.

7.3 Concluding Remarks

The risk assessment of bridges applied to a case study of Northern Cyprus is the first of its kind for the region and also equally important in terms of the seismic risk reduction findings in the country. The results of this thesis can provide responsible agencies with a framework that can visualize different scenarios, and consequently apply the best mitigation strategies to minimize the overall losses.

Analyzing network vulnerability and reliability can provide an in-depth understanding of the current and future impacts of seismic risks associated with highway-bridge networks. The three factors of sustainability (i.e., economic, social, and environmental) considering the resiliency of the transportation network following a seismic event can significantly influence the decisions taken in mitigation, planning, response, and recovery stages. Therefore, hazard-induced sustainability metrics have to be integrated into the risk assessment studies and planned in the initial design stage of the bridge transportation network.

While this thesis has focused on seismic risks, the major hazard that Northern Cyprus is usually faced with is flooding. In that sense, the general framework, models, and software used in this thesis can be extended to other hazards analysis. Thereby, the losses due to floods can also be included in the analysis to provide an all-in-one multi-hazards assessment tool.

The methods and concepts described in this study can be considered as the next step toward the future of the cyber-physical system (CPS) as part of the IoT paradigm shift. The future of the risk assessment of transportation network lies within the smart city and cloud technology. What will ensue from the shift to this paradigm is the applications of deep learning, artificial intelligence, drones, and virtual/augmented reality. These are some of the promising next-generation sensing and monitoring applications.

BIBLIOGRAPHY

[1] R. G. Little, "Controlling Cascading Failure: Understanding the Vulnerabilities of Interconnected Infrastructures," *J. Urban Technol.*, vol. 9, no. 1, pp. 109–123, Apr. 2002, doi: 10.1080/106307302317379855.

[2] Nesrin Basöz and Anne S. Kiremidjian, "Risk Assessment for Highway Transportation Systems," John A. Blume Earthquake Engineering Center, Technical Report 118, 1996. [Online]. Available: http://purl.stanford.edu/fr998kq2251.

[3] A. Rytter, "Vibrational based inspection of civil engineering structures," PhD Thesis, Dept. of Building Technology and Structural Engineering, Aalborg University, 1993.

[4] C. R. Farrar and K. Worden, "An introduction to structural health monitoring," *Philos. Trans. R. Soc. Math. Phys. Eng. Sci.*, vol. 365, no. 1851, pp. 303–315, Feb. 2007, doi: 10.1098/rsta.2006.1928.

[5] C. Arcadius Tokognon, B. Gao, G. Y. Tian, and Y. Yan, "Structural Health Monitoring Framework Based on Internet of Things: A Survey," *IEEE Internet Things J.*, vol. 4, no. 3, pp. 619–635, Jun. 2017, doi: 10.1109/JIOT.2017.2664072.

[6] D. Feng and M. Q. Feng, "Computer vision for SHM of civil infrastructure: From dynamic response measurement to damage detection – A review," *Eng. Struct.*, vol. 156, pp. 105–117, Feb. 2018, doi: 10.1016/j.engstruct.2017.11.018.

[7] S. Sony, S. Laventure, and A. Sadhu, "A literature review of next-generation smart sensing technology in structural health monitoring," *Struct. Control Health Monit.*, vol. 26, no. 3, p. e2321, Mar. 2019, doi: 10.1002/stc.2321.

[8] C. R. Farrar, S. W. Doebling, and D. A. Nix, "Vibration–based structural damage identification," *Philos. Trans. R. Soc. Lond. Ser. Math. Phys. Eng. Sci.*, vol. 359, no. 1778, pp. 131–149, Jan. 2001, doi: 10.1098/rsta.2000.0717.

[9] H. Sohn *et al.*, "A review of structural health monitoring literature: 1996–2001," Los Alamos National Laboratory, Los Alamos, NM, LA13976-MS, 2003.

[10] C. Farrar, G. Park, and K. Worden, "Complexity: A new axiom for structural health monitoring?," LOS ALAMOS NATIONAL LAB NM, 2010.

[11] H. Sohn, "Effects of environmental and operational variability on structural health monitoring," *Philos. Trans. R. Soc. Math. Phys. Eng. Sci.*, vol. 365, no. 1851, pp. 539–560, Feb. 2007, doi: 10.1098/rsta.2006.1935.

[12] B. Tomaszewski, *Geographic Information Systems (GIS) for Disaster Management*, 1 edition. Boca Raton: Routledge, 2014.

[13] D. L. Enke, C. Tirasirichai, and R. Luna, "Estimation of Earthquake Loss due to Bridge Damage in the St. Louis Metropolitan Area. II: Indirect Losses," *Nat. Hazards Rev.*, vol. 9, no. 1, pp. 12–19, Feb. 2008, doi: 10.1061/(ASCE)1527-6988(2008)9:1(12).

[14] W. Shi, P. G. Cheng, J. M. Ko, and C. Liu, "GIS-based bridge structural health monitoring and management system," San Diego, CA, Jun. 2002, pp. 12–19, doi: 10.1117/12.470725.

[15] M.-Y. Cheng, Y.-W. Wu, S.-J. Chen, and M.-C. Weng, "Economic evaluation model for post-earthquake bridge repair/rehabilitation: Taiwan case studies," *Autom. Constr.*, vol. 18, no. 2, pp. 204–218, Mar. 2009, doi: 10.1016/j.autcon.2008.08.004.

[16] Technical Activities Division, Transportation Research Board, and National Academies of Sciences, Engineering, and Medicine, *Dynamic Traffic Assignment: A Primer*. Washington, D.C.: Transportation Research Board, 2011, p. 22872.

[17] S. W. Doebling, C. R. Farrar, M. B. Prime, and D. W. Shevitz, “Damage identification and health monitoring of structural and mechanical systems from changes in their vibration characteristics: A literature review,” LA--13070-MS, 249299, May 1996. doi: 10.2172/249299.

[18] J. M. W. Brownjohn, “Structural health monitoring of civil infrastructure,” *Philos. Trans. R. Soc. Math. Phys. Eng. Sci.*, vol. 365, no. 1851, pp. 589–622, Feb. 2007, doi: 10.1098/rsta.2006.1925.

[19] J. P. Lynch, “An overview of wireless structural health monitoring for civil structures,” *Philos. Trans. R. Soc. Math. Phys. Eng. Sci.*, vol. 365, no. 1851, pp. 345–372, Feb. 2007, doi: 10.1098/rsta.2006.1932.

[20] A. B. Noel, A. Abdaoui, T. Elfouly, M. H. Ahmed, A. Badawy, and M. S. Shehata, “Structural Health Monitoring Using Wireless Sensor Networks: A Comprehensive Survey,” *IEEE Commun. Surv. Tutor.*, vol. 19, no. 3, pp. 1403–1423, 2017, doi: 10.1109/COMST.2017.2691551.

[21] M. Grossi, “A sensor-centric survey on the development of smartphone measurement and sensing systems,” *Measurement*, vol. 135, pp. 572–592, Mar. 2019, doi: 10.1016/j.measurement.2018.12.014.

[22] A. H. Alavi and W. G. Buttlar, “An overview of smartphone technology for citizen-centered, real-time and scalable civil infrastructure monitoring,” *Future Gener. Comput. Syst.*, vol. 93, pp. 651–672, Apr. 2019, doi: 10.1016/j.future.2018.10.059.

[23] S. Sony, S. Laventure, and A. Sadhu, “A literature review of next-generation smart sensing technology in structural health monitoring,” *Struct. Control Health Monit.*, vol. 26, no. 3, p. e2321, Mar. 2019, doi: 10.1002/stc.2321.

[24] P. Omenzetter, U. Yazgan, S. Soyoz, and M. P. Limongelli, “Quantifying the value of SHM for emergency management of bridges at-risk from seismic damage,” presented at the Joint Workshop of COST TU1402 - COST TU1406 – IABSE WC1, Zagreb, Croatia, 2017, Accessed: Jul. 30, 2019. [Online]. Available: https://abdn.pure.elsevier.com/en/publications/quantifying-the-value-of-shm-for-emergency-management-of-bridges-.

[25] C. Lan, H. Li, and J. Ou, “Traffic load modelling based on structural health monitoring data,” *Struct. Infrastruct. Eng.*, vol. 7, no. 5, pp. 379–386, May 2011, doi: 10.1080/15732470902726809.

[26] J. Jin, J. Gubbi, S. Marusic, and M. Palaniswami, “An Information Framework for Creating a Smart City Through Internet of Things,” *IEEE Internet Things J.*, vol. 1, no. 2, pp. 112–121, Apr. 2014, doi: 10.1109/JIOT.2013.2296516.

[27] S. M. Khan, S. Atamturktur, M. Chowdhury, and M. Rahman, “Integration of Structural Health Monitoring and Intelligent Transportation Systems for Bridge Condition Assessment: Current Status and Future Direction,” *IEEE Trans. Intell. Transp. Syst.*, vol. 17, no. 8, pp. 2107–2122, Aug. 2016, doi: 10.1109/TITS.2016.2520499.

[28] T. Wang, M. Z. A. Bhuiyan, G. Wang, Md. A. Rahman, J. Wu, and J. Cao, “Big Data Reduction for a Smart City’s Critical Infrastructural Health Monitoring,” *IEEE Commun. Mag.*, vol. 56, no. 3, pp. 128–133, Mar. 2018, doi: 10.1109/MCOM.2018.1700303.

[29] D. Skokandić, A. Žnidarič, A. Mandić-Ivanković, and M. Kreslin, “Application of Bridge Weigh-in-Motion measurements in assessment of existing road bridges,” presented at the Joint Workshop of COST TU1402 - COST TU1406 – IABSE WC1, Zagreb, Croatia, Mar. 2017.

[30] D. Pines and A. E. Aktan, “Status of structural health monitoring of long-span bridges in the United States,” *Prog. Struct. Eng. Mater.*, vol. 4, no. 4, pp. 372–380, Oct. 2002, doi: 10.1002/pse.129.

[31] M. Pervizpour, E. Kulcu, K. A. Grimmelsman, R. A. Barrish, and X. Qin, “REAL-TIME BRIDGE HEALTH-MONITORING FOR MANAGEMENT,” presented at the Second Workshop on Advanced Technologies in Urban Earthquake Disaster Mitigation, Kyoto Univ, Japan, Jul. 2000.

[32] A. Kiremidjian, J. Moore, Y. Y. Fan, O. Yazlali, N. Basoz, and M. Williams, “Seismic Risk Assessment of Transportation Network Systems,” *J. Earthq. Eng.*, vol. 11, no. 3, pp. 371–382, May 2007, doi: 10.1080/13632460701285277.

[33] A. H. Barbat, M. L. Carreño, L. G. Pujades, N. Lantada, O. D. Cardona, and M. C. Marulanda, “Seismic vulnerability and risk evaluation methods for urban areas. A review with application to a pilot area,” *Struct. Infrastruct. Eng.*, vol. 6, no. 1–2, pp. 17–38, Feb. 2010, doi: 10.1080/15732470802663763.

[34] Y. Zhou, S. Banerjee, and M. Shinozuka, “Socio-economic effect of seismic retrofit of bridges for highway transportation networks: a pilot study,” *Struct. Infrastruct. Eng.*, vol. 6, no. 1–2, pp. 145–157, Feb. 2010, doi: 10.1080/15732470802663862.

[35] A. Guo, Z. Liu, S. Li, and H. Li, “Seismic performance assessment of highway bridge networks considering post-disaster traffic demand of a transportation system in emergency conditions,” *Struct. Infrastruct. Eng.*, vol. 13, no. 12, pp. 1523–1537, Dec. 2017, doi: 10.1080/15732479.2017.1299770.

[36] R. G. Little, “Controlling Cascading Failure: Understanding the Vulnerabilities of Interconnected Infrastructures,” *J. Urban Technol.*, vol. 9, no. 1, pp. 109–123, Apr. 2002, doi: 10.1080/106307302317379855.

[37] I. Kilanitis and A. Sextos, “Integrated seismic risk and resilience assessment of roadway networks in earthquake prone areas,” *Bull. Earthq. Eng.*, vol. 17, no. 1, pp. 181–210, Jan. 2019, doi: 10.1007/s10518-018-0457-y.

[38] A. H. M. Muntasir Billah and M. Shahria Alam, “Seismic fragility assessment of highway bridges: a state-of-the-art review,” *Struct. Infrastruct. Eng.*, vol. 11, no. 6, pp. 804–832, Jun. 2015, doi: 10.1080/15732479.2014.912243.

[39] I. Gidaris *et al.*, “Multiple-Hazard Fragility and Restoration Models of Highway Bridges for Regional Risk and Resilience Assessment in the United States: State-of-the-Art Review,” *J. Struct. Eng.*, vol. 143, no. 3, p. 04016188, Mar. 2017, doi: 10.1061/(ASCE)ST.1943-541X.0001672.

[40] P. Omenzetter, S. Ramhormozian, P. Mangabhai, R. Singh, and R. Orense, “A framework for rapid post-earthquake assessment of bridges and restoration of transportation network functionality using structural health monitoring,” San Diego, California, USA, Apr. 2013, p. 86920J, doi: 10.1117/12.2008875.

[41] A. Guo, Z. Liu, S. Li, and H. Li, “Seismic performance assessment of highway bridge networks considering post-disaster traffic demand of a transportation system in emergency conditions,” *Struct. Infrastruct. Eng.*, vol. 13, no. 12, pp. 1523–1537, Dec. 2017, doi: 10.1080/15732479.2017.1299770.

[42] L. Chang, A. S. Elnashai, and B. F. Spencer, “Post-earthquake modelling of transportation networks,” *Struct. Infrastruct. Eng.*, pp. 1–19, May 2011, doi: 10.1080/15732479.2011.574810.

[43] J. E. Padgett, R. DesRoches, and E. Nilsson, “Regional Seismic Risk Assessment of Bridge Network in Charleston, South Carolina,” *J. Earthq. Eng.*, vol. 14, no. 6, pp. 918–933, Jul. 2010, doi: 10.1080/13632460903447766.

[44] M. Shinozuka, Y. Murachi, X. Dong, Y. Zhou, and M. J. Orlikowski, “Effect of seismic retrofit of bridges on transportation networks,” *Earthq. Eng. Eng. Vib.*, vol. 2, no. 2, pp. 169–179, Dec. 2003, doi: 10.1007/s11803-003-0001-0.

[45] E. C. Stergiou and A. S. Kiremidjian, “Risk assessment of transportation systems with network functionality losses,” *Struct. Infrastruct. Eng.*, vol. 6, no. 1–2, pp. 111–125, Feb. 2010, doi: 10.1080/15732470802663839.

[46] R. Luna, D. Hoffman, and W. T. Lawrence, “Estimation of Earthquake Loss due to Bridge Damage in the St. Louis Metropolitan Area. I: Direct Losses,” *Nat. Hazards Rev.*, vol. 9, no. 1, pp. 1–11, Feb. 2008, doi: 10.1061/(ASCE)1527-6988(2008)9:1(1).

[47] D. L. Enke, C. Tirasirichai, and R. Luna, “Estimation of Earthquake Loss due to Bridge Damage in the St. Louis Metropolitan Area. II: Indirect Losses,” *Nat. Hazards Rev.*, vol. 9, no. 1, pp. 12–19, Feb. 2008, doi: 10.1061/(ASCE)1527-6988(2008)9:1(12).

[48] R. Codermatz, R. Nicolich, and D. Slejko, “Seismic risk assessments and GIS technology: applications to infrastructures in the Friuli-Venezia Giulia region (NE Italy),” *Earthq. Eng. Struct. Dyn.*, vol. 32, no. 11, pp. 1677–1690, Sep. 2003, doi: 10.1002/eqe.294.

[49] J. R. Rozelle, “International Adaptation of the Hazus Earthquake Model Using Global Exposure Datasets,” Master, University of Colorado at Denver, United States -- Colorado, 2018.

[50] H. McGrath, E. Stefanakis, and M. Nastev, “Sensitivity analysis of flood damage estimates: A case study in Fredericton, New Brunswick,” *Int. J. Disaster Risk Reduct.*, vol. 14, pp. 379–387, Dec. 2015, doi: 10.1016/j.ijdrr.2015.09.003.

[51] S. Fallah-Aliabadi *et al.*, "Risk analysis of hospitals using GIS and HAZUS: A case study of Yazd County, Iran," *Int. J. Disaster Risk Reduct.*, vol. 47, p. 101552, Aug. 2020, doi: 10.1016/j.ijdrr.2020.101552.

[52] V. Silva, H. Crowley, M. Pagani, D. Monelli, and R. Pinho, "Development of the OpenQuake engine, the Global Earthquake Model's open-source software for seismic risk assessment," *Nat. Hazards*, vol. 72, no. 3, pp. 1409–1427, Jul. 2014, doi: 10.1007/s11069-013-0618-x.

[53] R. Jena, B. Pradhan, G. Beydoun, A. Al-Amri, and H. Sofyan, "Seismic hazard and risk assessment: a review of state-of-the-art traditional and GIS models," *Arab. J. Geosci.*, vol. 13, no. 2, p. 50, Jan. 2020, doi: 10.1007/s12517-019-5012-x.

[54] Z. Cagnan and G. B. Tanircan, "Seismic hazard assessment for Cyprus," *J. Seismol.*, vol. 14, no. 2, pp. 225–246, May 2009, doi: 10.1007/s10950-009-9163-1.

[55] Geological Survey Department Cyprus, "Cyprus Broadband Seismological Network," 2013, doi: 10.7914/SN/CQ.

[56] Bogazici University Kandilli Observatory And Earthquake Research Institute, "Bogazici University Kandilli Observatory And Earthquake Research Institute," 2001, doi: 10.7914/SN/KO.

[57] The SHARE Consortium *et al.*, "The 2013 European Seismic Hazard Model: key components and results," *Bull. Earthq. Eng.*, vol. 13, no. 12, pp. 3553–3596, Dec. 2015, doi: 10.1007/s10518-015-9795-1.

[58] J. L. Gross and L. T. Phan, "Implications for Earthquake Risk Reduction in the United States From the Kocaeli, Turkey, Earthquake of August 17, 1999," in *ASCE World Structural Engineering Conference (USGS Circular 1193)*, Aug. 2000, vol. 1193, Accessed: Jul. 14, 2020. [Online]. Available: https://www.nist.gov/publications/implications-earthquake-risk-reduction-united-states-kocaeli-turkey-earthquake-august.

[59] A. Barka and R. Reilinger, "Active tectonics of the Eastern Mediterranean region: deduced from GPS, neotectonic and seismicity data," *Ann. Geophys.*, vol. 40, no. 3, 1997, doi: 10.4401/ag-3892.

[60] M. Stucchi *et al.*, "The SHARE European Earthquake Catalogue (SHEEC) 1000–1899," *J. Seismol.*, vol. 17, no. 2, pp. 523–544, Apr. 2013, doi: 10.1007/s10950-012-9335-2.

[61] G. Grünthal, R. Wahlström, and D. Stromeyer, "The SHARE European Earthquake Catalogue (SHEEC) for the time period 1900–2006 and its comparison to the European-Mediterranean Earthquake Catalogue (EMEC)," *J. Seismol.*, vol. 17, no. 4, pp. 1339–1344, Oct. 2013, doi: 10.1007/s10950-013-9379-y.

[62] C. A. Cornell, "Engineering seismic risk analysis," *Bull. Seismol. Soc. Am.*, vol. 58, no. 5, pp. 1583–1606, Oct. 1968.

[63] J. W. Baker, "An introduction to probabilistic seismic hazard analysis," *White Pap. Version*, vol. 2, no. 1, p. 79, 2013.

[64] U.S. Geological Survey, "ShakeMap." U.S. Geological Survey, 2017, doi: 10.5066/F7W957B2.

[65] Z. Çağnan and D. Kalafat, "A new catalogue of eastern Mediterranean earthquakes, 2150 BC-2011," 2012.

[66] B. Gutenberg and C. F. Richter, "Frequency of earthquakes in California," *Bull. Seismol. Soc. Am.*, vol. 34, no. 4, pp. 185–188, 1944.

[67] D. M. Boore and W. B. Joyner, "The influence of rupture incoherence on seismic directivity," *Bull. Seismol. Soc. Am.*, vol. 68, no. 2, pp. 283–300, 1978.

[68] W. B. Joyner and D. M. Boore, "Peak horizontal acceleration and velocity from strong-motion records including records from the 1979 Imperial Valley, California, earthquake," *Bull. Seismol. Soc. Am.*, vol. 71, no. 6, pp. 2011–2038, 1981.

[69] John Douglas, "Ground motion prediction equations 1964-2019." http://www.gmpe.org.uk.

[70] C. A. Cornell, H. Banon, and A. F. Shakal, "Seismic motion and response prediction alternatives," *Earthq. Eng. Struct. Dyn.*, vol. 7, no. 4, pp. 295–315, Jul. 1979, doi: 10.1002/eqe.4290070402.

[71] D. M. Boore and G. M. Atkinson, “Ground-Motion Prediction Equations for the Average Horizontal Component of PGA, PGV, and 5%-Damped PSA at Spectral Periods between 0.01 and 10.0,” *Earthq. Spectra*, vol. 24, no. 1, pp. 99–138, Feb. 2008, doi: 10.1193/1.2830434.

[72] K. W. Campbell and Y. Bozorgnia, “NGA-West2 Ground Motion Model for the Average Horizontal Components of PGA, PGV, and 5% Damped Linear Acceleration Response Spectra,” *Earthq. Spectra*, vol. 30, no. 3, pp. 1087–1115, Aug. 2014, doi: 10.1193/062913EQS175M.

[73] S. Akkar and J. J. Bommer, “Empirical Equations for the Prediction of PGA, PGV, and Spectral Accelerations in Europe, the Mediterranean Region, and the Middle East,” *Seismol. Res. Lett.*, vol. 81, no. 2, pp. 195–206, Mar. 2010, doi: 10.1785/gssrl.81.2.195.

[74] C. B. Worden, *ShakeMap Manual*. U.S. Geological Survey, 2016.

[75] B. G. Nielson, “Analytical fragility curves for highway bridges in moderate seismic zones,” PhD Thesis, Georgia Institute of Technology, 2005.

[76] NIBS-FEMA, “Hazus®–MH 2.1 Multi-hazard Loss Estimation Methodology Technical Manual,” Department of Homeland Security Federal Emergency Management Agency Mitigation Division, Washington, D.C., 2013.

[77] Anne S. Kiremidjian and Evangelos Stergiou, “Treatment of Uncertainties in Seismic Risk Analysis of Transportation Systems,” John A. Blume Earthquake Engineering Center, Technical Report 154, 2006.

[78] J. B. Mander, “Fragility curve development for assessing the seismic vulnerability of highway bridges,” University at Buffalo, State University of New York, Technical Report, 1999.

[79] J. B. Mander and N. Basöz, “Seismic Fragility Curve Theory for Highway Bridges,” 1999, pp. 31–40, Accessed: May 02, 2019. [Online]. Available: https://cedb.asce.org/CEDBsearch/record.jsp?dockey=0118440.

[80] U. Hancilar, C. Tuzun, C. Yenidogan, and M. Erdik, “ELER software – a new tool for urban earthquake loss assessment,” *Nat. Hazards Earth Syst. Sci.*, vol. 10, no. 12, pp. 2677–2696, Dec. 2010, doi: 10.5194/nhess-10-2677-2010.

[81] R. D. Borcherdt, “Estimates of Site-Dependent Response Spectra for Design (Methodology and Justification),” *Earthq. Spectra*, vol. 10, no. 4, pp. 617–653, Nov. 1994, doi: 10.1193/1.1585791.

[82] D. J. Wald, V. Quitoriano, T. H. Heaton, and H. Kanamori, “Relationships between Peak Ground Acceleration, Peak Ground Velocity, and Modified Mercalli Intensity in California,” *Earthq. Spectra*, vol. 15, no. 3, pp. 557–564, Aug. 1999, doi: 10.1193/1.1586058.

[83] F. Al-Turjman, M. Abujubbeh, A. Malekloo, and L. Mostarda, “UAVs assessment in software-defined IoT networks: An overview,” *Comput. Commun.*, vol. 150, pp. 519–536, Jan. 2020, doi: 10.1016/j.comcom.2019.12.004.

[84] E. Ozer, “Multisensory Smartphone Applications in Vibration-Based Structural Health Monitoring,” PhD Thesis, Columbia University, New York, NY, USA, 2016.

[85] M. Feng, Y. Fukuda, M. Mizuta, and E. Ozer, “Citizen Sensors for SHM: Use of Accelerometer Data from Smartphones,” *Sensors*, vol. 15, no. 2, pp. 2980–2998, Jan. 2015, doi: 10.3390/s150202980.

[86] E. Ozer and M. Q. Feng, “Structural Reliability Estimation with Participatory Sensing and Mobile Cyber-Physical Structural Health Monitoring Systems,” *Appl. Sci.*, vol. 9, no. 14, p. 2840, Jul. 2019, doi: 10.3390/app9142840.

[87] “Sensor Kinetics Pro - Apps on Google Play.” https://play.google.com/store/apps/details?id=com.innoventions.sensorkineticspro&hl=en (accessed Jul. 29, 2020).

[88] Wasim Ramadan, “Finite Element Model Updating of Bridges with Mobile and Smart Technologies for Infrastructure-Related Decision-Making,” MSc Thesis, Middle East Technical University Northern Cyprus Campus, In progress.

[89] F. McKenna, G. L. Fenves, M. H. Scott, and B. Jeremic, “Open system for earthquake engineering simulation (OpenSees),” *Univ Calif. Berkeley CA Httpopensees Berkeley Edu*, 2000.

[90] A. Kiremidjian, J. Moore, Y. Y. Fan, O. Yazlali, N. Basoz, and M. Williams, "Seismic Risk Assessment of Transportation Network Systems," *J. Earthq. Eng.*, vol. 11, no. 3, pp. 371–382, May 2007, doi: 10.1080/13632460701285277.

[91] M. A. P. Taylor and G. M. D'Este, "Transport Network Vulnerability: a Method for Diagnosis of Critical Locations in Transport Infrastructure Systems," in *Critical Infrastructure: Reliability and Vulnerability*, A. T. Murray and T. H. Grubesic, Eds. Berlin, Heidelberg: Springer, 2007, pp. 9–30.

[92] M. G. H. Bell and Y. Iida, *Transportation network analysis*. Chichester ; New York: J. Wiley, 1997.

[93] J.-P. Rodrigue, *The geography of transport systems*, Fifth edition. Abingdon, Oxon ; New York, NY: Routledge, 2020.

[94] J. L. Gross, J. Yellen, and P. Zhang, Eds., *Handbook of graph theory*, Second edition. Boca Raton: CRC Press, Taylor & Francis Group, 2014.

[95] K. Kansky and P. Danscoine, "Measures of network structure," *FLUX Cah. Sci. Int. Réseaux Territ.*, vol. 5, no. 1, pp. 89–121, 1989.

[96] K. J. Kansky, *Structure of Transportation Networks: Relationships Between Network Geometry and Regional Characteristics*. University of Chicago., 1963.

[97] L.-G. Mattsson and E. Jenelius, "Vulnerability and resilience of transport systems – A discussion of recent research," *Transp. Res. Part Policy Pract.*, vol. 81, pp. 16–34, Nov. 2015, doi: 10.1016/j.tra.2015.06.002.

[98] A. Sevtsuk and M. Mekonnen, "Urban network analysis: a new toolbox for measuring city form in ArcGIS," in *Proceedings of the 2012 Symposium on Simulation for Architecture and Urban Design*, 2012, pp. 1–10.

[99] Atsu Okabe and Kei-ichi Okunuki, "SANET. A Spatial Analysis along Networks (Ver.4.1).," Tokyo, Japan.

[100] A. Hagberg, P. Swart, and D. S Chult, "Exploring network structure, dynamics, and function using networkx," Los Alamos National Lab. (LANL), Los Alamos, NM (United States), LA-UR-08-05495; LA-UR-08-5495, Jan. 2008. Accessed: Jul. 03, 2020. [Online]. Available: https://www.osti.gov/biblio/960616-exploring-network-structure-dynamics-function-using-networkx.

[101] L. C. Freeman, "Centrality in social networks conceptual clarification," *Soc. Netw.*, vol. 1, no. 3, pp. 215–239, Jan. 1978, doi: 10.1016/0378-8733(78)90021-7.

[102] Andres Sevtsuk, Michael Mekonnen, and Raul Kalvo, "Urban Network AnalysisToolbox for ArcGIS 10 / 10.1 / 10.2 Help Manual V1.01." City Form Lab, Jan. 20, 2016.

[103] S. L. Handy and D. A. Niemeier, "Measuring Accessibility: An Exploration of Issues and Alternatives," *Environ. Plan. Econ. Space*, vol. 29, no. 7, pp. 1175–1194, Jul. 1997, doi: 10.1068/a291175.

[104] A. Okabe and K. Sugihara, *Spatial analysis along networks: statistical and computational methods*. Hoboken, N.J: Wiley, 2012.

[105] A. Okabe, T. Satoh, and K. Sugihara, "A kernel density estimation method for networks, its computational method and a GIS-based tool," *Int. J. Geogr. Inf. Sci.*, vol. 23, no. 1, pp. 7–32, Jan. 2009, doi: 10.1080/13658810802475491.

[106] J. Benedek, S. M. Ciobanu, and T. C. Man, "Hotspots and social background of urban traffic crashes: A case study in Cluj-Napoca (Romania)," *Accid. Anal. Prev.*, vol. 87, pp. 117–126, Feb. 2016, doi: 10.1016/j.aap.2015.11.026.

[107] Z. Xie and J. Yan, "Kernel Density Estimation of traffic accidents in a network space," *Comput. Environ. Urban Syst.*, vol. 32, no. 5, pp. 396–406, Sep. 2008, doi: 10.1016/j.compenvurbsys.2008.05.001.

[108] Transportation Research Board, National Cooperative Highway Research Program, and Transportation Research Board, *Travel Demand Forecasting: Parameters and Techniques*. Washington, D.C.: National Academies Press, 2012, p. 14665.

[109] N. J. Garber and L. A. Hoel, *Traffic and highway engineering*, 4th ed. Australia ; United States: Cengage Learning, 2009.

[110] U. B. of P. R. O. of P. U. P. Division, *Traffic Assignment Manual for Application with a Large, High Speed Computer*. US Department of Commerce, 1964.

[111] J. C. Duthie *et al.*, "Investigating Regional Dynamic Traffic Assignment Modeling for Improved Bottleneck Analysis: Final Report," Center for Transportation Research, University of Texas, Austin, Technical Report FHWA/TX-13/0-6657-1, Jun. 2013. Accessed: Jul. 08, 2020. [Online].

[112] Z. Tian, D. Lin, K. Yin, and X. Zhou, "Development of a Dynamic Traffic Assignment Model for Northern Nevada," Center for Advanced Transportation Education and Research (CATER), University of Nevada, Reno, NDOT Research Report 342-13–803, Jun. 2014.

[113] X. Zhou and J. Taylor, "DTALite: A queue-based mesoscopic traffic simulator for fast model evaluation and calibration," *Cogent Eng.*, vol. 1, no. 1, Oct. 2014, doi: 10.1080/23311916.2014.961345.

[114] J. G. Wardrop, "ROAD PAPER. SOME THEORETICAL ASPECTS OF ROAD TRAFFIC RESEARCH.," *Proc. Inst. Civ. Eng.*, vol. 1, no. 3, pp. 325–362, May 1952, doi: 10.1680/ipeds.1952.11259.

[115] C.-C. Lu, H. S. Mahmassani, and X. Zhou, "Equivalent gap function-based reformulation and solution algorithm for the dynamic user equilibrium problem," *Transp. Res. Part B Methodol.*, vol. 43, no. 3, pp. 345–364, Mar. 2009, doi: 10.1016/j.trb.2008.07.005.

[116] E. National Academies of Sciences and Medicine (U. S.). and Transportation Research Board, *Highway capacity manual: a guide for multimodal mobility analysis.* 2016.

[117] R. Dowling, *Planning techniques to estimate speeds and service volumes for planning applications*, vol. 387. Transportation Research Board, 1997.

[118] J. Sloboden, J. Lewis, V. Alexiadis, Y.-C. Chiu, and E. Nava, "Traffic analysis toolbox volume xiv: Guidebook on the utilization of dynamic traffic assignment in modeling," United States. Federal Highway Administration. Office of Operations, 2012.

[119] O. Järv, R. Ahas, E. Saluveer, B. Derudder, and F. Witlox, "Mobile Phones in a Traffic Flow: A Geographical Perspective to Evening Rush Hour Traffic Analysis Using Call Detail Records," *PLoS ONE*, vol. 7, no. 11, p. e49171, Nov. 2012, doi: 10.1371/journal.pone.0049171.

[120] Center For International Earth Science Information Network-CIESIN-Columbia University, "Gridded Population of the World, Version 4 (GPWv4): Administrative Unit Center Points with Population Estimates, Revision 10." Palisades, NY: NASA Socioeconomic Data and Applications Center (SEDAC), 2017, doi: 10.7927/H46H4FCT.

[121] UNISDR, "Global Assessment Report on Disaster Risk Reduction 2015, Making Development Sustainable: The Future of Disaster Risk Management," United Nations Office for Disaster Risk Reduction (UNISDR), Geneva, Switzerland, 2015.

[122] B. Bhaduri, E. Bright, P. Coleman, and M. L. Urban, "LandScan USA: a high-resolution geospatial and temporal modeling approach for population distribution and dynamics," *GeoJournal*, vol. 69, no. 1, pp. 103–117, Jun. 2007, doi: 10.1007/s10708-007-9105-9.

[123] Global Administrative Areas, "GADM database of Global Administrative Areas, version 3.6." [Online]. Available: https://gadm.org/index.html.

[124] FEMA, "Earthquake Model Technical Manual (Hazus 2.1)." Department of Homeland Security Federal Emergency Management Agency Mitigation Division.

[125] NIBS-FEMA, "Hazus®–MH 2.1 Multi-hazard Loss Estimation Methodology User Manual," Department of Homeland Security Federal Emergency Management Agency Mitigation Division, Washington, D.C., 2013.

[126] Z. Cagnan, O. Yilmaz, and T. Yilmaz, "Site Classification of Newly Deployed Strong Motion Stations in the Eastern Mediterranean," presented at the 15th World Conference on Earthquake Engineering, Lisbon, Portugal, Sep. 2012.

[127] Geofabrik GmbH, "OpenStreetMap Data Extracts." http://download.geofabrik.de/.

[128] OpenStreetMap Wiki, "Road Identification Details in OpenStreetMap." https://wiki.openstreetmap.org/wiki/Key:highway.

[129] FEMA, "FEMA Flood Map Service Center | Hazus." https://msc.fema.gov/portal/resources/hazus.

[130] Z. Wang, "Understanding seismic hazard and risk: a gap between engineers and seismologists," 2008.

[131] D. L. Wells and K. J. Coppersmith, "New empirical relationships among magnitude, rupture length, rupture width, rupture area, and surface displacement," *Bull. Seismol. Soc. Am.*, vol. 84, no. 4, pp. 974–1002, 1994.

[132] E. M. Thompson and C. B. Worden, "Estimating Rupture Distances without a Rupture," *Bull. Seismol. Soc. Am.*, vol. 108, no. 1, pp. 371–379, Feb. 2018, doi: 10.1785/0120170174.

[133] Y. Zhou, S. Banerjee, and M. Shinozuka, "Socio-economic effect of seismic retrofit of bridges for highway transportation networks: a pilot study," *Struct. Infrastruct. Eng.*, vol. 6, no. 1–2, pp. 145–157, Feb. 2010, doi: 10.1080/15732470802663862.

[134] A. Guo, Z. Liu, S. Li, and H. Li, "Seismic performance assessment of highway bridge networks considering post-disaster traffic demand of a transportation system in emergency conditions," *Struct. Infrastruct. Eng.*, vol. 13, no. 12, pp. 1523–1537, Dec. 2017, doi: 10.1080/15732479.2017.1299770.

[135] Y. Dong, D. M. Frangopol, and D. Saydam, "Sustainability of Highway Bridge Networks Under Seismic Hazard," *J. Earthq. Eng.*, vol. 18, no. 1, pp. 41–66, Jan. 2014, doi: 10.1080/13632469.2013.841600.

[136] E. C. Stergiou and A. S. Kiremidjian, "Risk assessment of transportation systems with network functionality losses," *Struct. Infrastruct. Eng.*, vol. 6, no. 1–2, pp. 111–125, Feb. 2010, doi: 10.1080/15732470802663839.

[137] S. E. Chang, M. Shinozuka, and J. E. Moore, "Probabilistic Earthquake Scenarios: Extending Risk Analysis Methodologies to Spatially Distributed Systems," *Earthq. Spectra*, vol. 16, no. 3, pp. 557–572, Aug. 2000, doi: 10.1193/1.1586127.

[138] A. Malekloo, E. Ozer, and F. Al-Turjman, "Combination of GIS and SHM in Prognosis and Diagnosis of Bridges in Earthquake-Prone Locations," in *Smart Grid in IoT-Enabled Spaces*, 1st ed., CRC Press, 2020, pp. 139–158.

[139] F. Al-Turjman and A. Malekloo, "Smart parking in IoT-enabled cities: A survey," *Sustain. Cities Soc.*, vol. 49, p. 101608, Aug. 2019, doi: 10.1016/j.scs.2019.101608.

APPENDIX

A. Data Sources Used for the Case Study

In this appendix, we provide the data sources and models developed in this study. The supplementary files are uploaded on GitHub, in particular,

1. Northern Cyprus Hazus inventory and the python code are available at https://bit.ly/3kQZKlo
2. ShakeMap data files, including the sources files and the maps, are available at https://bit.ly/3g0sDYX
3. The dynamic traffic simulation files modeled in DTALite is available at https://bit.ly/2PY1cEG

B. The PGA Maps of Scenarios Simulated

Here we present the ShakeMap PGA maps of the four scenarios simulated in this study.

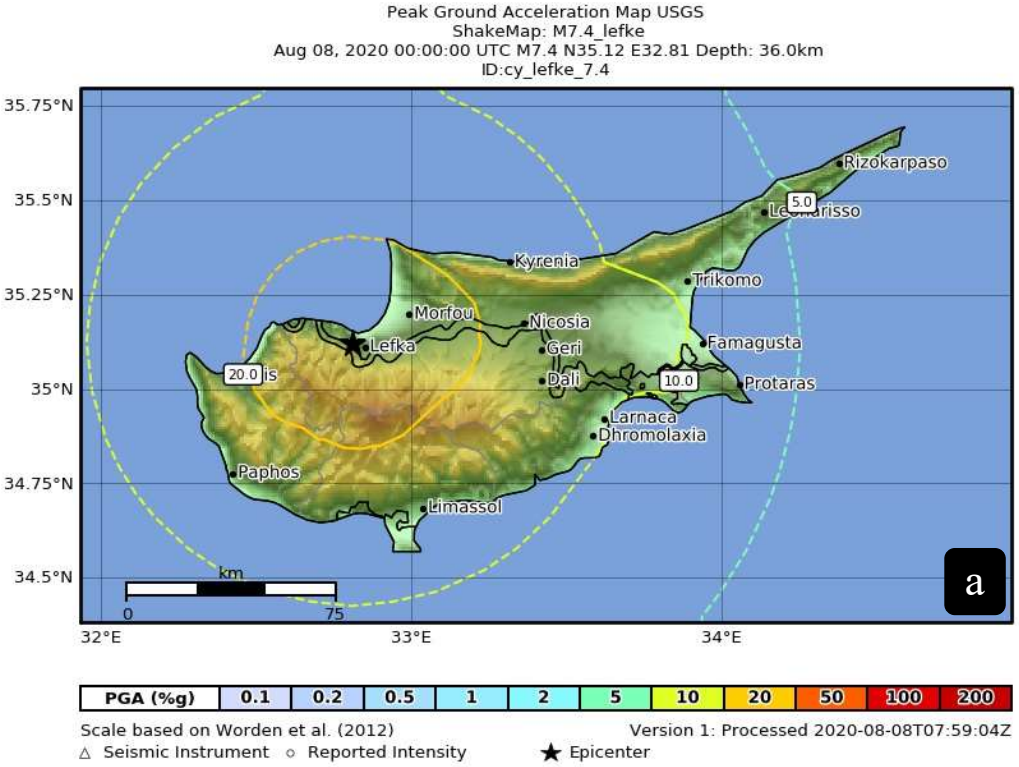

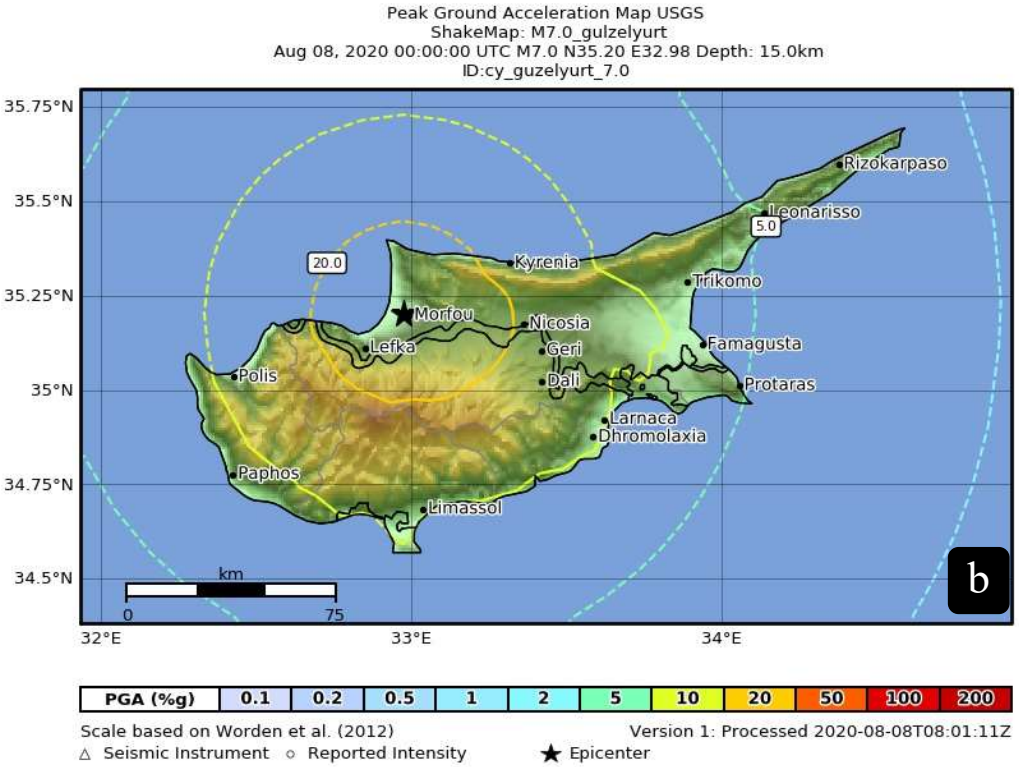

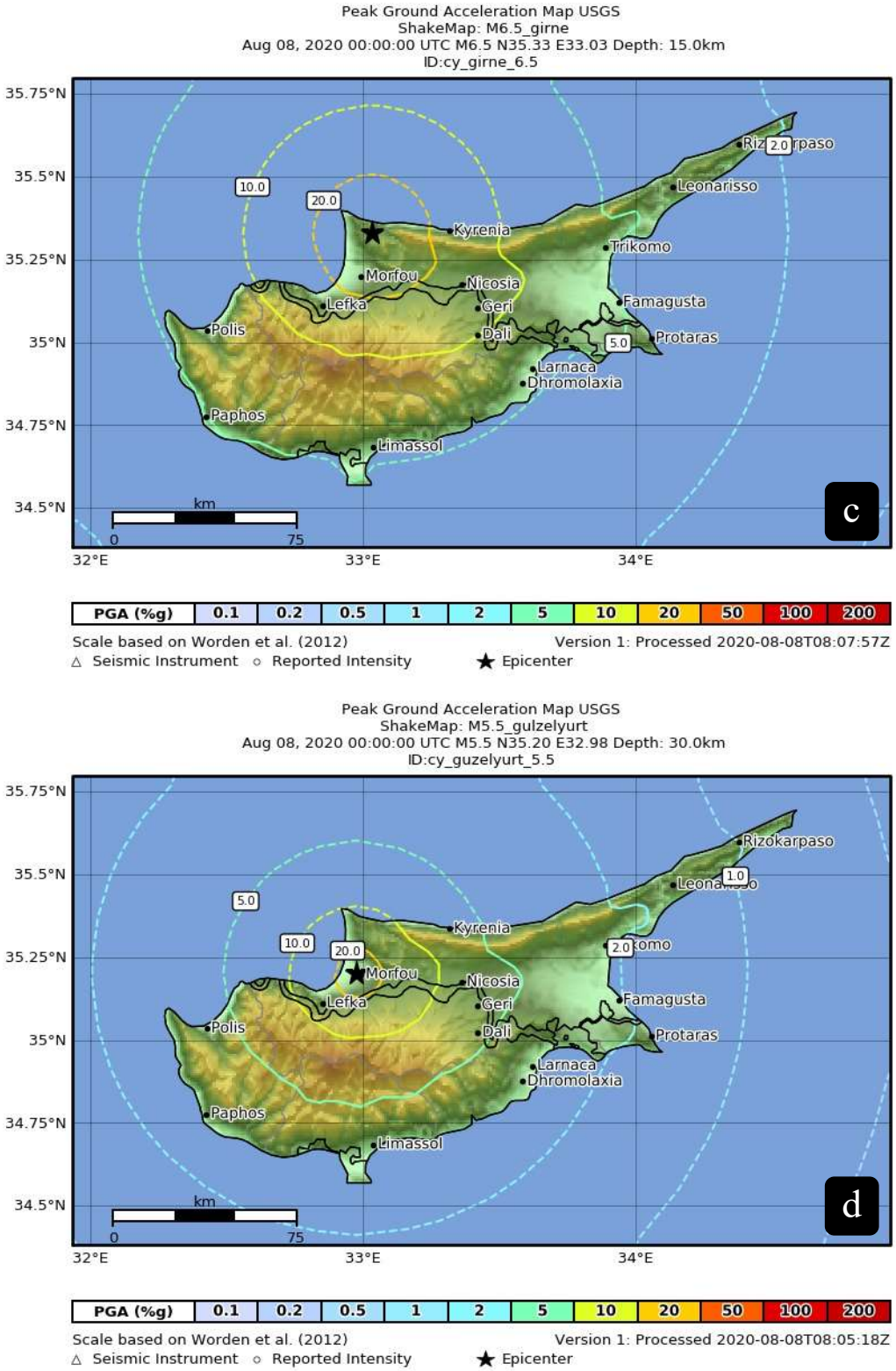

Figure B.1. ShakeMap PGA maps for a) Scenario 1 M7.4, b) Scenario 2 M7.0, c) Scenario 3, M6.5, and d) Scenario 4 M5.5

C. Bridge Damage State

In this appendix, we provide the damage state probabilities from Hazus based on the ShakeMap data for scenarios 2, 3, and 4.

Table C.1. Overall damage state description for Scenario 2

Bridge ID Number	Damage State $P(DS = k\|IM_m)$					Overall Damage		
	None	Slight	Moderate	Extensive	Complete	μ_1	σ_1	Mean Damage State
KK000001	0.511	0.161	0.110	0.138	0.080	0.101	0.172	Moderate
KK000002	0.974	0.013	0.007	0.005	0.001	0.003	0.037	None
KK000003	0.974	0.015	0.006	0.004	0.001	0.003	0.036	None
KK000004	0.694	0.103	0.081	0.085	0.037	0.068	0.187	Moderate
KK000005	0.973	0.000	0.000	0.021	0.005	0.010	0.078	Slight
KK000006	0.929	0.038	0.017	0.013	0.003	0.009	0.062	None
KK000007	0.850	0.070	0.036	0.032	0.011	0.024	0.111	Slight
KK000008	0.820	0.081	0.043	0.041	0.015	0.019	0.054	Slight
KK000009	0.991	0.006	0.002	0.001	0.000	0.001	0.009	None
KK000010	0.751	0.102	0.059	0.061	0.027	0.050	0.164	Moderate
KK000011	0.753	0.001	0.085	0.103	0.058	0.091	0.225	Moderate
KK000012	0.753	0.045	0.075	0.085	0.043	0.072	0.200	Moderate
KK000013	0.244	0.099	0.129	0.238	0.289	0.362	0.377	Extensive
KK000014	0.244	0.148	0.132	0.229	0.247	0.122	0.082	Moderate
KK000015	0.245	0.128	0.131	0.233	0.262	0.138	0.090	Moderate
KK000016	0.250	0.149	0.132	0.228	0.241	0.313	0.366	Extensive
KK000017	0.983	0.011	0.004	0.002	0.000	0.001	0.013	None
KK000018	0.974	0.016	0.006	0.004	0.001	0.003	0.036	None
KK000019	0.974	0.010	0.009	0.006	0.001	0.004	0.038	None
KK000020	0.991	0.004	0.003	0.002	0.000	0.001	0.012	None

Table C.2. Overall damage state description for Scenario 3

Bridge ID Number	Damage State $P(DS = k\|IM_m)$					Overall Damage		
	None	Slight	Moderate	Extensive	Complete	μ_1	σ_1	Mean Damage State
KK000001	0.908	0.051	0.021	0.015	0.003	0.009	0.048	None
KK000002	0.999	0.000	0.000	0.000	0.000	0.000	0.000	None
KK000003	0.999	0.001	0.000	0.000	0.000	0.000	0.001	None
KK000004	0.961	0.020	0.011	0.007	0.001	0.004	0.039	None
KK000005	0.999	0.000	0.000	0.001	0.000	0.000	0.008	None
KK000006	0.998	0.002	0.000	0.000	0.000	0.000	0.001	None
KK000007	0.993	0.005	0.001	0.001	0.000	0.000	0.009	None
KK000008	0.990	0.006	0.002	0.001	0.000	0.001	0.009	None
KK000009	1.000	0.000	0.000	0.000	0.000	0.000	0.000	None
KK000010	0.972	0.017	0.006	0.004	0.001	0.003	0.036	None
KK000011	0.969	0.000	0.016	0.012	0.003	0.007	0.061	None
KK000012	0.969	0.009	0.012	0.008	0.002	0.005	0.050	None
KK000013	0.690	0.094	0.085	0.091	0.041	0.073	0.196	Moderate
KK000014	0.663	0.136	0.080	0.084	0.036	0.039	0.070	Moderate
KK000015	0.637	0.126	0.090	0.099	0.047	0.047	0.078	Moderate
KK000016	0.601	0.149	0.093	0.105	0.051	0.089	0.213	Moderate
KK000017	0.947	0.030	0.012	0.009	0.002	0.006	0.051	None
KK000018	0.919	0.042	0.019	0.015	0.004	0.011	0.070	Slight
KK000019	0.919	0.025	0.027	0.022	0.007	0.015	0.090	Slight
KK000020	0.966	0.013	0.011	0.008	0.002	0.005	0.050	None

Table C.3. Overall damage state description for Scenario 4

Bridge ID Number	Damage State $P(DS = k\|IM_m)$					Overall Damage		
	None	Slight	Moderate	Extensive	Complete	μ_1	σ_1	Mean Damage State
KK000001	0.999	0.001	0.000	0.000	0.000	0.000	0.001	None
KK000002	1.000	0.000	0.000	0.000	0.000	0.000	0.000	None
KK000003	1.000	0.000	0.000	0.000	0.000	0.000	0.000	None
KK000004	1.000	0.000	0.000	0.000	0.000	0.000	0.000	None
KK000005	1.000	0.000	0.000	0.000	0.000	0.000	0.000	None
KK000006	1.000	0.000	0.000	0.000	0.000	0.000	0.000	None
KK000007	1.000	0.000	0.000	0.000	0.000	0.000	0.000	None
KK000008	0.999	0.001	0.000	0.000	0.000	0.000	0.001	None
KK000009	1.000	0.000	0.000	0.000	0.000	0.000	0.000	None
KK000010	0.999	0.000	0.000	0.000	0.000	0.000	0.000	None
KK000011	0.999	0.000	0.000	0.000	0.000	0.000	0.000	None
KK000012	0.999	0.000	0.000	0.000	0.000	0.000	0.000	None
KK000013	0.971	0.015	0.009	0.005	0.001	0.003	0.037	None
KK000014	0.969	0.020	0.007	0.004	0.001	0.002	0.018	None
KK000015	0.969	0.018	0.008	0.004	0.001	0.002	0.019	None
KK000016	0.972	0.018	0.006	0.003	0.001	0.003	0.035	None
KK000017	1.000	0.000	0.000	0.000	0.000	0.000	0.000	None
KK000018	1.000	0.000	0.000	0.000	0.000	0.000	0.000	None
KK000019	1.000	0.000	0.000	0.000	0.000	0.000	0.000	None
KK000020	1.000	0.000	0.000	0.000	0.000	0.000	0.000	None

D. A Simple Bridge Retrofit Prioritization

In this appendix, we present a very simple case-study for developing an optimal strategy for utilizing the funds available to retrofit the vulnerable overpasses for the network shown in Figure D.1. The strategy is based on the goal of transferring people from the vicinity of an event epicenter to 4 different evacuation centers. Assume five bridges have been identified to fail for an earthquake of M7.0 or above. We use MATLAB to develop this model as:

D.1 Creating the Sample Network

```
clc;
clear;
s=[1 1 2 2 2 3 3 3 3 4 4 4 5 5 5 6 6 6 7 7 7 8 8 8 9 9 9 9 10 10 10 11 11
11 12 12 12 13 13 13 13 14 14 14 14 15 15 15 16 16 17 17 17 18 18 18 19 19
19 20 20 20 21 21];
t=[2 3 1 3 4 1 2 4 6 2 3 5 4 6 7 3 5 8 5 9 11 6 9 12 7 8 10 13 9 11 14 7
10 15 8 13 16 9 12 14 17 10 13 15 18 11 14 20 12 17 13 16 18 14 17 19 18 20
21 15 19 21 19 20];

G=digraph(s,t,'omitselfloops')
plot(G)
```

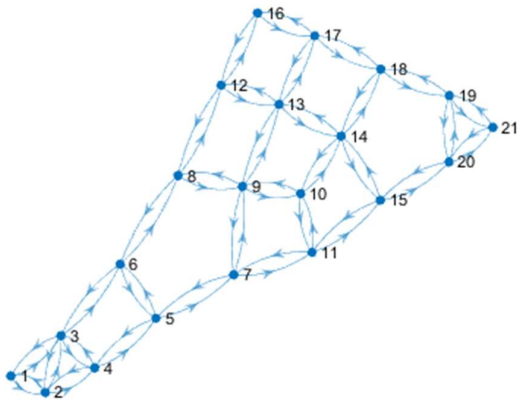

Figure D.1. A sample network for bridge retrofit prioritization

D.2 Creating Network Descriptions

```
cost=[20 25 20 20 25 25 20 15 30 25 15 15 15 20 20 30 20 10 20 10 20 10 15
20 10 15 5 10 5 5 10 20 5 15 20 10 10 10 10 5 15 10 5 15 10 15 15 10 10 5
15 5 5 10 5 20 20 10 10 10 10 5 10 5]';

cap=[3953 4941 3521 3219 5574 3670 3264 5006 5386 6213 5955 6640 4035 4532
5183 3369 4829 3799 4136 3255 3156 6892 3774 3389 5352 5472 5823 6164 4401
6497 4078 3067 6863 6739 5497 4278 5685 4848 3785 4356 3485 4567 5661 6901
3081 5238 6194 6722 1000 5435 5707 4071 6327 3690 3144 6903 5517 6340 4987
6237 6331 6040 6563 3428]';
```

```
G.Edges.cost=cost;
G.Edges.cap=cap;
```

where:

- Cost = Travel time
- Cap = Link reserve capacity during the evacuation (over and above usual traffic)

Decision to retrofit the vulnerable bridges should take into consideration both directions of the associated roadway, assuming no partial retrofitting is allowed:

```
vulinks_s=[9 11 12 15 20 10 15 13 20 21]';
vulinks_t=[10 15 13 20 21 9 11 12 15 20]';
retrocost=[2 3 4 5 4 2 3 4 5 4];
ff=G.findedge(vulinks_s,vulinks_t);
G.Edges.retro_cost=zeros(G.numedges,1);
G.Edges{ff,"retro_cost"}=retrocost';
G.Edges
```

D.3 Developing optimization parameters

To develop the mixed integer linear program optimization parameters (MILP), we have:

```
  flow1=optimvar('flow',G.numedges,"Type","integer","LowerBound",0);

  retrofit1=optimvar('retrofit',10,"Type","integer","LowerBound",0,"UpperB
ound",1)
```

The network flow constraint is modeled as:

```
  netflow1=optimexpr(1,G.numedges);
  for c=1:G.numnodes
      netf=0;
      for g=1:G.numedges
          if (G.Edges.EndNodes(g,2)==c)
              netf=netf+flow1(g);
          elseif G.Edges.EndNodes(g,1)==c
              netf=netf-flow1(g);
          end
      end
      netflow1(c)=sum(netf);
  end
```

Link constraints on flow capacity is modeled as:

```
  problem.Constraints.flowconst=flow1<=G.Edges.cap;
  problem.Constraints.retrofitflow=flow1(ff)<=retrofit1.*G.Edges{ff,"cap"}
```

Flow conservation constraint is:

```
  problem.Constraints.nodeconst1=netflow1(1:20) <= [2000 0 0 0 0 0 1000 500
0 0 0 1500 0 0 0 0 0 0 0 0];
  problem.Constraints.nodeconst2=netflow1(21)== -5000;
```

Note 1: source node has assumed to have a negative supply and has to fully dispersed the flow on the connected links

Note 2: Sink nodes (Evacuations centers) and transshipment nodes (internal network nodes) are assumed to have positive demand and 0 demand, respectively. The flow was defined in the variable section as positive with Lowerband=0

To formulate the budget constraint:

```
problem.Constraints.retrofitconst=sum(retrofit1.*retrocost')<= 30;
```

Finally, we can write the objective function as:

```
problem=optimproblem("ObjectiveSense","min");

problem.Objective = sum(flow1.*G.Edges.cost);
```

To solve the MILP optimization problem, some necessary parameters have to be set to ensure convergence and reaching optimum values.

```
options=optimoptions("intlinprog");
options.CutGeneration="advanced";
options.CutMaxIterations=50;
options.IntegerPreprocess="advanced";
options.RootLPAlgorithm="primal-simplex";
options.HeuristicsMaxNodes=100;
options.Heuristics="intermediate";

[sol,fval1,exitflag1,output1]=solve(problem,"Options",options)
```

Therefore, under a budget constraint, the optimum strategy is to Retrofit all five vulnerable bridges except the one on link 11-15 (or 15-11), as shown in Figure D.2. Link with +ve flow indicates the shortest paths between the source node and the sink nodes.

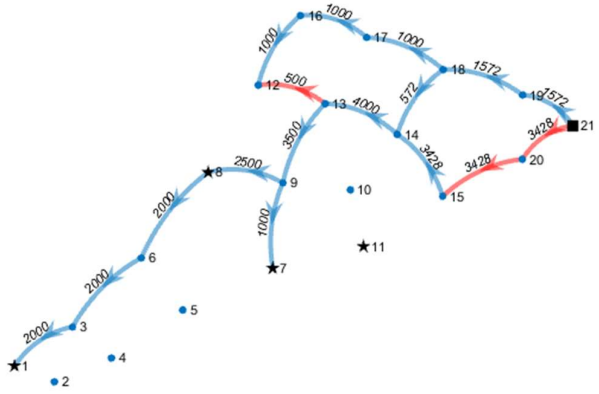

Figure D.2. A simple bridge retrofit prioritization model under a budget constraint